fodor.gyula_298_24

Exponentially small radiation of oscillons and oscillatons

A thesis for the Doctor of Sciences (D.Sc.) degree
of the Hungarian Academy of Sciences

Gyula Fodor

HUN-REN Wigner Research Centre for Physics,
Institute for Particle and Nuclear Physics

Budapest, 2025

Abstract

Numerical simulations show that a massive real scalar field in a nonlinear theory can form long-lived oscillating localized states. For a self-interacting scalar on a fixed background these objects are named oscillons, while for the self-gravitating case they are called oscillatons. This review discusses the history and various general properties of these solutions. However, the main emphasis is on the calculation of the small but nonzero classical scalar field radiation emitted by them. The radiation for higher amplitude states can be calculated by a spectral numerical method. For small and moderately large amplitudes an analytical approach based on complex extension, matching of asymptotic series, and Laplace transform can be used.

For ease of understanding, the complicated analytical methods are presented first for a linear inhomogeneous model problem. Then the analytic and numerical techniques are applied for the fifth-order generalization of the Korteweg-de Vries (KdV) equation. This hydrodynamically motivated problem also has weakly radiating localized solutions, but since there are time-independent configurations, the formalism is still considerably simpler than the procedure for the oscillating scalar field problem. This allows us to obtain higher order corrections to the leading order result in the KdV case. We continue with the simplest one-dimensional scalar oscillons, then generalize to $3+1$ dimensional oscillons, and finally to self-gravitating oscillatons based on that experience.

Contents

1 Introduction

A fundamental question of physics is how the available matter can form spatially localized lumps, and what prevents the formed objects from falling apart, evaporating or radiated out, such that the matter and energy occupy uniformly all the available space. In this review we approach this problem from a theoretical perspective where we study the simplest classical field theoretical and hydrodynamical models where long-lived localized states may appear. In this way we can get insight on what properties a theory must have so that these type of structures would be allowed to exist at all. The objects corresponding to the states appearing in the simplest models can also be expected to develop in more general, complicated, physically more relevant theories. The typical size of the formed structures may range from the size of particles to galaxy clusters, depending on the parameters in the theory, such as the mass of the scalar field, for example.

Some special models allow *soliton* solutions which are exponentially localized and do not lose energy by radiation. The discovery of solitons is associated to the name of John Scott Russell, a Scottish civil engineer, who in 1834 observed a stable wave packet propagating along a canal, and followed it on horseback for a few kilometers. Solitons are nonlinear wave packets that propagate with constant speed, keep their shape during the propagation, and they show considerable stability even when colliding with each other. The observed surface water waves can be well described by the stationarily propagating solutions of Korteweg-de Vries (KdV) equation.

For a certain range of the surface tension of the fluid it is necessary to extend the KdV equation by adding a fifth spatial derivative term, multiplied by ε^2, where ε is a small parameter [1]. For positive but not too large ε there are still solutions quite similar to solitons, but they are losing energy by weak scalar field radiation in the direction of the propagation [2]. There exist also solutions with essentially the same core region which are time-independent in a comoving system. These solutions are symmetric and have very small constant-amplitude spatially oscillating tails in both directions far from the center. The amplitude of this tail tends to zero exponentially when $\varepsilon \to 0$, hence it cannot be calculated by elementary perturbational methods. The main objective of this review is to pedagogically present the methods that can be used for the calculation of such exponentially small tail-amplitudes. Since these methods are quite complicated and technical, we start with introducing them in Section 2 for the simplest system for which they can be applied, a linear inhhomogeneous differential equation suggested by J. P. Boyd [3, 4, 5]. Then in Section 3 we continue with the calculation of the tail-amplitude for the fifth-order KdV problem. That procedure have been carried out to quite high orders in our papers [6, 7]. The application of the method for oscillating scalar field systems is described in Sections 4 and 5 of this review.

The procedure for the computation of the exponentially small tail-amplitude is based on the extension of the solutions to complex values of the spatial coordinate. This method was applied first by Pokrovskii and Khalatnikov in 1961 for the calculation of the amplitude of backscattering from a low potential barrier [8]. The ordinary WKB (Wentzel–Kramers–Brillouin) method cannot be applied for above-the-barrier scattering because of the lack of turning points. The key idea has been the use of turning points which exist for complex values of the spatial coordinate. Close to these points on the complex plane the reflected wave is not small anymore. However, it decays exponentially when going back to the real axis, so one can obtain the intended extremely small amplitude. For nonlinear problems Kruskal and Segur [9] was the first to apply the complex extension method for a model describing the growth of needle crystals, in a preprint in 1985. Soon after this, they have generalized the procedure for the calculation of the radiating tail of ϕ^4 oscillons [10]. Pomeau, Ramani and Grammaticos have applied the procedure for the fifth-order KdV equation, and they have realized that the inner equations can be solved by Borel summation instead of the earlier numerical method [11].

Presumably, the simplest classical relativistic field theoretical model is the theory in which there is only a single real (not complex) scalar field ϕ on a fixed $1+1$ dimensional Minkowski spacetime background. The scalar field ϕ depends on the time coordinate t and spatial coordinate x, and satisfies the differential equation

$$-\frac{\partial^2\phi}{\partial t^2}+\frac{\partial^2\phi}{\partial x^2}=U'(\phi)\ , \tag{1}$$

where $U'(\phi)$ denotes the derivative of the scalar potential $U(\phi)$ with respect to ϕ. For a large class of $U(\phi)$ potentials various localized but weakly radiating states can already appear in this simple model. The most widely investigated cases are the ϕ^4 potential with two symmetrically placed minimums, $U(\phi)=(\phi^2-1)^2/4$, and the sine-Gordon potential $U(\phi)=1-\cos\phi$, which has infinitely many identical minimums. In both models there are *kink* solutions, which appear at the boundary of two different vacuum domains. The kink solution belongs to the class of solitons.

If we observe the solution from a system moving along with the kink, then we obtain the simplest static kink solution. The shape of this solution for the case of the sine-Gordon theory is $\phi=4\arctan(\pm\exp x)$. Although the energy density of the one-dimensional kink is essentially restricted to a bounded region, it is not a localized solution in the sense that it tends to different vacuum states in the negative and positive x directions. The three-dimensional generalization of this solution is not a particle-like state localized around a point, but rather a domain wall. From Derrick's theorem we know that there are no stable static localized solutions for three or more spatial dimensions [12].

The other particle-like solution in the sine-Gordon theory is known as the *sine-Gordon breather*, the form of which will be written out later in equation (141). There is a one-

parameter family of sine-Gordon breather solutions, which can be parametrized by the frequency of the oscillation of the field. The breather is a time-periodically oscillating exponentially localized exact solution, which is stable and do not radiate energy out to infinity. For the sine-Gordon breather the scalar field tends to the same vacuum value at both the negative and positive directions, hence there is a possibility for the existence of a three-dimensional spherically symmetric generalization.

The spatially reflected version of the kink solution is named antikink. Surprisingly, a sine-Gordon breather cannot be formed by the collision of a kink and an antikink. According to the exact solution describing the collision, the two objects go through each other without any change in their velocity or shape. This is an exceptional property of the integrable sine-Gordon theory.

The one-dimensional sine-Gordon theory is also very special in the sense that it is the only theory involving a real scalar field where an exactly time-periodic localized breather can exist. In other models with analytic potential, including the higher dimensional sine-Gordon theory, not only an exact solution is not known, but even with numerical methods it is not possible to find a finite energy localized time-periodic solution. There are mathematical results showing that for the one-dimensional case families of breathers can only exist for the sine-Gordon potential [13, 14, 15]. In this way, from the intended properly localized solutions not only the static but the time-periodic solutions are also excluded.

Surprisingly, in spite of all this, as numerical experience shows, a self-interacting real scalar field can still form long-lived localized oscillating states. However, these solutions always lose energy slowly by the radiation of scalar field, and hence their frequency is also changing gradually. These objects were called pulsons originally [16, 17], but later the name *oscillon* became widespread in the literature [18, 19]. For example, in the one-dimensional ϕ^4 theory oscillons can easily form by the collision of a kink and an antikink, after radiating out the unnecessary energy [20].

The importance of oscillons is greatly increased by the observation that they are not exceptional states, they evolve from quite general initial data in several cases. For more than one spatial dimensions oscillons become spherically symmetric quickly by radiating out scalar field [21]. Oscillons can be produced rather easily by numerically following the spherically symmetric time-evolution of a general bell-shaped initial data. According to more general numerical simulations, oscillons can form from randomly chosen not spherically symmetric initial data as well [22, 23]. This makes it likely that they may have played a role in the early universe, evolving from the inflaton field or from some of the other scalars coupled to it [24, 25, 26, 27, 28, 29, 30]. At the forming and decaying of oscillons the emission of gravitational waves may be increased, which might be observed as peaks on the spectrum of gravitational waves [31, 32, 33, 34, 35, 36, 37, 38, 39, 40, 41, 42, 43].

The nonlinearity of the theory is an essential feature for the existence of oscillons. The structure of oscillons cannot be described by first-order linear perturbations. There are small-amplitude oscillons, but the smaller the amplitude is the larger their spatial size becomes. This is necessary in order to allow the influence of the nonlinearity become effective even for small amplitude states. The shape of the oscillon is getting determined from conditions arising at higher orders in the perturbational analysis.

Oscillons have been observed to form in theories containing several kind of interacting fields, such as for example in the bosonic sector of the standard model, when the Higgs mass is twice as large as the mass of the $W^{\pm}$ boson [44, 45, 46]. Oscillons can also form in Abelian Higgs models at the decay of sphalerons [47, 48, 49, 50, 51], at the collision of vortex antivortex pairs [52], or as a result of symmetry breaking [53, 54].

Although the scalar field oscillons are classical field theoretical solutions, they can also be considered as collective quantum states formed by large number of identical particles. Before the numerical discovery of oscillons, in their paper appeared in 1975, Dashen, Hasslacher and Neveu have already arrived at the study of the one-dimensional sine-Gordon breathers and ϕ^4 oscillons, while applying the semiclassical WKB method [55]. Considering the small-amplitude oscillons as stable time-periodic solutions and quantizing the perturbations around them they have calculated the energy levels at weak coupling. The semiclassical method for the calculation of the radiation of oscillons has been applied by Hertzberg [56, 57]. Considering the oscillons as quantum systems and using inhomogeneous Hartree approximation and numerical methods, the time evolution and radiation of oscillons have been investigated in paper [58]. The radiation of the sine-Gordon breather have been calculated by the classical-quantum correspondence method in [59].

In Section 4 of this review, after presenting the most important earlier articles about oscillons, the results that we have obtained in our papers [60, 61, 62, 63] concerning their structure and radiation are discussed in detail. Apart from the exceptional sine-Gordon breather, all oscillon solutions emit energy slowly by the radiation of scalar field. In certain cases this radiation can be so weak that one may have chance to detect it only by extremely precise numerical methods. For a long time it was unclear whether or not there may exist exactly periodic nonradiating solutions. By varying the parameters of a Gaussian-type initial data, in 2002 Honda and Choptuik found 125 resonance peaks, which appeared to correspond to periodic oscillons [64]. In our first paper about oscillons, we have shown that the states belonging to these peaks are actually oscillons belonging to the low amplitude unstable domain, which, even if very slightly, but necessarily radiate in a detectable way [60].

If we compensate the energy loss of an oscillon by a same amplitude and frequency incoming wave, then we obtain an exactly time-periodic state with a small amplitude standing wave tail outside the core region. The spherically symmetric standing wave tail goes out to

arbitrarily large distances, and the decrease of its amplitude is so slow that the whole energy of the system turns out to be infinite. Although the obtained solution is not localized, it still has a core region where the energy density is many orders of magnitude larger than in the tail zone. At some given frequency, for the solution with the minimal amplitude tail we have introduced the naming *quasibreather* [60]. The concept has been adopted in the literature [65, 56, 66, 67, 68, 69, 70, 71, 72, 73, 74]. The amplitude of the standing wave tail of the quasibreather agrees with the tail-amplitude of the radiating oscillon. A big advantage of the introduction of the quasibreather is that numerically it can be much more precisely calculated than the corresponding oscillon state.

The core region of oscillons can be described quite precisely by an asymptotic power series expansion in terms of an amplitude parameter [75, 55, 10, 76, 77, 14]. This parameter is usually denoted by ε. The relation between the oscillon's frequency ω and the amplitude parameter can always be chosen in the form $\omega^2 = 1 - \varepsilon^2$. The expansion worked out to higher orders has been presented in our paper [61]. The formalism also gives a result for the ε dependence of the oscillon's energy, which is valid for low and moderate amplitudes. For higher amplitude states we can obtain the precise value of the energy by a spectral numerical code. The dependence of the energy on the central amplitude is important because it determines the stability of the system. If increasing the central amplitude the total energy of the system also increases, then the system is stable, otherwise it is unstable. From the analysis it follows that three-dimensional oscillons are stable only if their amplitude is above a certain limit. If their amplitude decreases below that value because of the radiation loss, then they suddenly decay. In case of one and two spatial dimensions all oscillons are stable below a certain amplitude. Since the energy loss rate decreases exponentially when the amplitude decreases, these lower dimensional oscillons never decay.

Although the small-amplitude expansion gives a very good representation of the core region, it is unable to describe the radiating tail, which is exponentially small in ε. This is closely related to the fact that this expansion is not convergent, it is an asymptotic series representation. Extending the formalism to complex values of the radial coordinate r, it is possible to determine the amplitude of the tail by investigating the behavior of the quantities near a singularity on the complex r plane. This method was used by Segur and Kruskal in 1987, for the case of one-dimensional oscillons [10]. In our paper [62] we have extended the procedure by a Borel summation method, and for symmetric $U(\phi)$ potentials we have determined the radiation amplitude by a purely analytic way. For two and three spatial dimensions we have generalized the procedure in our paper [63]. In Subsection 4.4 of this review we explain in a more comprehensible way this rather complicated procedure, which has been presented in a rather concise way in our papers.

In Section 5 of this review we investigate localized states formed by a real scalar field

interacting with gravity in the framework of general relativity. In this case, the potential $U(\phi)$ determining the self-interaction of the scalar field may have the form $U(\phi) = \frac{1}{2}m\phi^2$ corresponding to the Klein-Gordon case, since gravity already provides the necessary non-linearity. On a fixed flat background the equations describing the Klein-Gordon scalar are linear, hence they cannot form oscillons. In the gravitational case the most studied case is just the Klein-Gordon scalar. Possibly this is the reason why the theory of localized states formed by self-gravitating scalars was born and developed in a completely separated way from that of the flat background oscillons. These configurations were discovered in 1991 by Seidel and Suen, who found apparently time-periodic localized states formed by a self-gravitating scalar field using numerical methods [78]. They gave the name *oscillaton* to these objects [79]. In spite of the markedly similar naming, generally there is no reference to the other topic in most publications.

Majority of the published studies on oscillatons are restricted to the physically important three-dimensional case. As we have mentioned earlier, oscillons defined on a 3+1 dimensional background suddenly decay after a few thousand oscillations, at most. In contrast to this, the lifetime of 3+1 dimensional self gravitating oscillatons is infinite, their behavior is similar to the $1+1$ and $2+1$ dimensional oscillons.

Oscillatons can easily develop from Gaussian shaped initial data, and non-symmetric initial data also develops into spherically symmetric oscillatons by quick radiation of the surplus mass. The radiation is so small that for a long time it was tacitly assumed that oscillatons are time-periodic and nonradiating. This is understandable if we know that even in the most favorable case, at the maximal mass oscillaton, when the ratio of the amplitude of the radiating tail to the central amplitude is maximal, the tail-amplitude is of the order 10^{-8}, while the central amplitude is about 0.5.

It was first pointed out by Don Page in 2003 that oscillatons must necessarily radiate, hence they cannot be exactly time periodic and localized [80]. Because of the mass loss, their amplitude and frequency slowly change as time passes. In our paper [81] the method applied for oscillons earlier has been generalized for the case of oscillatons. In a subsequent paper we have also calculated the strength of the radiation by a spectral numerical method, and we have obtained results consistent with our analytical calculations [82]. Small but positive cosmological constant further increases the amplitude of the radiation, but it still remains exponentially small in terms of the cosmological constant [83]. In Section 5 of this review the results published in our papers [81, 82] are presented in detail.

Several physical applications of oscillatons have been proposed in the literature up to now. Oscillatons formed by scalar fields in cosmological models may be suitable for describing dark matter in galaxies [84, 85, 86, 87, 88, 89, 90]. The real scalar field necessary for the formation of oscillons or oscillatons may be most naturally provided by axions [91, 92, 93, 22] or similar

weakly interacting hypothetical bosonic particles [94, 95, 96, 97, 98, 99, 100, 101]. If the self-interaction of the scalar field is determined by a potential $U(\phi)$ typical for axions, then in several papers the forming oscillatons are called axion stars, see e.g. [102, 103, 104, 105, 106, 107]. Cosmological simulations describing the evolution of axion-like fields show that in the central parts of the forming diffuse matter structures solitonic cores are developing, which also correspond to oscillatons [108, 109, 110, 111, 112]. Fuzzy dark matter constituting of very low mass axion-like particles may provide a solution for the core-cusp problem, explaining why in galaxies we cannot observe dark matter lumps which are below a certain size [113, 114, 115, 116, 117, 118, 119]. Scalar dark matter may also be accumulated inside stars, and may form oscillaton-like cores there [120, 121]. Massive real vector fields under the influence of gravitation can also form localized states, the so called Proca stars, with a time-periodically oscillating metric similar to that of oscillatons [122, 121, 123, 124, 125]. For complex massive vector fields there are Proca star solutions where the spacetime is stationary [126, 127, 128], similarly to boson stars.

2 Slowly driven fast oscillator – a model problem

In this section we consider a simple linear model problem, for which we can pedagogically present essentially all of the rather technical mathematical and perturbational methods that has to be applied to solve the physically more relevant nonlinear problems in the following sections. We focus our attention on the second-order linear ordinary differential equation for a function u that depends on x,

$$\varepsilon^2 \frac{\mathrm{d}^2 u}{\mathrm{d}x^2} + u = \operatorname{sech}^2 x \ , \tag{2}$$

where ε is a small positive constant. The source function $\operatorname{sech}^2 x = \cosh^{-2} x$ is symmetric and tends to zero when $|x| \to \infty$. Equation (2) has been studied first by J. P. Boyd, who interpreted it as a reduced wave equation obtained by factoring out harmonic time dependence [3, 4, 5]. Regarding x as time, one can consider (2) as an equation describing a fast oscillator driven by a relatively slowly varying force [129, 130]. Taking ε as a small parameter, we obviously have a singular perturbation problem, since the high frequency oscillations completely disappear when $\varepsilon = 0$.

The general solution can be obtained from any particular solution by adding $\alpha \sin(\frac{x}{\varepsilon} + \delta)$ with arbitrary amplitude α and phase δ. We are interested in solutions that are as localized as possible. The most important solution for our analysis is the even solution $u_{\mathrm{m}}(x) = u_{\mathrm{m}}(-x)$ that has a large core region, similarly shaped to the function $\operatorname{sech}^2 x$, and which for large $|x|$ tends to an oscillating tail $\alpha \sin \frac{|x|}{\varepsilon}$, with as small amplitude α as possible. We show this unique minimal tail solution for $\varepsilon = \frac{1}{4}$ in Fig. 1.

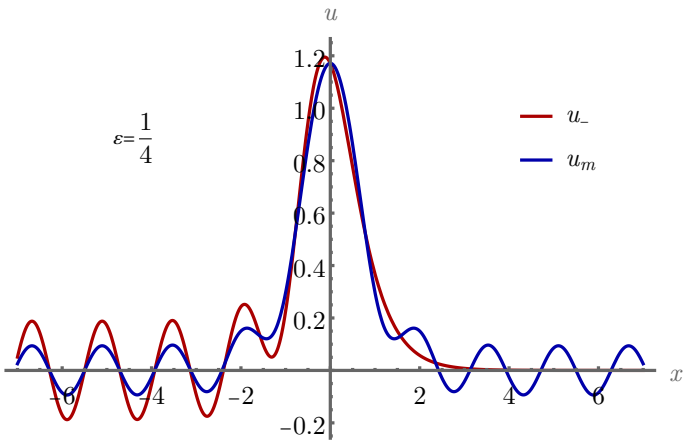

Figure 1: The right decaying u_- and the minimal tail symmetric u_{m} solutions for the specific choice of $\varepsilon = \frac{1}{4}$. For $\varepsilon > 0$ there is no localized configuration without tail.

For $\varepsilon > 0$ no symmetric solution without tail is possible, i.e. $\alpha > 0$. The second important solution, u_-, has a similar core, but it decays to zero exponentially for $x \to +\infty$. This can

be obtained from $u_{\rm m}$ by subtracting the homogeneous solution $\alpha \sin \frac{x}{\varepsilon}$, canceling the tail on the right hand side, but doubling the tail-amplitude on the left hand side. Logarithmic plots of the solutions for smaller values of ε are shown in Fig. 2.

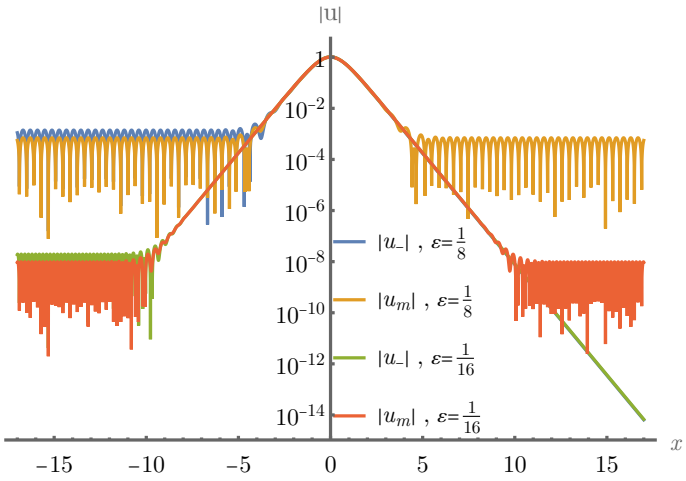

Figure 2: Absolute values of u_- and $u_{\rm m}$ for $\varepsilon = \frac{1}{8}$ and $\varepsilon = \frac{1}{16}$. The downward spikes, corresponding to zero crossings, should go all the way down for high enough plotting resolution. The core region of the solutions are quite similar, hence the other curves run below the red one. The blue curve is below the green one on the right side.

Since Eq. (2) is linear, it can be solved by the method of Green's functions. The solution of $\varepsilon^2 \frac{\mathrm{d}^2 u}{\mathrm{d}x^2} + u = \delta(x-s)$ also depends on the boundary conditions. Assuming $u \to 0$ as $x \to +\infty$, the Green's function is $G(x,s) = \frac{1}{\varepsilon} H(s-x) \sin \frac{s-x}{\varepsilon}$, where H is the Heaviside step function. The asymmetric right decaying solution can be calculated as

$$\begin{aligned} u_- &= \frac{1}{\varepsilon} \int_x^\infty \sin \frac{s-x}{\varepsilon} \, \mathrm{sech}^2 s \, \mathrm{d}s \\ &= \frac{1}{\varepsilon} \cos \frac{x}{\varepsilon} \int_x^\infty \sin \frac{s}{\varepsilon} \, \mathrm{sech}^2 s \, \mathrm{d}s - \frac{1}{\varepsilon} \sin \frac{x}{\varepsilon} \int_x^\infty \cos \frac{s}{\varepsilon} \, \mathrm{sech}^2 s \, \mathrm{d}s \ . \end{aligned} \tag{3}$$

Since $\mathrm{sech}^2 s$ is an even function, the first integral tends to zero for $x \to -\infty$, and the tail-amplitude on the left hand side can be calculated as

$$\alpha_- = \left| \frac{1}{\varepsilon} \int_{-\infty}^\infty \cos \frac{s}{\varepsilon} \, \mathrm{sech}^2 s \, \mathrm{d}s \right| = \left| \int_{-\infty}^\infty \cos s \ \mathrm{sech}^2(\varepsilon s) \mathrm{d}s \right| \ . \tag{4}$$

The symmetric minimal tail solution can be obtained as $u_{\rm m} = u_- + \frac{1}{2}\alpha_- \sin \frac{x}{\varepsilon}$, making the tail-amplitude $\alpha_{\rm m} = \frac{1}{2}\alpha_-$ on both sides. There is no $\cos \frac{x}{\varepsilon}$ part in the tails of u_- and $u_{\rm m}$. Adding the homogeneous solution $\cos \frac{x}{\varepsilon}$ with any nonzero factor to $u_{\rm m}$ would further increase the tail of the symmetric solution with respect to the minimal amplitude $\alpha_{\rm m} = \frac{1}{2}\alpha_-$. The difference between the two solutions is

$$u_{\rm m} - u_- = \alpha_{\rm m} \sin \frac{x}{\varepsilon} \ , \tag{5}$$

and the phase of the tail is that corresponding to the $\sin \frac{x}{\varepsilon}$ function.

The integral in (4) can be calculated, and the minimal tail-amplitude of symmetric solutions is given as

$$\alpha_{\rm m} = \frac{\pi}{2\varepsilon^2}\ \mathrm{csch}\left(\frac{\pi}{2\varepsilon}\right)\ . \tag{6}$$

The integrals in (3) can be expressed in terms of Hypergeometric functions ${}_2F_1$, and the right decaying solution can be written in the explicit form

$$u_- = \frac{2\mathrm{e}^{-2x}}{1+4\varepsilon^2}\Bigg[(1+2i\varepsilon)\ {}_2F_1\left(2, 1+\frac{i}{2\varepsilon}; 2+\frac{i}{2\varepsilon}; -\mathrm{e}^{-2x}\right) \\ +(1-2i\varepsilon)\ {}_2F_1\left(2, 1-\frac{i}{2\varepsilon}; 2-\frac{i}{2\varepsilon}; -\mathrm{e}^{-2x}\right)\Bigg]\ . \tag{7}$$

This can be used for fast and very precise numerical calculation of the solutions u_- and $u_{\rm m}$ for given values of ε, and also for plots, even on the complex x plane.

Equation (2) can be solved by the method of Green's functions because it is linear. For more complicated nonlinear problems spectral methods can be used to obtain very precise numerical solutions. The matched asymptotic expansions methods described in the next subsections can provide valuable information even for very complicated nonlinear systems, such as time-periodic scalar fields coupled to Einstein's gravity.

2.1 Outer expansion

We search the solution in the series expansion form:

$$u = \sum_{n=0}^{\infty} u_n \varepsilon^{2n}\ . \tag{8}$$

Although we do not assume convergence for the sum, we substitute into Eq. (2) and assume that the coefficients of the various ε powers are zero. We obtain $u_0 = \mathrm{sech}^2 x$ and $u_n = -\frac{\mathrm{d}^2}{\mathrm{d}x^2} u_{n-2}$, which yields

$$u_n = (-1)^n \frac{\mathrm{d}^{2n}}{\mathrm{d}x^{2n}} \mathrm{sech}^2 x\ . \tag{9}$$

The first few functions are

$$u_1 = 2\,\mathrm{sech}^2 x \left(3\,\mathrm{sech}^2 x - 2\right)\ , \tag{10}$$

$$u_2 = 8\,\mathrm{sech}^2 x \left(15\,\mathrm{sech}^4 x - 15\,\mathrm{sech}^2 x + 2\right)\ , \tag{11}$$

$$u_3 = 16\,\mathrm{sech}^2 x \left(315\,\mathrm{sech}^6 x - 420\,\mathrm{sech}^4 x + 126\,\mathrm{sech}^2 x - 4\right)\ . \tag{12}$$

We call (8) as *outer expansion* because, as we will see, it fails close to singularities on the complex x plane, and in those "smaller" regions, after a rescaling of x, a different, so-called *inner expansion* will be applied.

Since the perturbation problem is singular, the expansion (8) is not convergent for any fixed $\varepsilon > 0$, but it is *asymptotic* to some (non-unique) function $u(x, \varepsilon)$. For more information on asymptotic expansions and perturbation methods the reader may consult the popular textbooks [131, 132, 133]. Defining the partial sum

$$u^{(N)} = \sum_{n=0}^{N} u_n \varepsilon^{2n} \ , \tag{13}$$

asymptotic behavior means that the difference $\left|u(x,\varepsilon) - u^{(N)}\right|$ tends to zero faster than ε^{2N} as $\varepsilon \to 0$ for all $N \geq 0$ fixed integers. Taking various ε values, the solution families u_- and u_{m} both can be considered as appropriate $u(x, \varepsilon)$, since their difference and their tails are exponentially small in terms of ε. In Figure 3 the difference $\left|u_{\mathrm{m}} - u^{(N)}\right|$ is plotted for $\varepsilon = \frac{1}{8}$.

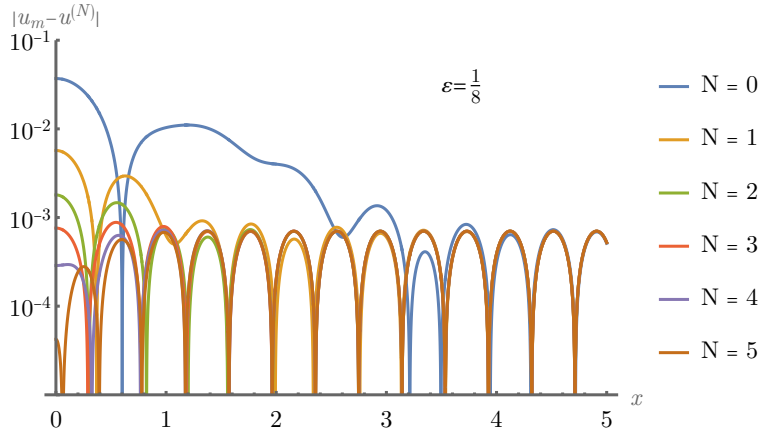

Figure 3: Difference of the minimal tail solution u_{m} from various N-th order expansion approximations $u^{(N)}$ for $\varepsilon = \frac{1}{8}$. All these functions are symmetric, so only $x \geq 0$ is shown. For this ε value the optimal truncation order is $N_{\mathrm{opt}} = 5$, for larger N the difference becomes larger and larger in the central region. For large x the difference tends to the oscillating tail, with amplitude $\alpha_{\mathrm{m}} \approx 7.0117 \cdot 10^{-4}$.

The optimal order of the truncation may depend on the choice of the position x. This is especially apparent when we compare the functions $u^{(N)}$ to the right decaying solution u_-. In Fig. 4 the difference $|u_- - u^{(N)}|$ is plotted for the same ε as in Fig. 3. For large positive x extremely small relative error with respect to the already small u_- can be obtained by taking N very large, even if ε is not small. At the central region the best approximation still has an error of the order of α_{m}, and much less terms in the sum has to be used. In a certain sense, expansion (8) can be considered as a boundary condition for u_- at $x \to +\infty$.

The error of the partial sum $u^{(N)}$ can be estimated by the absolute value of the first neglected term, $|u_{N+1}|\varepsilon^{2N+2}$. The optimal truncation order $N \equiv N_{\mathrm{opt}}$ of the asymptotic series can be generally well estimated by stopping the summation when the first neglected term,

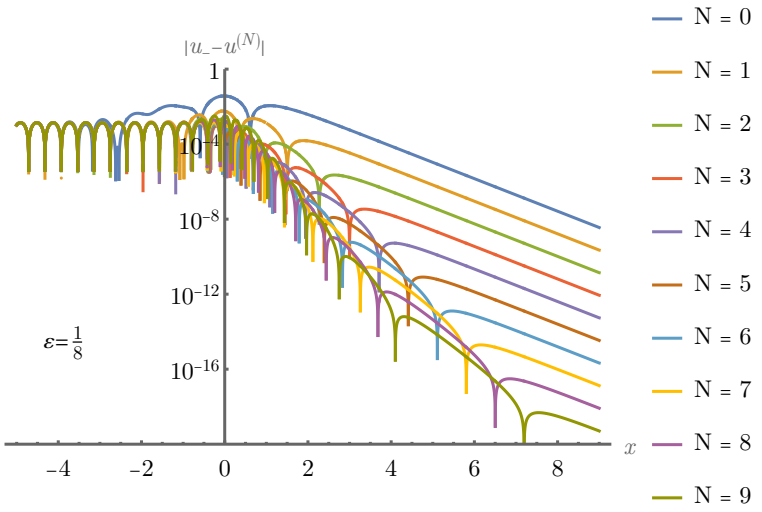

Figure 4: Difference of the right decaying solution u_- from various N-th order expansion approximations $u^{(N)}$ for $\varepsilon = \frac{1}{8}$. Although it cannot be seen well from the figure, the optimal truncation order in the central region is $N_{\rm opt} = 5$, just as for $u_{\rm m}$ in Fig. 3. However, for large enough positive x the optimal order $N_{\rm opt}$ can become arbitrarily large and the relative error with respect to u_- arbitrarily small.

$|u_{N+1}|\varepsilon^{2N+2}$, is minimal. When ε decreases, the optimal order increases approximately as $1/\varepsilon$, and the error decreases exponentially, $\sim \exp(-a/\varepsilon)$, where a is some positive constant. For general asymptotic series these type of "beyond all order small" corrections [9, 134] has been called *exponential asymptotics* [135, 136]. The optimally truncated expansion has been named *superasymptotics* [137], while even more precise approximations can be obtained by methods called *hyperasymptotics* [138, 139]. In Table 1 we show the how the function $u_{\rm m}$ and its approximations depend on ε at the center $x = 0$.

All functions u_n in the ε expansion tend to zero exponentially when $|x| \to \infty$. Hence this procedure cannot describe the tail region of the solutions u_- and $u_{\rm m}$. However, it provides a very good approximation for the core region of both functions, with error that tends to zero exponentially when $\varepsilon \to 0$. When we set the coefficients of the various powers of ε to zero after substituting the formal expansion (8) into (2), we implicitly assume that the second derivative of u_n has the same order in ε as u_n itself. This assumption is clearly false for the homogeneous solution $\sin \frac{x}{\varepsilon}$, which has very high frequency oscillations when ε is small. Similarly, taking repeated derivatives of $\mathrm{sech}^2 x$, higher and higher frequency oscillations appear in u_n close to $x = 0$, and the expansion loses its validity when the wavelength of these oscillations become as small as ε. This happens when N is near the optimal truncation order, as illustrated by Fig. 5.

The procedure we apply in (2) and (8) is essentially *multiple scale analysis*[131, 132, 133], where only the slow scale x dependence is used. The fast scale x contributions cannot be

ε	N	$u_{N+1}\varepsilon^{2N+2}$	$u^{(N)} - u_{\mathrm{m}}$	$u^{(N+1)} - u_{\mathrm{m}}$	α_{m}
2^{-2}	1	$6.25 \cdot 10^{-2}$	$-4.63 \cdot 10^{-2}$	$\mathbf{1.62 \cdot 10^{-2}}$	$9.39 \cdot 10^{-2}$
2^{-3}	5	$3.26 \cdot 10^{-4}$	$\mathbf{4.23 \cdot 10^{-5}}$	$3.68 \cdot 10^{-4}$	$7.01 \cdot 10^{-4}$
2^{-4}	11	$3.12 \cdot 10^{-9}$	$\mathbf{-4.61 \cdot 10^{-10}}$	$2.66 \cdot 10^{-9}$	$9.78 \cdot 10^{-9}$
2^{-5}	23	$1.08 \cdot 10^{-19}$	$-7.73 \cdot 10^{-20}$	$\mathbf{3.04 \cdot 10^{-20}}$	$4.76 \cdot 10^{-19}$
2^{-6}	49	$4.50 \cdot 10^{-41}$	$\mathbf{6.77 \cdot 10^{-42}}$	$5.18 \cdot 10^{-41}$	$2.81 \cdot 10^{-40}$
2^{-7}	99	$2.77 \cdot 10^{-84}$	$\mathbf{-3.16 \cdot 10^{-85}}$	$2.46 \cdot 10^{-84}$	$2.46 \cdot 10^{-83}$
2^{-8}	199	$3.75 \cdot 10^{-171}$	$-2.42 \cdot 10^{-171}$	$\mathbf{1.33 \cdot 10^{-171}}$	$4.71 \cdot 10^{-170}$
2^{-9}	400	$2.43 \cdot 10^{-345}$	$-1.72 \cdot 10^{-345}$	$\mathbf{7.11 \cdot 10^{-346}}$	$4.32 \cdot 10^{-344}$
2^{-10}	802	$3.61 \cdot 10^{-694}$	$-3.00 \cdot 10^{-694}$	$\mathbf{6.09 \cdot 10^{-695}}$	$9.06 \cdot 10^{-693}$

Table 1: We consider quantities at $x = 0$, where $u_{\mathrm{m}} = u_{-}$. For decreasing values of ε, in the second column we give the value of N for which the (positive) term $u_{N+1}\varepsilon^{2N+2}$ is the smallest, and give its value in the third column. In the fourth and fifth column we give the difference of the partial sums $u^{(N)}$ and $u^{(N+1)}$ from the precise value of u_{m}, setting the better approximation bold faced. The error of these approximations at the center are similar order but somewhat smaller than the minimal tail-amplitude α_{m} listed in the last column. The central value of u_{m} remains close to 1 for all these ε values.

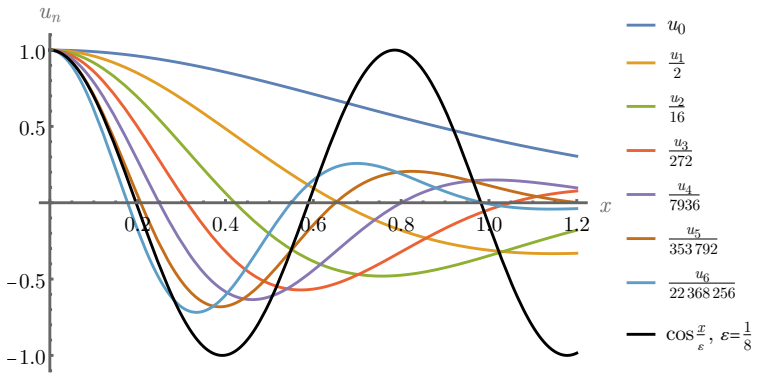

Figure 5: The functions u_n are shown up to $n = 6$, rescaled to make the central values 1. The wavelength of the oscillation at the center decreases as n grows. For $n = 5$ the wavelength becomes approximately equal to that of the function $\cos(8x)$, which is a solution of the homogeneous problem for $\varepsilon = \frac{1}{8}$, consistently with the value $N_{\mathrm{opt}} = 5$ in that case.

determined by this method, since they are exponentially small in terms of ε. The most well-known and widely applicable method for obtaining these exponentially small corrections is the extension of the solutions to the complex x plane and studying the behavior near the singularity closest to the real axis.

2.2 Complex extension

Since $\mathrm{sech}^2 x$ is a meromorphic function, we can consider (2) as a differential equation for functions u on the complex x plane. We are looking for complex analytic solutions u taking

real values on the real x axis, especially the complex extensions of the solutions u_- and u_m. Since u is real for $\mathrm{Im}\, x = 0$, it follows from the Schwarz reflection principle that $u(\overline{x}) = \overline{u(x)}$, where the overline denotes complex conjugate. Hence we will consider only the behavior of the functions on the upper half of the complex plane. Since the original real function u_m is symmetric at $x = 0$, the extension will naturally satisfy $u_\mathrm{m}(x) = u_\mathrm{m}(-x)$ for complex x values as well. Combining these two symmetries it follows that the mirror image with respect to the imaginary axis is just the complex conjugate of the original function, $u_\mathrm{m}(-\overline{x}) = \overline{u(x)}$. Consequently, the function u_m must take real values on the imaginary axis. The slightly asymmetric u_- function will have a small imaginary part along the line $\mathrm{Re}\, x = 0$.

The source function $\mathrm{sech}^2 x \equiv \cos^{-2}(ix)$ has second-order poles at $x = \frac{i\pi}{2}(1 + 2j)$ for all integer j. To study the behavior close to $x = \frac{i\pi}{2}$, which is the nearest pole above the real axis, we define y by $x = \frac{i\pi}{2} + y$. The function $\mathrm{sech}^n x$ has the Laurent series expansion

$$\mathrm{sech}^n x = \frac{1}{(iy)^n}\left[1 - \frac{ny^2}{6} + \frac{n(5n+2)y^4}{360} - \frac{n(35n^2+42n+16)y^6}{45360} + \dots\right], \qquad (14)$$

which is convergent for $|y| < \pi$, since π is the distance to the neighboring singularity. All solutions u of (2) will have singularities also at the points $x = \frac{i\pi}{2}(1 + 2j)$, and since the equation is linear, there will be no spontaneous (movable) singularities at other places. In Fig. 6 we show the behavior of the function u_- on the complex plane for $\varepsilon = \frac{1}{8}$. There is

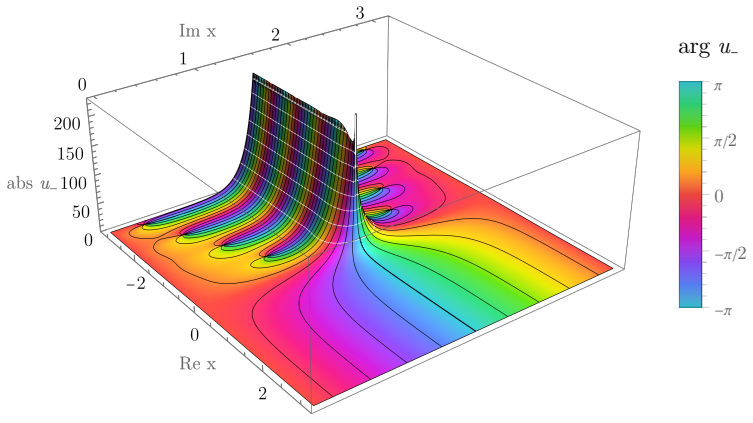

Figure 6: Three-dimensional complex plot of the solution u_- for $\varepsilon = \frac{1}{8}$, vertically showing the absolute value colored by the complex argument. The function is periodic along the imaginary direction, $u_-(x + i\pi) = u_-(x)$.

a branch cut for $\mathrm{Re}\, x < 0$ along the line $\mathrm{Im}\, x = \frac{\pi}{2}$ and the singularity is logarithmic at the point $x = \frac{i\pi}{2}$.

The coefficient functions u_n, which can be calculated by (9), also can be uniquely extended to the complex x plane, and one can form the asymptotic series expansion in terms of ε on the complex plane by (8). All u_n are built up from powers of $\operatorname{sech} x$, which has the Laurent series expansion presented in (14). The ε expansion will not only fail in the tail region of the real axis, but also close to the singularities on the complex plane. If $|y| \lesssim \varepsilon$ then the second derivative $\frac{\mathrm{d}^2 u}{\mathrm{d}x^2}$ will become so large that we cannot assume that it remains the same order in ε as u.

2.3 Inner expansion

The behavior of the solutions u in a region close the singularity at $x = \frac{i\pi}{2}$ can be described by a different ε expansion, focusing on that region by introducing a rescaled independent variable q by $y = \varepsilon q$. Since the relation to the original variable is

$$x = \frac{i\pi}{2} + \varepsilon q \ , \tag{15}$$

the factor ε^2 in Eq. (2) will be canceled in front of the second derivative. It is useful to scale down u by introducing the function

$$v = \varepsilon^2 u \ . \tag{16}$$

Equation (2) on the complex plane can be written into the equivalent form

$$\frac{\mathrm{d}^2 v}{\mathrm{d}q^2} + v = -\varepsilon^2 \operatorname{csch}^2(\varepsilon q) \ , \tag{17}$$

which is usually named *inner equation*, using the nomenclature from *boundary layer theory* [131, 132, 133]. We note that usually the inner and outer equations are obtained by making approximations that make them valid only in their respective regions. In our case both equations (2) and (17) remain exact everywhere, but the validity of the inner and outer ε expansions will determine the size of the inner and outer regions.

The solution of the inner equation (17) will be uniquely determined only after specifying appropriate boundary conditions. The simplest and most obvious solution will be the function $v^{(-)}$, which tends to zero to the right side, i.e. for $|q| \to \infty$ when $\operatorname{Re} q > 0$. We are interested in the downwards directions, when $\operatorname{Im} q \leq 0$. Up to a factor ε^2, this $v^{(-)}$ should correspond to the complex extension of the original right decaying solution u_-, which was defined on the real x line. Adding the homogeneous solutions $\cos q$ and $\sin q$ with appropriate complex valued factors, one may obtain the solution $v^{(\mathrm{m})}$, which corresponds to the extension of the minimal tail solution u_m that is symmetric on the real x axis. On the complex q plane this symmetry means that $v^{(\mathrm{m})}(-\overline{q}) = \overline{v^{(\mathrm{m})}(q)}$, at least for $\operatorname{Im} q < 0$. In particular, $\operatorname{Im} v^{(\mathrm{m})} = 0$ along the lower half of the imaginary axis.

The $\varepsilon \to 0$ limit is not singular when we use the variables q and v. Using the Laurent expansion (14) we can write the right hand side of (17) into a form expanded in powers of ε,

$$\frac{\mathrm{d}^2 v}{\mathrm{d}q^2} + v = -\frac{1}{q^2}\left[1 - \frac{q^2}{3}\varepsilon^2 + \frac{q^4}{15}\varepsilon^4 - \frac{2q^6}{189}\varepsilon^6 + \frac{q^8}{675}\varepsilon^8 - \frac{2q^{10}}{10395}\varepsilon^{10} + \ldots\right] . \tag{18}$$

The ε series expansion on the right hand side is convergent at those points q for which $|q| < \frac{\pi}{\varepsilon}$. This is quite a large region, considering that the real x axis is only at a distance $\frac{\pi}{2\varepsilon}$ from the singularity. Assuming that ε is small enough we can solve order by order, seeking the solution in the *inner expansion* form

$$v = \sum_{n=0}^{\infty} v_n \varepsilon^{2n} , \tag{19}$$

where v_n are ε independent functions. The differential equations for v_n are called the $2n$-*th order inner equations*. They have the form

$$\frac{\mathrm{d}^2 v_n}{\mathrm{d}q^2} + v_n = C_n q^{2n-2} , \tag{20}$$

where C_n are constants, the first few of them can be read off from (18). It is important to notice, that the ε expansions of the solutions $v^{(-)}$ and $v^{(\mathrm{m})}$ are different, specifically the coefficient functions $v_n^{(-)}$ and $v_n^{(\mathrm{m})}$ are generally not equal, as is will be illustrated in the next subsection. This is in contrast with Eq. (8), which is a valid expansion, with identical coefficient functions u_n, for both u_- and u_{m}, since their difference is exponentially small in ε. Inner equations and expansions can be similarly constructed for more complicated nonlinear problems as well.

2.4 Leading order inner equation

We discuss in more detail the leading order inner equation, which has the form

$$\frac{\mathrm{d}^2 v_0}{\mathrm{d}q^2} + v_0 = -\frac{1}{q^2} . \tag{21}$$

The unique solution which tends to zero as $|q| \to \infty$ in the half plane $\mathrm{Re}\, q > 0$ is

$$v_0^{(-)} = \sin q\, \mathrm{si}(q) + \cos q\, \mathrm{Ci}(q) , \tag{22}$$

where $\mathrm{Ci}(q)$ is the cosine integral function and $\mathrm{si}(q)$ is the sine integral function. In Fig. 7 we show a plot of this solution. Since the leading order behavior for small $|q|$ is $\log q$, there is a branch cut along the negative part of the real q axis. The function $v_0^{(-)}$ is real for real $q > 0$, hence $v_0^{(-)}(\overline{q}) = \overline{v_0^{(-)}(q)}$ for all q apart from the branch cut. However, the function is not symmetric with respect to the point $q = 0$. We define the function $v_0^{(+)}(q) = v_0^{(-)}(-q)$, which

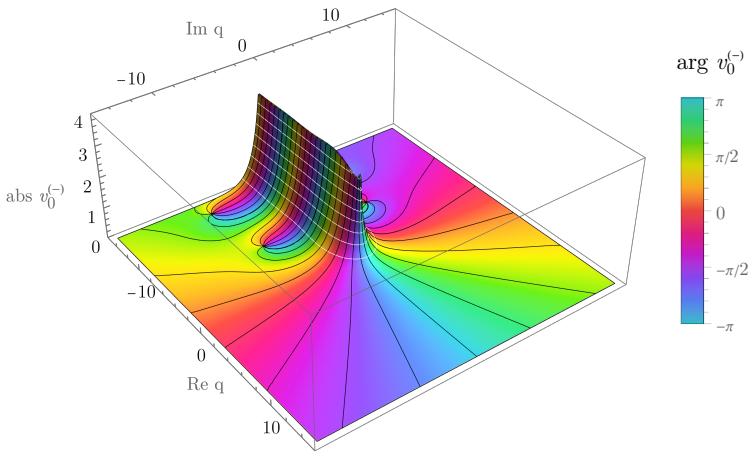

Figure 7: Three-dimensional complex plot of $v_0^{(-)}$. The local behavior is very similar to that of u_- in Fig. 6, but this function is not periodic along the imaginary direction.

is the unique solution that decays to zero asymptotically on the left side of the imaginary axis. It can be checked that

$$v_0^{(+)}(q) - v_0^{(-)}(q) = \begin{cases} i\pi \exp(-iq) & \text{if } \operatorname{Im} q < 0 \ , \\ -i\pi \exp(iq) & \text{if } \operatorname{Im} q > 0 \ . \end{cases} \tag{23}$$

It follows that the failure of symmetry for the reflection to the imaginary axis can be written as

$$\overline{v_0^{(-)}(-\overline{q})} - v_0^{(-)}(q) = \begin{cases} i\pi \exp(-iq) & \text{if } \operatorname{Im} q < 0 \ , \\ -i\pi \exp(iq) & \text{if } \operatorname{Im} q > 0 \ . \end{cases} \tag{24}$$

This shows that going downwards along the lower half of the imaginary axis the imaginary part of $v_0^{(-)}$ decays exponentially,

$$\operatorname{Im} v_0^{(-)}(q) = -\frac{\pi}{2} \exp(-iq) \quad \text{for} \quad \operatorname{Re} q = 0 \text{ and } \operatorname{Im} q < 0 \ . \tag{25}$$

For our purposes it is important to study the asymptotic behavior of the solution $v_0^{(-)}$ along constant $\operatorname{Im} q = q_i$ lines in the lower half plane $\operatorname{Im} q < 0$. If $\operatorname{Re} q = q_r$ tends to infinity in the $q_r > 0$ direction, then $v_0^{(-)} \to 0$ as q_r^{-2}. However, the function $v_0^{(-)}$ asymptotically oscillates as $-i\pi \exp q_i \exp(-iq_r)$ when $q_r \to -\infty$ for fixed q_i.

Canceling out the asymmetry, we define the other important solution as

$$v_0^{(\mathrm{m})} = v_0^{(-)} + i\frac{\pi}{2} \exp(-iq) \ , \tag{26}$$

which has the property $v_0^{(\mathrm{m})}(-\overline{q}) = \overline{v_0^{(\mathrm{m})}(q)}$ for $\operatorname{Im} q < 0$. This solution tends to zero when $|q| \to \infty$ in the lower half plane along constant $\arg q$ lines, i.e. for $-\pi < \arg q < 0$. If we add

the homogeneous solution $c_r \exp(-iq)$ to the function $v_0^{(\mathrm{m})}$ with any real constant factor c_r, the reflection symmetry to the imaginary axis and the decay properties remain unchanged, however, the amplitude of the tail oscillations along the constant $q_i < 0$ lines necessarily increase from the minimal value $\frac{\pi}{2} \exp q_i$. For constant $q_i < 0$, when considering $q_r \gg 0$, the asymptotic behavior of the solution necessarily has a fixed amplitude $i\frac{\pi}{2} \exp q_i \exp(-iq_r)$ part, which has a real part proportional to $\sin q_r$. However, adding $c_r \exp(-iq)$ can always be used to completely cancel the part of the solution that has real part proportional to $\cos q_r$.

The inner solutions $v_0^{(-)}$ and $v_0^{(\mathrm{m})}$, respectively, describe the leading order behavior for small ε of the exact solutions u_- and u_m, respectively, near the singularity. The main advantage of going out to the complex plane is that close to the singularity, in the inner region, the difference of these two solutions is not exponentially small in ε anymore, as it was on the real x line. In fact, the difference is not even vanishing in the $\varepsilon \to 0$ limit, as we have just seen.

There are two places where the difference of the symmetric and asymmetric solutions is particularly apparent. On the real x line for $x \gg 0$ the difference $u_\mathrm{m} - u_-$ is just the oscillating tail. The calculation of the amplitude of these type of tails is the main aim of this review paper. The other important place is the lower half of the imaginary q axis. There the extension of solutions that are even on the real x axis, in particular $v^{(\mathrm{m})}$, and hence $v_n^{(\mathrm{m})}$, cannot have any imaginary part. At this place the difference of the imaginary parts of $v^{(-)}$ and $v^{(\mathrm{m})}$ is determined just by $\mathrm{Im}\, v^{(-)}$.

In our linear problem the difference $u_\mathrm{m} - u_-$ is necessarily given by (5), which is exactly valid everywhere, including the tail region and the close neighborhood of the singularity. Then from (15) and (16) follows that $v^{(\mathrm{m})} - v^{(-)} = \varepsilon^2 \alpha_\mathrm{m} \sin\left(\frac{i\pi}{2\varepsilon} + q\right)$. Neglecting terms which are exponentially small in ε, we get

$$v^{(\mathrm{m})} - v^{(-)} = \frac{i}{2} \varepsilon^2 \alpha_\mathrm{m} \exp\left(\frac{\pi}{2\varepsilon}\right) \exp(-iq) \ . \tag{27}$$

To leading order in ε we can approximate the left hand side by $v_0^{(\mathrm{m})} - v_0^{(-)}$. Comparing with (26), we can solve for the tail-amplitude:

$$\alpha_\mathrm{m} = \frac{\pi}{\varepsilon^2} \exp\left(-\frac{\pi}{2\varepsilon}\right) \ . \tag{28}$$

Note that to obtain α_m it is enough to know that (26) and (27) hold on the lower part of the imaginary axis. Actually, even less information is needed, only the knowledge of the imaginary part of $v_0^{(-)}$ is enough for the calculation of the tail-amplitude. The quantity corresponding to $\mathrm{Im}\, v_0^{(-)}$ can be obtained relatively easily even for nonlinear problems when exact solutions are not known.

The tail-amplitude (28) agrees with the leading order behavior of the exact result in (6),

which can be expanded as

$$\alpha_{\rm m} = \frac{\pi}{\varepsilon^2}\exp\left(-\frac{\pi}{2\varepsilon}\right)\left[1+\exp\left(-\frac{\pi}{\varepsilon}\right)+\exp\left(-\frac{2\pi}{\varepsilon}\right)+\exp\left(-\frac{3\pi}{\varepsilon}\right)+\ldots\right] \ . \qquad (29)$$

The exponentially suppressed higher order terms in (29) can be interpreted as contributions from the singularities at $x = \frac{3i\pi}{2}$, $\frac{5i\pi}{2}$, $\frac{7i\pi}{2}\ldots$, which are $\frac{3\pi}{2\varepsilon}$, $\frac{5\pi}{2\varepsilon}$, $\frac{7\pi}{2\varepsilon}\ldots$ distances from the real line in terms of the variable q. Since the solution u_- is periodic, $u_-(x+i\pi) = u_-(x)$, it seems natural that the other singularities give similar contributions, only their amplitudes decay according to the corresponding larger distances. It might seem surprising that there are no $\varepsilon^n \exp\left(-\frac{\pi}{2\varepsilon}\right)$ contributions in (29) with $n > -2$ integers. In order to understand why the higher order inner equations do not give contributions, we study them in more detail.

2.5 Higher order inner equations

The inner equations we have to solve are given by (20), with $C_0 = -1$, $C_1 = \frac{1}{3}$, $C_2 = -\frac{1}{15}$, $C_3 = \frac{2}{189}$, $C_4 = -\frac{1}{675}\ldots$. The right decaying solution for v_0 has been given in (22). All the other inner equations have polynomial particular solutions, the first few are

$$\begin{aligned} v_1 =& \frac{1}{3} \ , \quad v_2 = -\frac{1}{15}\left(q^2-2\right) \ , \quad v_3 = \frac{2}{189}\left(q^4-12q^2+24\right) \ , \\ v_4 =& -\frac{1}{675}\left(q^6-30q^4+360q^2-720\right) \ . \end{aligned} \qquad (30)$$

These solutions are unique in the sense that they are not showing any oscillations or exponential blowup when $|q|$ is large, which necessarily appear in the general solution when we add $\exp(\pm iq)$ terms. However, these v_n functions have a rather puzzling feature, they are not tending to zero when $|q| \to \infty$, in fact they are growing polynomially. This might seem to be inconsistent with the decaying boundary conditions of the full inner equation (17). However, the inner ε expansion (19) can be convergent only if the right hand side of (18) is convergent, i.e. if $|q| < \frac{\pi}{\varepsilon}$. The analytic extension of the solution v beyond the convergence radius can be asymptotically decaying even if the coefficient functions v_n are divergent but have alternating signs.

We discuss the appropriate and consistent boundary conditions for the inner solutions v_n in the next subsection. However, it is apparent that the polynomial solutions (30) are the ones which do not contain any oscillations asymptotically. Additionally, they are purely real on the imaginary q axis, hence correspond to symmetric solutions. This means that for $n \geq 1$ the solutions $v_n^{(-)}$ and $v_n^{(\rm m)}$ completely agree. Consequently, at these orders we do not obtain any contributions to the tail oscillations at large x, as it has been already noted after Eq. (29). For our simple linear problem only the inner solution v_0 gives contribution to the tail. If instead of (2) we would solve the equation $\varepsilon^2 \frac{{\rm d}^2 u}{{\rm d}x^2} + u = \mathrm{sech}^4 x$ then v_0 and v_1 would give contributions.

2.6 Boundary conditions for the inner equations

Although in our linear problem the exact solution u_- can be written as in (7), it in not easy to deduce from this the ε dependence of its behavior near the singularity on the complex plane. However, there is a general method to obtain the behavior of the inner solutions v_n in an intermediate region, close to the singularity, but not very close to it. In an overlapping region where both the outer and inner ε expansions are valid we can use the outer expansion (8) of u with the known coefficient functions u_n, starting with (10)-(12), to provide boundary conditions to the various order inner equations. This procedure is known as the *method of matched asymptotic expansions* in the literature [131, 132, 133].

Since all x dependence is through powers of $\operatorname{sech} x$ we can use the Laurent series expansion presented in (14) with $y = \varepsilon q$. Multiplying with ε^2 to obtain $v = \varepsilon^2 u$ and collecting ε^n terms we obtain approximations to the inner solutions v_n. For the leading order inner solution we get

$$v_0 = -\frac{1}{q^2} + \frac{6}{q^4} - \frac{120}{q^6} + \frac{5040}{q^8} - \frac{362880}{q^{10}} + \frac{39916800}{q^{12}} - \dots \ , \tag{31}$$

while for all other v_n with $n \geq 1$ we obtain exactly the polynomial solutions of the inner equations, the first few of which are listed in (30). The coefficients in (31) increase so fast that the series in $1/q$ is not convergent for any q, but it is a series asymptotic to the function $v_0^{(-)}$ given in (22). On the other hand, considering the functions v_n as coefficients in the ε power series, the decrease of the highest coefficients of the polynomials in (30) suggest that the ε expansion (19) is likely to have a finite convergence radius for any fixed q, just as the source term expansion on the right hand side is convergent in (18) for $\varepsilon|q| < \pi$.

Although (31) is not convergent, its optimal truncation can give better and better approximation to a certain solution as $|q|$ is increasing, for example along a constant $\arg q$ or constant $\operatorname{Im} q$ line in the half plane $\operatorname{Re} q > 0$. In this case (31) can be considered as a valid boundary condition that selects the right decaying $v_0^{(-)}$ solution. The polynomials v_n for $n > 1$ obtained from the outer ε expansion also can be considered as boundary conditions for the n-th order inner equations, determining the unique solutions $v_n^{(-)}$ which are not oscillating on the right hand side. For this simple linear problem they happen to agree with the actual polynomial solutions everywhere, not just for large $|q|$ and $\operatorname{Re} q > 0$.

2.7 Borel summation

The leading order inner equation is generally nonlinear, and usually no exact solutions are known. We present a general method for studying its solution, which can be applied for more complicated systems as well. The Borel summation approach we discuss in this subsection has been applied first by Pomeau, Ramani and Grammaticos [11] for the fifth-order Korteweg-de Vries equation.

The complex extension of the outer expansion has provided the $1/q$ series approximation (31) to the solution of the inner equation (21). The coefficients in the series (31) increase very fast, actually, they are factorials in this case. To construct this expansion to arbitrary order, we can directly search the solution in the form

$$v_0 = \sum_{n=1}^{\infty} \frac{b_n}{q^{2n}} \ , \tag{32}$$

where b_n are constants. Substituting into equation (21) and setting the coefficients of the various powers of q to zero we obtain that $b_1 = -1$ and $b_n = -(2n-1)(2n-2)b_{n-1}$. This yields $b_n = (-1)^n(2n-1)!$,

$$v_0 = \sum_{n=1}^{\infty} \frac{(-1)^n(2n-1)!}{q^{2n}} \ . \tag{33}$$

The factorial divergence shows that the series cannot have any finite convergence radius.

Dividing each coefficient $b_n = (-1)^n(2n-1)!$ in the divergent sum (33) by $(2n)!$ we obtain a series with a finite radius of convergence. This Borel transformed series in our case is defined as

$$B(s) = \sum_{n=1}^{\infty} \frac{(-1)^n}{2n} s^{2n} \ , \tag{34}$$

which is convergent for $|s| < 1$. It can be summed as

$$B(s) = -\frac{1}{2}\log(1+s^2) = -\frac{1}{2}\left[\log(1+is) + \log(1-is)\right] \ . \tag{35}$$

The Borel sum of the series (33) is defined as the integral

$$v_0^{[B]}(q) = \int_\Gamma \exp(-t) B\left(\frac{t}{q}\right) \mathrm{d}t \ , \tag{36}$$

where the contour Γ runs from $t = 0$ to infinity in the half plane $t > 0$, along a path for which $\mathrm{Re}\, t \to \infty$. The path can be specified as a complex function of a real variable τ as $\Gamma \equiv \{t(\tau) : 0 \le \tau < \infty\}$. Choosing two paths going to infinity in different directions, the result of the integrals will be the same, provided the two contours are not separated by a branch cut or pole.

Substituting (34) and exchanging the order of the integral and summation (see e.g. [132]), we obtain

$$v_0^{[B]}(q) \sim \sum_{n=1}^{\infty} \frac{(-1)^n}{2n} \frac{1}{q^{2n}} \int_0^{\infty} \exp(-\tau)\tau^{2n} \mathrm{d}\tau = \sum_{n=1}^{\infty} \frac{(-1)^n(2n-1)!}{q^{2n}} \ , \tag{37}$$

where $\sim$ indicates that the divergent series is asymptotic to the function $v_0^{[B]}(q)$. It also follows that if the integral in (36) exists, the function $v_0^{[B]}(q)$ will be a solution of the inner differential equation (21).

The contour of the integral in

$$v_0^{[B]}(q) = -\frac{1}{2}\int_\Gamma \exp(-t)\log\left(1+\frac{t^2}{q^2}\right)\mathrm{d}t \tag{38}$$

can be taken simply the positive half of the real t line when $\mathrm{Re}\, q > 0$, but it should move out to complex t plane when $\mathrm{Re}\, q \le 0$, as we will see shorty. Taking the real path for t, it can be shown that as $|q| \to \infty$ along fixed $-\frac{\pi}{2} < \arg q < \frac{\pi}{2}$ lines, the integral tends to zero as $-1/q^2$ (see e.g. Sec. 6.4 of [132]), hence the function has no asymptotic oscillations. Not surprisingly, for positive real q the integral (38) can be evaluated exactly, obtaining the right decaying solution $v_0^{(-)}(q)$ already given in (22). Instead of using that expression, we proceed by a method that can be applied even when no result for the integral is known.

Fixing q, the integrand in (38) has logarithmic branch points at $t = \pm iq$. The usual branch cuts associated to the principal branch are along the lines $t = \pm iqa$, for $1 < a < \infty$. In Fig. 8 we show how the branch cuts are located on the complex t plane as q is rotated

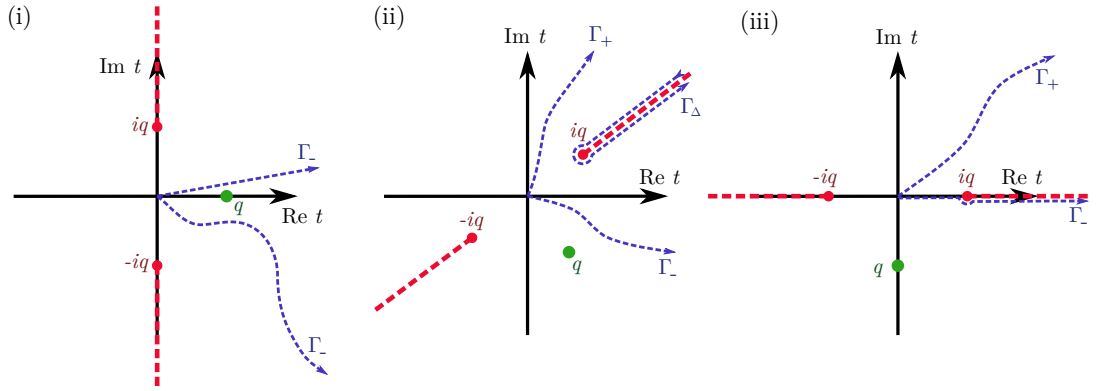

Figure 8: The red dashed lines show the branch cuts of the integrand for various values of q. In the left drawing q is positive real, in the middle $\mathrm{Re}\, q > 0$, $\mathrm{Im}\, q < 0$, and on the right q is purely imaginary. The integral along any of blue curves denoted by Γ_- gives the right decaying solution $v_0^{(-)}(q)$, while integrating along Γ_+ yields the left decaying $v_0^{(+)}(q)$. The difference can be obtained by integrating around the branch cut from infinity and back along Γ_Δ. For purely imaginary q one has to integrate below the cut to obtain a smooth extension of $v_0^{(-)}(q)$.

around in a circle. For positive real q the branch cuts are on the imaginary t axis, and because of the exponential decay of the integrand, any contour for which $\mathrm{Re}\, t \to \infty$ gives the same integral, $v_0^{[B]}(q) = v_0^{(-)}(q)$. In particular, one can choose any straight line starting from the center with $-\frac{\pi}{2} < \arg t < \frac{\pi}{2}$ constant. As q moves down into the quadrant $\mathrm{Re}\, q > 0$, $\mathrm{Im}\, q < 0$, the branch cut is also rotated, and then only contours in the region $-\frac{\pi}{2} < \arg t < \arg q + \frac{\pi}{2}$ give the solution $v_0^{(-)}(q)$. Integrating at the other side of the branch cut, for $\arg q + \frac{\pi}{2} < \arg t < \frac{\pi}{2}$

one would obtain the left decaying solution, $v_0^{[B]}(q) = v_0^{(+)}(q) = v_0^{(-)}(-q)$. The difference of the two solutions can be obtained by integrating along the left hand side of the branch cut from infinity to the branch point $t = iq$ and back to infinity on the other side. Since the difference of the values of the logarithm at the two sides of the branch cut is exactly $2i\pi$, taking into account the factor $-1/2$ in (38), we have to integrate $-i\pi \exp(-t)$ from iq to infinity, yielding $v_0^{(+)}(q) - v_0^{(-)}(q) = i\pi \exp(-iq)$, in agreement with (23) for $\mathrm{Im}\, q < 0$.

When q is exactly on the lower half of the imaginary axis, the branch cut has moved to the real axis for $t > iq$. For continuity, to obtain $v_0^{(-)}(q)$, the contour has to go around the branch point from below, and go to infinity along the rotated branch cut, approaching it from below. Since the singularity is only logarithmic, shrinking the half circle to the branch point gives no contribution to the integral. For $t > iq$ the imaginary part of the integrand is exactly $\pi \exp(-t)$. Integrating one gets

$$\mathrm{Im}\, v_0^{[B]}(q) = -\frac{1}{2}\int_{iq}^{\infty} \exp(-\tau)\pi \mathrm{d}\tau = -\frac{\pi}{2}\exp(-iq) \quad \text{for} \quad \mathrm{Re}\, q = 0 \text{ and } \mathrm{Im}\, q < 0\ , \qquad (39)$$

in agreement with (25). Note that this imaginary part is the only information we need for the calculation of the tail-amplitude on the real x axis. Now we have obtained it as a very simple integral, without actually calculating the full complex valued solution $v_0^{(-)}(q)$ of the inner equation on the complex q plane.

Rotating q further, into the quadrant $\mathrm{Re}\, q < 0$, $\mathrm{Im}\, q < 0$, if we use the principal branch cut of the logarithm, the contour of the integration has to remain in the region $-\frac{\pi}{2} < \arg t < \arg q + \frac{\pi}{2}$ in order to give the analytic extension of the right decaying solution, $v_0^{[B]}(q) = v_0^{(-)}(q)$, as we show it in Fig. 9. Any contour in the larger region $\arg q + \frac{\pi}{2} < \arg t < \frac{\pi}{2}$, in

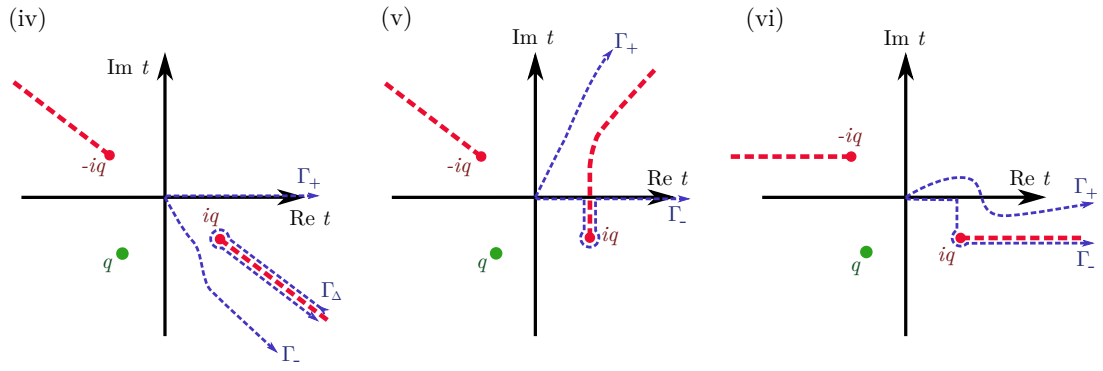

Figure 9: Different ways of choosing the branch cuts when q is in the quadrant $\mathrm{Re}\, q < 0$, $\mathrm{Im}\, q < 0$.

particular along the real t line, would yield the left decaying solution $v_0^{[B]}(q) = v_0^{(+)}(q)$, which

cannot be matched smoothly with $v_0^{(-)}(q)$ at the imaginary q axis. Even for this choice of q it is possible to obtain $v_0^{(-)}(q)$ by integrating along a path which goes out to infinity along the real t line, but the contour must go down to the singularity at $t = iq$ and come back to the real axis on the other side of a rotated version of the branch cut, as it is shown in the middle drawing of Fig. 9 (see also Fig. 4.6 of [5]). Choosing the branch cut of the logarithm in a nonstandard direction, or even making it not a straight line, the integral along a contour Γ_Δ coming from infinity and going back on the other side remains invariant. In the right drawing the integral path is chosen parallelly to the real t axis, similarly to Fig. 2 of [11]. In case of the figure in [11] the singularity is above the real axis because left decaying solutions are considered.

2.8 Laplace transform

The integration by parts and Laplace transform method presented in this subsection has been applied first by Grimshaw and Joshi in [140] for the inner equation of the fifth-order Korteweg-de Vries problem. Since $B(0) = 0$, one can apply integration by parts in (36) to obtain

$$v_0^{[B]}(q) = \frac{1}{q}\int_\Gamma \exp(-t)B'\left(\frac{t}{q}\right)\mathrm{d}t = \int_\Gamma \exp(-t)\frac{-t}{q^2+t^2}\mathrm{d}t \ . \tag{40}$$

The integrand has now simple poles at $t = \pm iq$ and no branch cuts, allowing the use of the residue theorem, hence leading to a somewhat simpler analysis than in the previous subsection. Changing variables by introducing $s = t/q$, one can see that this integral is just the Laplace transform of $B'(s)$,

$$v_0^{[B]}(q) = \int_\gamma \exp(-qs)B'(s)\mathrm{d}s \ , \tag{41}$$

where

$$B'(s) = \frac{-s}{1+s^2} \ , \tag{42}$$

and the parametrization of the contour γ is related to that of Γ as $s(\tau) = t(\tau)/q$. The expression (42) for $B'(s)$ can be obtained directly, by substituting the Laplace transform integral (41) into the inner equation (21), without using the Borel summation procedure from the previous subsection.

The contour γ in (41) can be any path going from the center $s = 0$ to infinity, along which $\mathrm{Re}(qs) \to \infty$. The result of the integral will depend on how the contour is situated with respect to the poles at $s = \pm i$. If q is real and positive, the contour naturally runs in the $\mathrm{Re}\, s > 0$ half plane (at least asymptotically), and the Laplace transform of the function $B'(s)$ is given by the right decaying solution $v_0^{(-)}$ presented in equation (22). If q is moved down to the quadrant $\mathrm{Re}\, q > 0$, $\mathrm{Im}\, q < 0$, the contour should run in the half-plane $\mathrm{Re}(qs) > 0$, as shown in Fig. 10. If γ is on the right side of the pole at $s = i$ then the integral gives $v_0^{(-)}$,

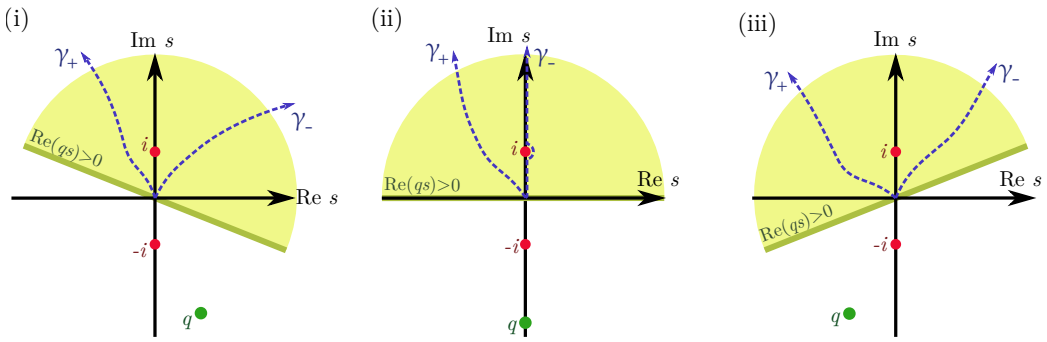

Figure 10: Rotation of the half plane in which the contour γ should tend to infinity, as q is moved. The integral along the contours denoted by γ_- gives the right decaying solution $v_0^{(-)}(q)$, while integrating along the curves γ_+ yields the left decaying $v_0^{(+)}(q)$.

at the other side one gets $v_0^{(+)}$ (see also Fig. 1 of [140]). When q is rotated to the quadrant $\mathrm{Re}\, q < 0$, $\mathrm{Im}\, q < 0$, it is not possible anymore to use the trivial straight contour $\mathrm{Im}\, s = 0$, $\mathrm{Re}\, s \leq 0$ to obtain a finite value for the Laplace transform.

For the calculation of the tail-amplitude of the original function u on the real x axis we only need to know the imaginary part of $v_0^{(-)}$ along the lower half of the imaginary q axis. In this case the most natural contour to obtain $v_0^{(-)}$ is to use the upper half of the imaginary s axis. However, the contour should avoid the pole at $s = i$, going around it from the right side, as shown in the middle drawing of Fig. 10. Parametrizing the straight sections as $s = i\tau$, the integrand is purely real along the imaginary s axis, hence only the small half-circle can give contribution to the imaginary part of the result. Since reflection with respect to the imaginary s axis corresponds to -1 times complex conjugation, the integral along the half-circle is exactly the half of the full circle integral, which can be obtained easily by the residue theorem. The residue at $s = i$ is $-\exp(-iq)/2$, hence the imaginary part of the integral gives

$$\mathrm{Im}\, v_0^{[B]}(q) = -\frac{\pi}{2}\exp(-iq) \quad \text{for} \quad \mathrm{Re}\, q = 0 \text{ and } \mathrm{Im}\, q < 0\ , \tag{43}$$

in agreement with (25) and (39). Now we can use the earlier presented reasoning about the difference of the symmetric minimal tail and asymmetric right decaying solutions to obtain the leading order expression (28) for the minimal tail α_m.

Considering more complicated problems, where the leading order inner equation is nonlinear, one obtains integral equations for $B'(s)$ when looking for the solution in terms of the Laplace transform (41). However, the coefficients b_n of the asymptotic series expansion solution (32) for v_0 can be obtained even in those cases. The calculation of this expansion

is necessary anyway, since it provides the boundary condition for the inner equation. Since the Laplace transform of s^n is $n!q^{-n-1}$, it follows that the expansion of the function $B'(s)$ is

$$B'(s) = \sum_{n=0}^{\infty} \frac{b_{n+1}}{(2n+1)!} s^{2n+1} \ . \tag{44}$$

This sum is generally convergent, in the same way as the Borel transformed series (34) defined earlier. For our linear problem, according to (33) we have $b_n = (-1)^n(2n-1)!$, hence

$$B'(s) = \sum_{n=0}^{\infty} (-1)^{n+1} s^{2n+1} = \frac{-s}{1+s^2} \tag{45}$$

in agreement with (42). Even in those cases when there is no simple general expression for b_n, it turns out that only the large n behavior of the coefficients is important for the calculation of the imaginary part of the inner solution along the imaginary q axis, which is directly related to the minimal tail-amplitude of the original problem.

3 Stationary solutions of the fifth-order KdV equation

The Korteweg-de Vries (KdV) equation modified by a fifth derivative term (fKdV equation) can be written as

$$\varepsilon^2 \frac{\partial^5 u}{\partial y^5} + \frac{\partial^3 u}{\partial y^3} + 6u\frac{\partial u}{\partial y} + \frac{\partial u}{\partial t} = 0 \ , \tag{46}$$

where u is a function of the time t and spatial coordinate y, and ε is a small non-negative parameter. It has been also named as Kawahara equation [141, 142], originally obtained by studying magnetohydrodynamical waves in plasma physics. The fKdV equation in a hydrodynamical context has been derived by Hunter and Scheurle [1], considering small amplitude, long waves in shallow water. Adding the fifth derivative term, the well known solitary wave solutions of the KdV equation are deformed into almost localized objects that are losing continuously some of their energy by radiating small amplitude waves in the direction of propagation [2]. It has been proven that the spatially localized solitary traveling wave solutions of the KdV equation cease to exist when a fifth-order dispersion term is added [143, 144].

We consider stationary solutions traveling to the right with speed $c > 0$, so that u is time independent when $x = y - ct$ is used as a comoving spatial coordinate. The obtained ordinary differential equation can be integrated once, yielding the stationary fKdV equation

$$\varepsilon^2 \frac{\mathrm{d}^4 u}{\mathrm{d}x^4} + \frac{\mathrm{d}^2 u}{\mathrm{d}x^2} + 3u^2 - cu = 0 \ . \tag{47}$$

For $\varepsilon = 0$ this reduces to the familiar stationary KdV equation, which for $c > 0$ has the solitary wave (or soliton) solutions $u = \frac{c}{2}\mathrm{sech}^2\left(\frac{\sqrt{c}}{2}x\right)$. Since the amplitude is always positive, there are only elevation waves in the $\varepsilon = 0$ case. The KdV equation can be obtained from the fluid dynamical equations when considering surface water waves for shallow depth and long wavelength. Long wavelength sinusoidal waves move to the right with speed $c_s = \sqrt{hg}$, where h is the average water depth and g is the gravity of Earth. The coordinate system used in (46) is already moving to the right with this speed. Solitary waves move with even higher physical speed, $c_{ph} \sim c_s + c$, hence they are supercritical.

The KdV equation can also describe shallow water waves when there is a nonzero surface tension σ. In that case the equation can be written as $\left(\frac{1}{3} - B\right)\frac{\mathrm{d}^2 u}{\mathrm{d}x^2} + 3u^2 - cu = 0$ where $B = \dfrac{\sigma}{\rho g h^2}$ is the Bond number and ρ is the fluid density. The signature of the second derivative term changes when $B = \frac{1}{3}$. For $B > \frac{1}{3}$ there are depression solitary waves with subcritical speed and no oscillating tail. For $B \approx \frac{1}{3}$ the influence of the second derivative term becomes small, hence a previously neglected fourth derivative term appears in the equation. Assuming that B is close to but below $\frac{1}{3}$ one obtains the stationary fKdV equation (47). The main problem we would like to address in this section is how the soliton solutions change when there is a fourth derivative term with a small factor $\varepsilon > 0$.

Equation (47) remains invariant under the rescalings

$$u = \xi^2 \bar{u} \ , \quad x = \frac{1}{\xi} \bar{x} \ , \quad c = \xi^2 \bar{c} \ , \quad \varepsilon = \frac{1}{\xi} \bar{\varepsilon} \ , \tag{48}$$

for any $\xi > 0$ constant. Note that $\varepsilon^2 c$ remains invariant. It is possible to use this freedom to scale either of the constants ε or c to some given positive value. For example, it is sufficient to perform numerical simulations only for $c = 1$.

Outside the core in the tail region u is small, so the quadratic term can be neglected in (47). Since we expect asymptotic oscillations with spatial frequency increasing when $\varepsilon \to 0$, we search for the tail in the form

$$u = \alpha \sin\left(\frac{kx}{\varepsilon} - \delta\right) \ , \tag{49}$$

where $\frac{k}{\varepsilon}$ is the wave number, and the amplitude α and phase δ may be different on the two sides of the core. From the linearized equation follows that $k^4 - k^2 - c\varepsilon^2 = 0$. This equation has two real and two imaginary roots. In the following we take k as the positive real root,

$$k = \sqrt{\frac{1}{2}\left(1 + \sqrt{1 + 4c\varepsilon^2}\right)} = 1 + \frac{c}{2}\varepsilon^2 - \frac{5c^2}{8}\varepsilon^4 + \dots \ . \tag{50}$$

It can be seen that for small ε the wavelength is proportional to ε.

Instead of calculating the imaginary roots, in order to agree with the notations in [140], we directly search for the exponentially decaying or blowup solutions in the form $u = \beta \exp(\pm 2\gamma x)$ with $\gamma > 0$. From the linearized equation we get

$$c = 4\gamma^2(1 + 4\gamma^2\varepsilon^2) \ . \tag{51}$$

The constant γ expressed in terms of ε and c can be written as

$$\gamma = \sqrt{\frac{1}{8\varepsilon^2}\left(-1 + \sqrt{1 + 4c\varepsilon^2}\right)} = \frac{\sqrt{c}}{2}\left(1 - \frac{c}{2}\varepsilon^2 + \frac{7c^2}{8}\varepsilon^8 - \dots\right) \ . \tag{52}$$

The relation between k and γ is

$$k^2 = 1 + 4\gamma^2\varepsilon^2 \ . \tag{53}$$

Comparing with (51) also follows that $c = 4\gamma^2 k^2$.

A conserved quantity can be defined as

$$F = -\frac{1}{2}cu^2 + 2u^3 + u\frac{\mathrm{d}^2 u}{\mathrm{d}x^2} - \frac{1}{2}\left(\frac{\mathrm{d}u}{\mathrm{d}x}\right)^2 + \varepsilon^2\left[u\frac{\mathrm{d}^4 u}{\mathrm{d}x^4} - \frac{\mathrm{d}u}{\mathrm{d}x}\frac{\mathrm{d}^3 u}{\mathrm{d}x^3} + \frac{1}{2}\left(\frac{\mathrm{d}^2 u}{\mathrm{d}x^2}\right)^2\right] \ , \tag{54}$$

which can be interpreted as an energy flux [2, 140]. Using (47) it is easy to check that $\frac{\mathrm{d}F}{\mathrm{d}x} = 0$, so F is constant. Substituting the form (49) of the tail, to leading order the energy

flux turns out to be $F = \alpha^2/(2\varepsilon^2)$. It follows that the amplitude of the tail at the two sides of the core must necessarily agree, at least for small amplitudes. Numerical simulations also support the conjecture that solutions which have a single large core and small tails in both the positive and the negative directions are necessarily reflection symmetric, $u(-x) = u(x)$. An important consequence is that there is no solution for which there is a small tail in one direction and exponential decay without any tail in the other direction. We have seen such solutions in Figs. 1 and 2 in case of the linear model problem in Section 2. Our numerical simulations for the fKdV problem show that for sufficiently small ε there is a solution u_- which decays exponentially to zero for $x > 0$, has a core region similar to the KdV solitary wave, but continuing further to the negative direction the solution blows up at some finite $x < 0$, before a standing wave tail could appear. This solution is unique up to translations in x. We show a few such solutions in Fig. 11.

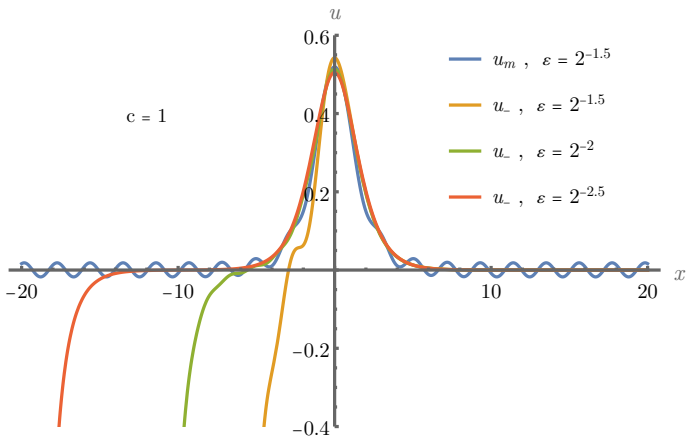

Figure 11: For $c = 1$, the yellow, green and red curves show the asymmetric right decaying solutions u_- for three different values of ε. These solutions run into a singularity at some value of $x < 0$, which moves farther from the center as ε decreases. The blue curve shows the minimal tail symmetric solution $u_{\rm m}$ for the largest ε value. Since the tail-amplitude decreases exponentially with decreasing ε, the symmetric solutions are not plotted for the smaller ε values. The green and yellow curves are below the red one for $x > 2$.

It appears to be a plausible that all solutions that can be defined for all $-\infty < x < \infty$ are symmetric, $u(-x) = u(x)$. It has been shown[145, 146] that for sufficiently small fixed ε there exists a one-parameter family of symmetric solutions, parametrized by the phase δ of the small-amplitude tail. Physically the most important is the solution $u_{\rm m}$ that has the minimal tail-amplitude $\alpha \equiv \alpha_{\rm m}$, belonging to the phase $\delta = \delta_{\rm m}$. This $\alpha_{\rm m}$ agrees with the amplitude of the minimal outgoing radiating tail in the dynamical time dependent case, hence $\alpha_{\rm m}$ is a crucial quantity that can be used to determine the energy loss rate of the system. The amplitude $\alpha_{\rm m}$ always larger than zero when $\varepsilon > 0$.

Our numerical solutions have been obtained by a high precision numerical code that is

based on spectral methods [147, 148] and uses arbitrary digits precision arithmetics [149, 150, 151]. The details of the method can be found in our papers [6, 7]. The present review is focused on the analytic and perturbational methods that can be used to describe solutions with small amplitude tails. The main difficulty of the problem is the exponentially fast decrease of the tail-amplitude when ε becomes smaller. In Fig. 12 we show logarithmic plots

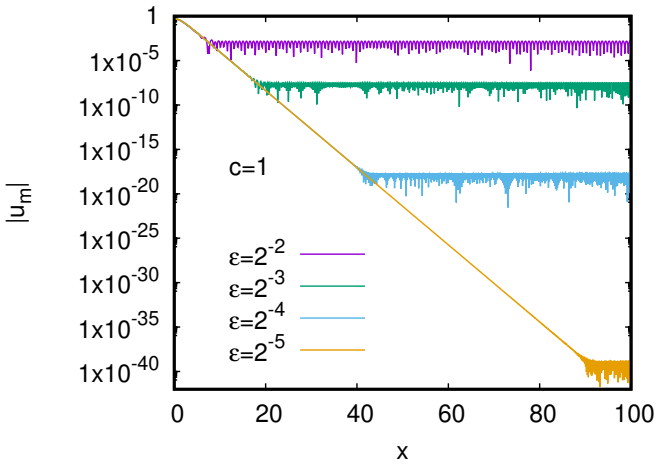

Figure 12: Logarithmic plot of the absolute value of the minimal tail symmetric solution $u_{\rm m}$ for decreasing values of ε. The downward spikes correspond to zero crossings. They would go all the way down for higher plotting resolution.

of $|u_{\rm m}|$ for various values of ε. The core region, with an exponential decay, remains similar for all cases, but the tail oscillations start at larger x values for smaller ε. In Table 2 we list

ε	$\alpha_{\rm m}$	$\delta_{\rm m}$	$\frac{{\rm d}^3}{{\rm d}x^3}u_-(0)$
2^{-1}	$4.8\cdot 10^{-2}$	1.2	$7.10760589389\cdot 10^{-1}$
2^{-2}	$1.53\cdot 10^{-3}$	0.749	$8.11499816225\cdot 10^{-2}$
2^{-3}	$3.2525301\cdot 10^{-8}$	0.37253582	$1.62487857959\cdot 10^{-5}$
2^{-4}	$1.94383743304\cdot 10^{-18}$	0.187147747984	$7.92099610003\cdot 10^{-15}$
2^{-5}	$1.27243717968\cdot 10^{-39}$	0.0937046561766	$4.16436578363\cdot 10^{-35}$
2^{-6}	$1.17039547447\cdot 10^{-82}$	0.0468692914439	$3.06718215011\cdot 10^{-77}$
2^{-7}	$2.29646599329\cdot 10^{-169}$	0.0234367851656	$4.81567051778\cdot 10^{-163}$
2^{-8}	$2.12961253593\cdot 10^{-343}$	0.0117186606062	$3.57282878973\cdot 10^{-336}$
2^{-9}	$4.49453680829\cdot 10^{-692}$	0.00585936382454	$6.03243642172\cdot 10^{-684}$

Table 2: Numerically calculated values of the minimal tail-amplitude $\alpha_{\rm m}$ and the corresponding phase $\delta_{\rm m}$ for the case $c=1$. The last column gives the central third derivative of the asymmetric solution u_-.

high precision numerical results for the minimal tail-amplitude and phase. The asymmetry of the solution u_- can be most naturally described by the third derivative of the function at

the point where it is maximal, i.e. where its first derivative vanishes. This third derivative is listed in the last column of Table 2. The extremely small numbers show the necessity of exceptionally high precision spectral numerical methods. From the exponential decrease also follows that standard perturbational methods cannot be used for the determination of the tail-amplitude.

3.1 Outer expansion

Assuming that ε is small, we search for solutions of the stationary fKdV equation (47) in a power series expansion form

$$u = \sum_{n=0}^{\infty} u_n \varepsilon^{2n} \,, \tag{55}$$

where u_n are ε independent functions of x. Since the fKdV equation also contains a second parameter, c, the most obvious assumption would be to assume that c is independent of ε. However, it turns out that the expansion procedure becomes technically significantly simpler if one uses a certain ε dependence in c, namely the form given by (51), with the assumption that γ is ε independent. With this choice all coefficient functions u_n turn out to be polynomials in $\mathrm{sech}^2(\gamma x)$. Otherwise, there would also appear terms containing $x\sinh(\gamma x)$ type factors. This would not only mean much longer expressions for u_n, but also slower decay for large $|x|$. The assumption that γ is constant actually means that the decay rate of the core is ε independent. We are not losing any solutions of (47) by this choice, since we have still two parameters (ε, γ) instead of (ε, c).

Substituting the expansion (55) into the stationary fKdV equation, the vanishing of the ε independent part gives the KdV equation

$$\frac{\mathrm{d}^2 u_0}{\mathrm{d}x^2} + 3u_0^2 - 4\gamma^2 u_0 = 0 \,, \tag{56}$$

which has the well-known solitary wave solution $u_0 = 2\gamma^2 \,\mathrm{sech}^2(\gamma x)$. For a given γ this is the unique localized solution when symmetry with respect to $x = 0$ is assumed. For $n > 0$, the vanishing of the coefficient of ε^{2n} yields

$$\frac{\mathrm{d}^4 u_{n-1}}{\mathrm{d}x^4} + \frac{\mathrm{d}^2 u_n}{\mathrm{d}x^2} + 3\sum_{j=0}^{n} u_j u_{n-j} - 4\gamma^2 u_n - 16\gamma^4 u_{n-1} = 0 \,. \tag{57}$$

Assuming that the functions are known up to order $n-1$, this equation can be considered as a linear inhomogeneous differential equation for determining u_n,

$$\frac{\mathrm{d}^2 u_n}{\mathrm{d}x^2} + 6u_0 u_n - 4\gamma^2 u_n = R_n \,, \tag{58}$$

where

$$R_n = -\frac{\mathrm{d}^4 u_{n-1}}{\mathrm{d}x^4} - 3\sum_{j=1}^{n-1} u_j u_{n-j} + 16\gamma^4 u_{n-1} \,. \tag{59}$$

The homogeneous problem with $R_n = 0$ has two independent solutions. The first solution is $\frac{\mathrm{d}u_0}{\mathrm{d}x}$, which is antisymmetric. The other solution blows up exponentially at infinity. This shows that the inhomogeneous equation has a unique symmetric and localized solution.

Proceeding order by order in n, it turns out that both R_n and u_n can be written as finite sums of powers of $\mathrm{sech}^2(\gamma x)$,

$$R_n = \gamma^{2n+4} \sum_{j=1}^{n+2} R_{n,j} \, \mathrm{sech}^{2j}(\gamma x) \ , \tag{60}$$

$$u_n = \gamma^{2n+2} \sum_{j=1}^{n+1} u_{n,j} \, \mathrm{sech}^{2j}(\gamma x) \ . \tag{61}$$

The powers of γ are included in order to make $R_{n,j}$ and $u_{n,j}$ rational numbers without γ factors. At leading order we have already seen that $u_{0,1} = 2$. Using identities for the derivatives of $\mathrm{sech}^j x$, from (59) follows that

$$\begin{aligned} R_{n,j} = & -16j^4 u_{n-1,j} + 8(j-1)(2j-1)(2j^2-2j+1)u_{n-1,j-1} \\ & - (2j-4)(2j-3)(2j-2)(2j-1)u_{n-1,j-2} \\ & - 3\sum_{l=1}^{n-1}\sum_{m=1}^{l+1} u_{l,m}u_{n-l,j-m} + 16u_{n-1,j} \ . \end{aligned} \tag{62}$$

Here we substitute zero for every $u_{n,j}$ when $j < 1$ or $j > n+1$. If the coefficients $u_{n,j}$ are known up to order $n-1$ in the first index, then (62) can be used to calculate the source term R_n in (58). It turns out that $R_{n,1} = 0$ for all n, which is necessary for the consistency of the method.

Substituting the expansions of R_n and u_n into (58), it follows that for $2 \le j \le n+1$

$$4(j^2-1)u_{n,j} + [12 - (2j-1)(2j-2)] \, u_{n,j-1} = R_{n,j} \ . \tag{63}$$

The equation for $j = n+2$ is

$$[12 - (2n+3)(2n+2)] \, u_{n,n+1} = R_{n,n+2} \ , \tag{64}$$

while for $j = 1$ we get $R_{n,1} = 0$. If all $R_{n,j}$ coefficients are already known at order n, then $u_{n,n+1}$ can be calculated from (64). After this, all $u_{n,j-1}$ can be obtained one by one in decreasing order in j using (63). This algorithm can be implemented using any algebraic manipulation software. A Mathematica notebook (wkb.nb) is attached as a Supplemental Material to our paper [7], which contains an implementation that can be used to calculate u_n up to order $n = 50$ in a few minutes. Results up to $n = 4$ are listed in Table 3.

All coefficient functions u_n in the expansion (55) are decaying exponentially when $x \to \pm\infty$, hence this approximation cannot describe any oscillating tails. This is consistent

$n\downarrow\ j\rightarrow$	1	2	3	4	5
0	2	-	-	-	-
1	-20	30	-	-	-
2	60	-930	930	-	-
3	-2472	21036	-66216	49662	-
4	$-\frac{240780}{7}$	$-\frac{3177030}{7}$	$\frac{23319570}{7}$	$-\frac{48197250}{7}$	$\frac{28918350}{7}$

Table 3: Values of $u_{n,j}$ up to order $n = 4$.

with the observation that the tail-amplitude decreases faster than any power of ε, so the appearance of the tail is a beyond all orders small effect. Since the expansion cannot converge to the true solution with a tail, it is not surprising that the sum in (55) is not convergent. However, it is a series which is asymptotic to some solution u. This solution can be either u_- or $u_{\rm m}$, since their difference is exponentially small, assuming that we are not considering the blow-up region of u_- on the left side of the core.

The error of the Nth order ε expansion approximation with respect to the precise numerically calculated minimal tail solution can be defined as

$$\Delta u_N = u_{\rm m} - \sum_{n=0}^{N} u_n \varepsilon^{2n} \ . \tag{65}$$

In Fig. 13 the functions Δu_N are plotted for three values of N for which the error is the

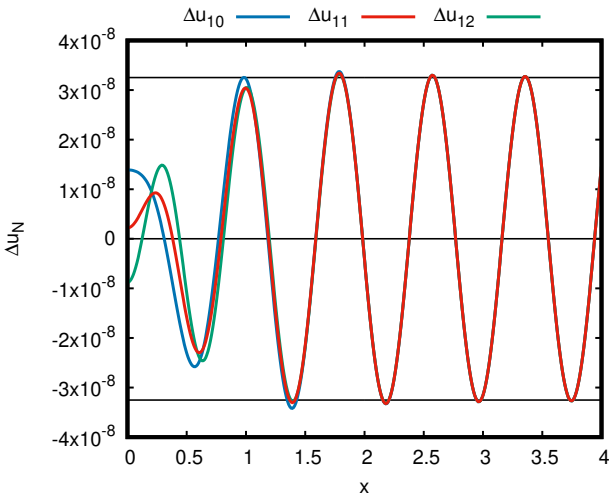

Figure 13: Difference of the Nth order approximation of the outer expansion (55) from the minimal tail symmetric solution $u_{\rm m}$ for $\varepsilon = 2^{-3}$ and $c = 1$. The black horizontal lines show the tail-amplitude $\alpha_m \approx 3.25 \cdot 10^{-8}$.

smallest for the case $\varepsilon = 2^{-3}$ and $c = 1$. For this ε value the optimal truncation is at $N_{\rm opt} = 11$, corresponding to the red curve. Since all coefficient functions u_n decay exponentially,

outside the core region the difference should agree with the oscillating tail. The values of $N_{\rm opt}$ for various ε parameters are listed in Table 4. For small ε values the optimal truncation

ε	2^{-1}	2^{-2}	2^{-3}	2^{-4}	2^{-5}	2^{-6}	2^{-7}	2^{-8}	2^{-9}
$N_{\rm opt}$	1	4	11	23	49	99	199	400	802

Table 4: Order of optimal truncation for decreasing ε values when $c = 1$.

behaves as $N_{\rm opt} \sim 1.56/(\varepsilon\sqrt{c})$.

The spectral numerical calculation of the solutions u_- or $u_{\rm m}$ can be made significantly more efficient by calculating first analytically the optimal approximation $u_{N_{\rm opt}}$, then numerically solving the nonlinear differential equation for the difference $\Delta u_{N_{\rm opt}} = u - u_{N_{\rm opt}}$ (see [7]). Then functions remain as small as the tail even in the central region. However, high frequency oscillations remain, so it is still necessary to use more than 16 digits arithmetics.

3.2 Linearized solution

For given ε and c the minimal tail symmetric solution $u_{\rm m}$ is unique, and the right decaying asymmetric solution u_- is also unique if we assume that the maximum is at $x = 0$. In Fig. 14 we plot the difference of these two solutions, $\Delta u = u_{\rm m} - u_-$, for a certain choice of parameters.

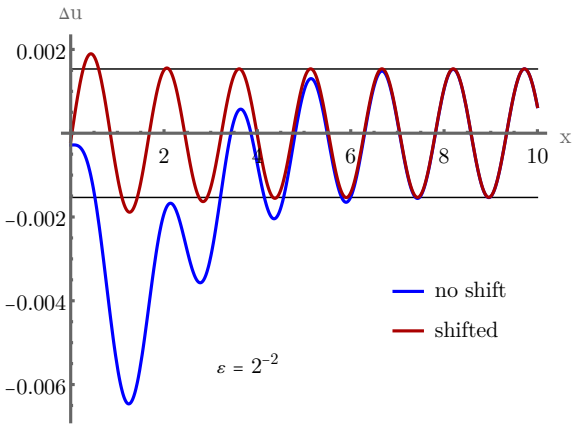

Figure 14: Plot of the difference $\Delta u = u_{\rm m} - u_-$ for $\varepsilon = 2^{-2}$ and $c = 1$.

The difference is already much smaller than the core amplitude, but if u_- is shifted in x to the left by 0.022, the difference becomes quite similar to the sine function, with amplitude agreeing with the tail-amplitude of $u_{\rm m}$. In the following we show that Δu can be calculated very precisely using the WKB (Wentzel–Kramers–Brillouin) method. This step was trivial for the model problem in Sec. 2, since the system was linear, and the homogeneous solutions have been simply the sine and cosine functions.

We linearize the stationary fKdV equation (47) around some solution u by substituting $u \to u + w$ and dropping the quadratic term,

$$\varepsilon^2 \frac{\mathrm{d}^4 w}{\mathrm{d}x^4} + \frac{\mathrm{d}^2 w}{\mathrm{d}x^2} + 6uw - cw = 0 \ . \tag{66}$$

The only property of u we use is that it can be approximated well by the asymptotic expansion (55). For example, it may be the solution u_{m} or u_-. We assume that w is exponentially small in terms of ε, hence the linear approximation is well justified, and exponentially small contributions can be neglected in the background solution u. Here we also substitute c from (51), and assume that γ is independent of ε. One of the solutions of equation (66) is $w = \frac{\mathrm{d}u}{\mathrm{d}x}$, which corresponds to a small shift of the original solution.

Since in the asymptotic region there are high frequency oscillations, we use the WKB method to search for other bounded solutions of (66). We first substitute $w = \beta_c \exp A$, where A is a function of x, and β_c is a complex constant. Then we expand A in powers of ε, starting with an ε^{-1} term,

$$A = \sum_{n=-1}^{\infty} A_n \varepsilon^n \ , \tag{67}$$

and solve order by order in ε. Since A_n appear in the equations only in differentiated form, there is additive complex scalar freedom in all A_n, which can be absorbed into β_c. Proceeding order by order in ε one can solve the resulting equations for A_n. Each odd indexed function contains a term proportional to x, which can be absorbed into the ε^{-1} term by defining the odd indexed $\tilde{A}_n$ functions as

$$A_{2n-1} = i\tilde{A}_{2n-1} - ix\gamma^{2n} \frac{(-1)^{n+1}(2n)!}{(2n-1)(n!)^2} \ . \tag{68}$$

The general solution of the linearized problem that takes real values for real x can be written as

$$w = \beta \exp\left(\sum_{\substack{n=2 \\ \text{even}}}^{\infty} A_n \varepsilon^n \right) \sin\left(\frac{kx}{\varepsilon} - \delta_w - \sum_{\substack{n=1 \\ \text{odd}}}^{\infty} \tilde{A}_n \varepsilon^n \right) \ . \tag{69}$$

Here β and δ_w are real constants with arbitrary ε dependence, and k is given by (53). Note that the leading order behavior for very small ε is simply $w = \beta \sin\left(\frac{x}{\varepsilon} - \delta_w\right)$, just as if we would linearize around the trivial $u = 0$ solution.

All coefficient functions in (69) are real. At leading orders we obtain $A_{-1} = -ix$ and

$A_0 = 0$, which shows that $\tilde{A}_{-1} = 0$. The next few functions are

$$\tilde{A}_1 = 6\gamma \tanh(\gamma x) \ , \tag{70}$$

$$A_2 = 15\gamma^2 \mathrm{sech}^2(\gamma x) \ , \tag{71}$$

$$\tilde{A}_3 = 111\gamma^3 \mathrm{sech}^2(\gamma x) \tanh(\gamma x) \ , \tag{72}$$

$$A_4 = \frac{525}{2}\gamma^4 \mathrm{sech}^2(\gamma x) \left[3\mathrm{sech}^2(\gamma x) - 2\right] \ , \tag{73}$$

$$\tilde{A}_5 = \frac{3}{5}\gamma^5 \left[12267\mathrm{sech}^4(\gamma x) - 4089\mathrm{sech}^2(\gamma x) + 632\right] \tanh(\gamma x) \ , \tag{74}$$

$$A_6 = \frac{3}{2}\gamma^6 \mathrm{sech}^2(\gamma x) \left[49317\mathrm{sech}^4(\gamma x) - 49317\mathrm{sech}^2(\gamma x) + 8050\right] \ . \tag{75}$$

A Mathematica notebook (wkb.nb) is attached as a Supplemental Material to our paper [7], which can be used to calculate A_n and $\tilde{A}_n$ up to order $n \approx 100$. The even indexed functions A_{2n} are symmetric and tend to zero as $x \to \pm\infty$. The odd indexed functions $\tilde{A}_{2n-1}$ are antisymmetric with respect to $x = 0$, and at infinity they tend to constants,

$$\lim_{x\to+\infty} \tilde{A}_{2n-1} = \gamma^{2n-1}\delta_{2n-1} \ . \tag{76}$$

The first few values of δ_{2n-1} are:

n	1	3	5	7	9	11	13	15
δ_n	6	0	$\frac{1896}{5}$	$\frac{67140}{7}$	$\frac{2662320}{7}$	$\frac{1301363652}{77}$	$\frac{864462595116}{1001}$	$\frac{49936729868796}{1001}$

The constants δ_{2n-1} are important, since they determine the asymptotic phase shift of the minimal tail configuration,

$$\delta_{\mathrm{m}} = \sum_{\substack{n=1 \\ \mathrm{odd}}}^{\infty} \delta_n \gamma^n \varepsilon^n \ . \tag{77}$$

The sums in (69) and (77) are not convergent, they are asymptotic series, with the same order of optimal truncation N_{opt} as in the original core expansion (55).

When $\delta_w = \frac{\pi}{2}$ the linearized solution (69) is symmetric, $w(-x) = w(x)$, hence the tail part corresponding to the phase $\delta_{\mathrm{m}} + \frac{\pi}{2}$ can be canceled, decreasing its overall amplitude. It follows that the minimal tail-amplitude symmetric solution u_{m} necessarily has the tail form $\alpha_{\mathrm{m}} \sin\left(\frac{kx}{\varepsilon} - \delta_{\mathrm{m}}\right)$ at large distances. The amplitude α_{m} cannot be determined by the WKB method, it will be considered in the next subsections. However, the phase δ_{m} can be very precisely calculated from (77), and the result agrees extremely well with the high precision numerical calculations (see Fig. 3 of [6]). Symmetric solutions with arbitrary phase δ have generally higher tail-amplitude, given by the simple relation $\alpha = \alpha_{\mathrm{m}}/\cos(\delta - \delta_{\mathrm{m}})$.

If we take the minimal tail symmetric solution u_{m} and subtract the linearized solution w in (69) with $\delta_{\mathrm{m}} = 0$ and $\beta = \alpha_{\mathrm{m}}$, then the tail on the right hand side disappears. Hence we obtain a very good approximation for a slightly shifted version of the asymmetric solution,

$u_{\rm m}(x) - w(x) = u_-(x - x_0)$. Defining the shifted version of the asymmetric solution by $\hat{u}_-(x) = u_-(x - x_0)$, dropping the argument we can write

$$u_{\rm m} - w = \hat{u}_- \ . \tag{78}$$

Since the shift x_0 is exponentially small in terms of ε, we can approximate the shifted function as $\hat{u}_- = u_- - x_0 \frac{\rm d}{{\rm d}x} u_-$. Since the first derivative of u_- is multiplied by a small number, u_- in that term can be replaced by an appropriately truncated version of the core expansion (55). Taking derivatives of the resulting equation at $x = 0$ it is possible to obtain a relation for the tail-amplitude $\alpha_{\rm m}$ in terms of the central third derivative of u_-,

$$\alpha_{\rm m} = \frac{{\rm d}^3}{{\rm d}x^3} u_-(0)\, \varepsilon^2 \left(1 + 5\gamma^2\varepsilon^2 + 311\gamma^4\varepsilon^4 + 13407\gamma^6\varepsilon^6 + \frac{1643903}{2}\gamma^8\varepsilon^8 + \dots \right) \ . \tag{79}$$

This relation is very useful, since it is considerably easier to calculate the asymmetric solution u_- than the minimal tail solution $u_{\rm m}$, both numerically and analytically. Numerically, for u_- there is no need for the minimization of the tail, and since there are no infinitely many oscillations in the tail region, it is possible to apply compactification to transform the infinite region $0 \le x < \infty$ into a finite interval. Analytically, a convergent expansion method to construct u_- has been published by Hammersley and Mazzarino [152], which has been discussed and somewhat improved in our paper [7]. It is natural to determine first the central third derivative $\frac{{\rm d}^3}{{\rm d}x^3} u_-(0)$ of the asymmetric solution and then use a higher order version of (79) for the calculation of the tail-amplitude $\alpha_{\rm m}$ of the symmetric solution. However, we expect that the Hammersley-Mazzarino method will not be generalizable for the more complicated scalar field systems that we discuss in the next sections. Hence we continue with the more general and widely applicable complex extension procedure in the next subsections.

The small shift can also be expressed in terms of an asymptotic series expression,

$$x_0 = -\frac{\alpha_{\rm m}}{4\gamma^4\varepsilon} \left[1 - 9(\gamma\varepsilon)^2 - 113(\gamma\varepsilon)^4 - 4987(\gamma\varepsilon)^6 - \frac{663031}{2}(\gamma\varepsilon)^8 - \mathcal{O}\left(\varepsilon^{10}\right) \right] \ . \tag{80}$$

3.3 Complex extension

Analogously to our procedures in Subsections 2.2 - 2.6 for the linear model problem, we extend the stationary fKdV equation (47), the solutions u, and the coefficient functions u_n in the outer expansion (55) to the complex x plane. Since all u_n are polynomials in $\mathrm{sech}^2(\gamma x)$, we investigate the solutions close to the first singularity above the real axis, defining the independent variable q by

$$x = \frac{i\pi}{2\gamma} + \varepsilon q \ . \tag{81}$$

To make the $\varepsilon \to 0$ limit regular we also define a rescaled function,

$$v = \varepsilon^2 u \ . \tag{82}$$

Substituting (81) into the asymptotic expansion (55) and (61), expanding in powers of $1/q$, and then also in powers of ε, we obtain that

$$v = \sum_{n=0}^{\infty} v_n \gamma^{2n} \varepsilon^{2n} \ , \tag{83}$$

where the expansions of the first four functions are

$$v_0 = -\frac{2}{q^2} + \frac{30}{q^4} - \frac{930}{q^6} + \frac{49662}{q^8} - \frac{28918350}{7q^{10}} + \frac{3495722130}{7q^{12}} + \dots \ , \tag{84}$$

$$v_1 = \frac{2}{3} \ , \tag{85}$$

$$v_2 = -\frac{2q^2}{15} + \frac{2}{3} + \frac{64}{q^2} + \frac{5856}{5q^4} - \frac{827520}{7q^6} + \frac{11936160}{q^8} + \dots \ , \tag{86}$$

$$v_3 = \frac{4q^4}{189} - \frac{40q^2}{63} - \frac{1220}{63} + \frac{7424}{7q^2} + \frac{1761280}{49q^4} - \frac{170074880}{49q^6} + \dots \ . \tag{87}$$

Since there are only even powers of q with real coefficients, any truncated versions of the above series correspond to the complex extension of symmetric functions. The expansion of each v_n starts with a q^{2n-2} term, even at higher orders not shown here. Apart from the exactly known constant v_1 all other v_n functions are given here in terms of asymptotic expansions in $1/q$. We will use these expansions as outer boundary conditions for the inner equations in a matching domain where both $\varepsilon|q|$ and $1/|q|$ are small, hence the inner and outer expansions are both valid.

The linear correction w given in (69) can be also extended to the complex x plane and considered close to the singularity in terms of the independent variable q by substituting (81). Expressing the sine function in terms of exponentials, we can neglect the term proportional to $\exp[-k\pi/(2\gamma\varepsilon)]$. The result becomes simpler if we use (68) to restore the non-tilde version of A_n,

$$w = \frac{i\beta}{2} \exp\left(\frac{k\pi}{2\gamma\varepsilon}\right) \exp\left(-iq + i\delta_w\right) \exp\left(-\frac{(k-1)\pi}{2\gamma\varepsilon} + \sum_{n=1}^{\infty} A_n \varepsilon^n\right) \ . \tag{88}$$

We keep k in the first exponential, but substitute $k = \sqrt{1 + 4\gamma^2\varepsilon^2}$ from (53) into the last term. Then we proceed by expanding in powers of $1/q$ and ε. The result up to order ε^6 is

$$w = \frac{i\beta}{2} \exp\left(\frac{k\pi}{2\gamma\varepsilon}\right) \exp\left(-iq + i\delta_w\right) \left[\left(1 + 5\gamma^2\varepsilon^2\right) Q_0(q) + \gamma^4\varepsilon^4 Q_2(q) + \gamma^6\varepsilon^6 Q_3(q) \dots\right] \ , \tag{89}$$

where

$$Q_0(q) = 1 + \frac{6i}{q} - \frac{33}{q^2} - \frac{237i}{q^3} + \frac{1890}{q^4} + \frac{17028i}{q^5} - \frac{167733}{q^6} + \dots \ , \tag{90}$$

$$Q_2(q) = -\frac{2iq^3}{15} - \frac{q^2}{5} + \frac{39iq}{5} - 25 + \frac{234i}{q} - \frac{14343}{5q^2} - \frac{181119i}{5q^3} + \dots \ , \tag{91}$$

$$Q_3(q) = \frac{4iq^5}{315} + \frac{26q^4}{315} - \frac{782iq^3}{315} - \frac{29q^2}{5} + \frac{4267iq}{21} - \frac{41749}{105} + \frac{327162i}{35q} - \frac{25898121}{245q^2} + \dots \ . \tag{92}$$

The q dependence of w in (89) is through terms proportional to $q^n \exp(-iq)$ with various integer n exponents. However, for the calculation of the tail-amplitude we will only need the purely exponential terms terms with $n = 0$, i.e. only those proportional to $\exp(-iq)$. We also only need the antisymmetric solutions with $\delta_w = 0$. The first few such terms are

$$w \overset{0}{\approx} \frac{i\beta}{2} \exp\left(\frac{k\pi}{2\gamma\varepsilon}\right) \exp\left(-iq\right) \left(1 + 5\gamma^2\varepsilon^2 - 25\gamma^4\varepsilon^4 - \frac{41749}{105}\gamma^6\varepsilon^6 - \frac{81737609}{7350}\gamma^8\varepsilon^8 - \dots\right) \ , \tag{93}$$

where $\overset{0}{\approx}$ indicates that we only keep $q^0 \exp(-iq)$ terms.

Equation (78), relating $u_{\rm m}$, $\hat{u}_-$ and w, will remain valid also on the complex plane. The singularities of the shifted asymmetric solution $\hat{u}_-$ will be at the same places as that of $u_{\rm m}$. Actually, this fixes the freedom in the shift of the asymmetric solution. The relation (78) is valid when $\delta_{\rm m} = 0$ and $\beta = \alpha_{\rm m}$ in (69). In this case w is antisymmetric on the real x line, implying that it is purely imaginary on the imaginary q axis. On the other hand, $u_{\rm m}$, which corresponds to a symmetric function, is purely real for $\mathrm{Re}\, q = 0$. Hence

$$\mathrm{Im}\, \hat{u}_- = -\,\mathrm{Im}\, w \quad \text{for } \ \mathrm{Re}\, q = 0 \ , \ \mathrm{Im}\, q < 0 \ . \tag{94}$$

This equation is extremely useful for the determination of the tail-amplitude. The consideration of the inner equations in the next subsections will provide the imaginary part of $\hat{u}_-$ along the imaginary axis, and then (94) can be used to obtain $\alpha_{\rm m} = \beta$. Since (94) is valid to any orders in ε and $1/q$, we can obtain very precise high order results.

3.4 Inner equations

The inner equation can be obtained from the stationary fKdV equation (47) by using the rescaled function $v = \varepsilon^2 u$ and the complex coordinate q,

$$\frac{\mathrm{d}^4 v}{\mathrm{d}q^4} + \frac{\mathrm{d}^2 v}{\mathrm{d}q^2} + 3v^2 - \varepsilon^2 c\, v = 0 \ , \tag{95}$$

We substitute $c = 4\gamma^2 + 16\gamma^4\varepsilon^2$ and keep γ fixed, as in case of the outer expansion. We expand v in powers of ε according to (83). For the coefficient functions v_j we obtain the

$2j$-th order inner equations

$$\frac{\mathrm{d}^4 v_j}{\mathrm{d}q^4} + \frac{\mathrm{d}^2 v_j}{\mathrm{d}q^2} + 3\sum_{l=0}^{j} v_l v_{j-l} - 4v_{j-1} - 16v_{j-2} = 0 \ . \tag{96}$$

This general form is valid for all j, including $j = 0$ and 1, if we substitute $v_n = 0$ when $n < 0$ in the last two terms.

Motivated by the results (84)-(87) that come from the outer expansion, we expand each v_j in even powers of $1/q$, starting with a q^{2j-2} term,

$$v_j = \sum_{n=1-j}^{\infty} b_n^{(j)} q^{-2n} \ . \tag{97}$$

Substituting into (96), for the coefficients $b_n^{(j)}$ we obtain the equations

$$\begin{aligned}(2n+1)(2n)(2n-1)(2n-2)b_{n-1}^{(j)} + (2n+1)(2n)b_n^{(j)} \\ + 3\sum_{l=0}^{j}\sum_{m=1-l}^{n+j-l} b_m^{(l)} b_{n-m+1}^{(j-l)} - 4b_{n+1}^{(j-1)} - 16b_{n+1}^{(j-2)} = 0 \ .\end{aligned} \tag{98}$$

These relations are valid for all $j \geq 0$ and $n \geq 1-j$ if we substitute zero for $b_n^{(j)}$ if $j < 0$ or $n < 1-j$. Eq. (98) can be used to calculate $b_n^{(j)}$ in increasing orders of j and n up to very high orders, using some algebraic manipulation software. However, the solution is not unique, some coefficients must be determined from the matching to the outer expansion solution. For the lowest order we have to choose the nonzero solution $b_1^{(0)} = -2$. For $j \geq 3$ no condition follows for $b_{-2}^{(j)}$, hence we have to obtain those coefficients from the outer expansion. The first few of those values are

j	3	4	5	6	7
$b_{-2}^{(j)}$	$\frac{4}{189}$	$\frac{2}{9}$	$\frac{3800}{2079}$	$\frac{524312}{15925}$	$\frac{13451096}{14553}$

All other coefficients become determined by equation (98), in complete agreement with the results in (84)-(87).

At ε^2 order we obtain $b_0^{(1)} = \frac{2}{3}$, and all other $b_n^{(1)}$ components turn out to be zero, yielding $v_1 = \frac{2}{3}$. Exceptionally, this is an exact solution of the first-order inner equation, satisfying the appropriate boundary conditions. All other v_j, including the leading order v_0, are known only as non convergent asymptotic expansions in terms of $1/q$.

3.5 Laplace transform

Our aim is to determine the imaginary part of the asymmetric solution $\hat{u}_-$ along the imaginary axis, close to the singularity. The inner solution corresponding to $\hat{u}_-$ is $\hat{v}^{(-)} = \varepsilon^2 \hat{u}_-$,

expressed in terms of the variable q. At order ε^{2j} of the inner expansion this function is represented by the function $\hat{v}_j^{(-)}$, according to (83). We intend to apply the Laplace transform method that we have already discussed for the linear model problem in Subsection 2.8. However, for $n \geq 0$ integer we cannot obtain q^n as the Laplace transform of a smooth function. Hence we have to separate those terms, defining

$$\tilde{v}_j = v_j - \sum_{n=1-j}^{0} b_n^{(j)} q^{-2n} = \sum_{n=1}^{\infty} b_n^{(j)} q^{-2n} \ . \tag{99}$$

According to (85)-(87), for the first three functions this is equivalent to

$$v_1 = \frac{2}{3} + \tilde{v}_1 \ , \quad v_2 = -\frac{2}{15} q^2 + \frac{2}{3} + \tilde{v}_2 \ , \quad v_3 = \frac{4}{189} q^4 - \frac{40}{63} q^2 - \frac{1220}{63} + \tilde{v}_3 \ . \tag{100}$$

It follows that $\tilde{v}_1 = 0$, but we keep it for the time being to make the formalism technically simpler.

We can now look for the solution $\tilde{v}_j$ of the order $2j$ inner equation as the Laplace transform of a function that we denote by $V_j'(s)$,

$$\tilde{v}_j = \int_\gamma I_j(s) \mathrm{d}s \quad , \quad I_j(s) = \exp(-qs) V_j'(s) \ , \tag{101}$$

where the contour γ can be any path from $s = 0$ to infinity, along which $\mathrm{Re}(qs) \to \infty$. Using the identity for the Laplace transform of powers of s it follows from (99) that $V_j'(s)$ can be expanded as

$$V_j'(s) = \sum_{n=0}^{\infty} a_n^{(j)} s^{2n+1} \ , \tag{102}$$

where

$$a_n^{(j)} = \frac{b_{n+1}^{(j)}}{(2n+1)!} \quad , \qquad b_n^{(j)} = (2n-1)!\, a_{n-1}^{(j)} \ . \tag{103}$$

It can be shown that the series (102) is convergent for $|s| < 1$ and the functions $V_j'(s)$ can be analytically extended for larger $|s|$. The functions $V_j'(s)$ satisfy integral equations that can be obtained from (96). The zeroth-order equation has been presented in Eq. (31) of [140]. All singularities are located on the imaginary axis at $s = \pm ni$, where n is any positive integer. There is no singularity at $s = 0$.

Although the functions $V_j'(s)$ are unique, the result of the Laplace transform integral (101) depends on how the contour γ is located with respect to the singularities of $V_j'(s)$. The change from one path to another can be calculated easily using the residue theorem. One only need to consider the pole at $s = i$, since the contribution from the others are exponentially suppressed.

To obtain the residue at order j we only need to study the behavior of the function $V_j'(s)$ close to the singularity at $s = 1$, which is determined by the large n behavior of the

coefficients $a_n^{(j)}$. Calculating coefficients up to large n, at leading ε order it is apparent that $a_n^{(0)} \approx K(-1)^n$, where $K \approx 19.97$. The value of the constant K is very important, because it can be used to determine the leading order radiation amplitude. To allow us to get more precise value for K, and to reach higher order results, we look for a more precise version of the large n behavior of the coefficients in the form of an $1/n$ expansion. To compensate the alternating signs, we define a non-alternating version of the coefficients by

$$a_n^{(j)} = (-1)^n \, \tilde{a}_n^{(j)} \ . \tag{104}$$

Then the large n behavior for $j = 0$ is

$$\tilde{a}_n^{(0)} = K G_0(n) \quad , \qquad G_0(n) = 1 + \sum_{l=1}^{\infty} \frac{\tilde{g}_l^{(0)}}{n^l} \ . \tag{105}$$

At ε^2 order all $a_n^{(1)}$ are zero. At higher orders the leading order behaviors are $a_n^{(j)} \sim (-1)^n n^{2j-1}$. For $j \geq 2$ we look for the large n behavior of the coefficients in the form

$$\tilde{a}_n^{(j)} = \sum_{l=1-2j}^{\infty} \frac{\tilde{g}_l^{(j)}}{n^l} \ . \tag{106}$$

The constants $\tilde{g}_l^{(j)}$ should be determined by substituting these expansions into (98). We assume that n is large and fixed. If we are interested in a finite number of $\tilde{g}_l^{(j)}$ constants we do not have to take into account all terms of the summation in (98). The middle terms in the inner sum for m turn out to be higher order in $1/n$ than those close to the limits $m = 1 - l$ and $m = n + j - l$. Taking m_m as a positive integer, if we use only the first $m_m + l$ and the last $m_m + l$ terms in the inner sum, we can still get the first $2m_m$ coefficients $\tilde{g}_m^{(j)}$ correctly. When the lower index in $b_n^{(j)}$ is large, in (98) we use (103) to express the constants in terms of $a_n^{(j)}$. For small lower index we keep $b_n^{(j)}$, especially since $a_n^{(j)}$ is not defined for negative indices. The obtained equation is

$$\begin{aligned} &\tilde{a}_{n-2}^{(j)} - \tilde{a}_{n-1}^{(j)} - \tilde{4} a_n^{(j-1)} - 16 \tilde{a}_n^{(j-2)} \\ &\quad + \frac{3}{(2n+1)!} \sum_{l=0}^{j} \sum_{m=1-l}^{m_m} (-1)^m (2n - 2m + 1)! \, b_m^{(l)} \tilde{a}_{n-m}^{(j-l)} \\ &\quad + \frac{3}{(2n+1)!} \sum_{l=0}^{j} \sum_{m=1-j+l}^{m_m} (-1)^m (2n - 2m + 1)! \, b_m^{(j-l)} \tilde{a}_{n-m}^{(l)} = 0 \ . \end{aligned} \tag{107}$$

If the constants $b_m^{(l)}$ are already calculated up to order m_m then (107) can be considered as a system of linear equations for $\tilde{a}_n^{(j)}$, which is valid for large n. Substituting the expansions (105) and (106) and expanding in $1/n$, one can solve the resulting equations for the coefficients $\tilde{g}_l^{(j)}$. At leading ε order, when $j = 0$, we get

$$G_0(n) = 1 - \frac{3}{n} + \frac{39}{4n^2} - \frac{69}{2n^3} + \frac{1929}{16n^4} - \frac{3381}{8n^5} + \frac{46041}{32n^6} - \frac{1089483}{224n^7} + \dots \ . \tag{108}$$

At higher ε orders we get inhomogeneous linear equations, where at each order l the lower order solutions with smaller l also appear with appropriate factors. The general solution is

$$\tilde{a}_n^{(j)} = K \sum_{l=0}^{j} K_l G_{j-l}(n) \ , \tag{109}$$

where K_l are constants and $G_j(n)$ are $1/n$ expansions starting with n^{2j-1} terms. For $j \geq 2$

$$G_j(n) = \sum_{l=1-2j}^{\infty} \frac{g_l^{(j)}}{n^l} \ . \tag{110}$$

In (109) the constants $K_0 = 1$, $K_1 = 0$ and the trivial expansion $G_1(n) = 0$ has been introduced only to make the expression look simpler. The constants $g_l^{(j)}$ can be calculated from (107) up to relatively high orders using an algebraic manipulation software. Here we list the next two orders:

$$G_2(n) = \frac{16}{15}n^3 + \frac{28}{5}n^2 + \frac{368}{15}n - \frac{132}{n} + \frac{4122}{5n^2} - \frac{50833}{10n^3} + \frac{3144915}{112n^4} + \dots \ , \tag{111}$$

$$G_3(n) = \frac{128}{315}n^5 + \frac{1696}{315}n^4 + \frac{12448}{315}n^3 + \frac{43304}{315}n^2 + \frac{18296}{35}n - \frac{25530}{7n} + \frac{11490537}{490n^2} - \frac{20719647}{140n^3} + \frac{3342753723}{3920n^4} + \dots \ . \tag{112}$$

For all $j \geq 2$ we chose the unique particular solution $G_j(n)$ in which there is no n^0 term.

The next step is to calculate the constants K and K_j. For this we need to calculate the constants $b_n^{(j)}$ and $a_n^{(j)}$ up to quite large n using (98) and (103). Instead of calculating exact rational numbers it is much more efficient to use floating point numbers with hundreds or even thousands of digits precision. A natural way to get K is to use (105) to calculate $\tilde{a}_n^{(0)}/G_0(n)$ using an appropriately high order truncation of the $1/n$ expansion (108) of $G_0(n)$. An equivalent, but technically simpler and more flexible method is to use Richardson extrapolation [132]. Richardson extrapolation uses $m+1$ numbers starting from $\tilde{a}_n^{(0)}$ up to $\tilde{a}_{n+m}^{(0)}$, approximating the large n limit by

$$R_{n;m} = \sum_{l=0}^{m} \tilde{a}_{n+l}^{(0)} \frac{(-1)^{m+l}(n+l)^m}{l!\,(m-l)!} \ . \tag{113}$$

This method provides the same precision as the earlier one with m terms used in the expansion (108) of $G_0(n)$, without the need for explicitly calculating the expansion constants $\tilde{g}_l^{(0)}$. For example, starting with lower index $n = 1000$, taking $m = 182$ terms, and using 500 digits arithmetics $R_{n;m}$ gives a value for K in a few seconds, which turns out to be correct to 237 digits precision. The result up to 40 digits is

$$K = -19.968947358760960518270975287461846342 54 \ . \tag{114}$$

High precision for K is necessary if we intend to calculate the constants K_j for larger j, in order to obtain higher order results for the tail-amplitude.

As it follows from the general expression (109), at ε^4 order the asymptotic behavior of the constants is $\tilde{a}_n^{(2)} = K(G_2(n) + K_2 G_0(n))$. Separating the positive powered terms in $G_2(n)$, the constant K_2 can be obtained by taking the limit

$$K_2 = \lim_{n\to\infty} \left(\frac{\tilde{a}_n^{(2)}}{K} - \frac{16}{15}n^3 - \frac{28}{5}n^2 - \frac{368}{15}n \right) , \tag{115}$$

which can be calculated to high precision using Richardson extrapolation. At higher orders the constants can be obtained similarly from

$$K_j = \lim_{n\to\infty} \left(\frac{\tilde{a}_n^{(j)}}{K} - \sum_{l=0}^{j-2} K_l \sum_{m=1}^{2j-2l-1} g_{-m}^{(j-l)} n^m \right) , \tag{116}$$

where we have to take $K_0 = 1$ and $K_1 = 0$. The results up to ε^{12} order and 25 digits are

$$K_2 \approx -36.5440681935837442934686 8 , \tag{117}$$

$$K_3 \approx -359.9341804574073953698025 , \tag{118}$$

$$K_4 \approx -2929.408154629231406658329 , \tag{119}$$

$$K_5 \approx 98251.223732216092353505 08 , \tag{120}$$

$$K_6 \approx 12208129.307132461043502 86 . \tag{121}$$

The advantage of the Richardson extrapolation method, in addition to the easier coding, is that one only has to calculate the first $2j-1$ negative indexed $g_n^{(j)}$ coefficients in the expansion (110) of $G_j(n)$. These components will be also necessary for the computation of the residue as well, as we shall see soon.

3.6 Asymmetric solution

The imaginary part of of the asymmetric function $\hat{v}_j^{(-)}$ along the lower part of the imaginary q axis can be calculated using the residue theorem. Similarly to the procedure for the model problem at Subsection 2.8, one can choose the contour γ in (101) as the upper half of the imaginary s axis, avoiding the singularities at $s = ni$ by going around them in small half-circles. Since the coefficients $b_n^{(j)}$ in (97) are real, the straight sections along the axis give no imaginary contributions to $\tilde{v}_j$, and hence neither to $v_j \equiv \hat{v}_j^{(-)}$. One only needs to consider the pole at $s = i$ since the contribution from the others are exponentially suppressed. The result from the half-circle will be exactly half of the full-circle integral, which can be obtained from the residue theorem.

The residue of the function $I_j(s) = \exp(-qs)V_j'(s)$ at $s = i$ will be $\exp(-iq)$ times the residue of $V_j'(s)$. Substituting (104) and (109) into the expansion (102), we obtain

$$V_j'(s) = \sum_{n=0}^{\infty} s^{2n+1}(-1)^n K \sum_{l=0}^{j} K_l G_{j-l}(n) \ . \tag{122}$$

Here each $G_j(n)$ can be expanded in powers of $1/n$ according to (105) and (110) in terms of the constants $\tilde{g}_l^{(0)}$ and $g_l^{(j)}$. The result will be sum of terms proportional to $(-1)^n n^m s^{2n+1}$, where m is integer. For a given m the sum for n can be evaluated in a closed form, but we could not find an expression for the sum valid for general m. However, the residue of these functions turn out to be very simple

$$\operatorname*{Res}_{s=i} \sum_{n=0}^{\infty} (-1)^n n^m s^{2n+1} = \begin{cases} \frac{1}{2}(-1)^m & \text{if } m \geq 0 \ , \\ 0 & \text{if } m < 0 \ . \end{cases} \tag{123}$$

From (122) we obtain that the residue is

$$\operatorname*{Res}_{s=i} V_j'(s) = \frac{K}{2} \left(K_j + \sum_{l=2}^{j} K_{j-l} \sum_{m=0}^{2l-1} (-1)^m g_{-m}^{(l)} \right) \ , \tag{124}$$

where we have to substitute $K_0 = 1$ and $K_1 = 0$. Interpreting the sum as zero for $j = 0$, the result is also valid for the leading order, showing that the residue of $V_0'(s)$ is simply $K/2$. The residue of $V_1'(s)$ is zero, since the solution $v_1 = \frac{2}{3}$ is real on the imaginary axis.

The value of the imaginary part of the function $v_j \equiv \hat{v}_j^{(-)}$ at the imaginary q axis will be half of this residue multiplied by $2\pi \exp(-iq)$,

$$\operatorname{Im} \hat{v}_j^{(-)} \overset{0}{\approx} \frac{\pi K}{2} \exp(-iq) \left(K_j + \sum_{l=2}^{j} K_{j-l} \sum_{m=0}^{2l-1} (-1)^m g_{-m}^{(l)} \right) \ , \tag{125}$$

where $\overset{0}{\approx}$ indicates that we neglect terms proportional to $q^m \exp(-iq)$ with $m \neq 0$, similarly as we did at Eq. (93). There are also terms with $m > 0$, which are generated from lower orders in j contributions. They have fixed amplitude, hence do not affect our results for the tail-amplitude.

Using $v = \varepsilon^2 u$ and (83), for the original non-expanded function u we obtain

$$\begin{aligned} \operatorname{Im} \hat{u}_- \overset{0}{\approx} \frac{\pi K}{2\varepsilon^2} \exp(-iq) \Bigg[1 + (K_2 - 20)\, \gamma^4 \varepsilon^4 + \left(K_3 - \frac{8816}{21} \right) \gamma^6 \varepsilon^6 \\ + \left(K_4 - 20 K_2 - \frac{2340812}{175} \right) \gamma^8 \varepsilon^8 + O(\varepsilon^{10}) \Bigg] \end{aligned} \tag{126}$$

for $\operatorname{Re} q = 0$, $\operatorname{Im} q < 0$. Higher order terms can be obtained using (125).

3.7 Tail-amplitude

Because of its importance in the tail-amplitude calculation we repeat Eq. (94),

$$\mathrm{Im}\,\hat{u}_- = -\,\mathrm{Im}\,w \quad \text{for } \mathrm{Re}\,q = 0\ ,\ \mathrm{Im}\,q < 0\ . \tag{127}$$

Here the linearized solution w is given by (93), and the imaginary part of the asymmetric solution $\hat{u}_-$ by (126), both include only the $q^0\exp(-iq)$ terms. We have to match the two expressions at various orders in ε. However, the constant $\beta = \alpha_\mathrm{m}$, which give the minimal tail-amplitude, is also ε dependent. We search it in the form

$$\alpha_\mathrm{m}^{(N)} = \alpha_\mathrm{m}^{(0)}\left(1 - \sum_{n=1}^{N}\xi_n(\gamma\varepsilon)^{2n}\right)\ , \tag{128}$$

where $\alpha_\mathrm{m}^{(0)}$ contains the ε dependent leading behavior, and the constants ξ_n represent corrections up to order ε^{2N}. Substituting $\beta = \alpha_\mathrm{m}^{(N)}$ into (93) we get

$$\mathrm{Im}\,w \overset{0}{\approx} \frac{1}{2}\alpha_\mathrm{m}^{(0)}\exp\left(\frac{k\pi}{2\gamma\varepsilon}\right)\exp(-iq)\Bigg[1 - (\xi_1 - 5)\,\gamma^2\varepsilon^2 - (\xi_2 + 5\xi_1 + 25)\,\gamma^4\varepsilon^4 - \left(\xi_3 + 5\xi_2 - 25\xi_1 + \frac{41749}{105}\right)\gamma^6\varepsilon^6 - \ldots\Bigg]\ . \tag{129}$$

Comparing the main factors in (126) and (129), we obtain the leading order behavior of the minimal tail-amplitude,

$$\alpha_\mathrm{m}^{(0)} = \frac{\mathcal{K}}{\varepsilon^2}\exp\left(-\frac{k\pi}{2\gamma\varepsilon}\right)\ , \tag{130}$$

where

$$\mathcal{K} = -K\pi \approx 62.734298322204738878836844164883360007 42\ . \tag{131}$$

Note that the constant k also has ε dependence, since according to (53), $k = \sqrt{1 + 4\gamma^2\varepsilon^2}$. The exponential term can be expanded as

$$\exp\left(-\frac{k\pi}{2\gamma\varepsilon}\right) = \exp\left(-\frac{\pi}{2\gamma\varepsilon}\right)\left[1 - \pi\gamma\varepsilon + \frac{\pi^2}{2}\gamma^2\varepsilon^2 - \left(\frac{\pi^3}{6} + \pi\right)\gamma^3\varepsilon^3 + O(\varepsilon^4)\right]\ . \tag{132}$$

This shows that the expression for $\alpha_\mathrm{m}^{(0)}$ in (130) is correct also to first-order in ε. The leading order result, i.e. (130) with $k = 1$ has been obtained first by Pomeau et al. [11]. The more precise result with the k factor in the exponential has been presented by Grimshaw and Joshi [140]. However, contrary to a claim in [140], the result (130) is not valid to ε^2 order.

To obtain the constants ξ_n we have to compare the ε^{2n} order corrections in (126) and (129) in increasing order in n. There is no ε^2 term in $\mathrm{Im}\,\hat{u}_-$ in (126), hence the corresponding term should vanish in $\mathrm{Im}\,w$ as well, implying that

$$\xi_1 = 5\ . \tag{133}$$

The corresponding approximation to the tail-amplitude is

$$\alpha_{\rm m}^{(1)} = \frac{\mathcal{K}}{\varepsilon^2} \exp\left(-\frac{k\pi}{2\gamma\varepsilon}\right)\left(1 - 5\gamma^2\varepsilon^2\right) \ . \tag{134}$$

The value $\xi_1 = 5$ agrees well with the high precision numerical results of Boyd [153], where the inconsistency with the incorrect value $\xi_1 = 0$ in [140] has been pointed out.

At order ε^4 the identity (127) gives the equation $K_2 - 20 = \xi_2 + 5\xi_1 + 25$, which yields

$$\xi_2 = -K_2 - 30 \approx 6.544068193583744293468677 \ . \tag{135}$$

The numerical results for the next few orders are

$$\xi_3 \approx 474.4138394894886739024592 \ , \tag{136}$$

$$\xi_4 \approx 4233.412359374196554531744 \ , \tag{137}$$

$$\xi_5 \approx 111053.9527095014662305753 \ , \tag{138}$$

$$\xi_6 \approx 1782156.514208953766632473 \ . \tag{139}$$

The method for the calculation of the constants ξ_n and the above presented values have been published in our papers [6, 7]. The coefficients ξ_n appear to increase in a rate which is slower than factorial increase. From this we might conjecture that the expansion in (128) is possibly convergent, but this requires further justification.

In Fig. 15 we show the extremely quick decrease of the numerically obtained minimal amplitude $\alpha_{\rm m}$ as a function of ε, and also show the relative difference $\Delta\alpha_{\rm m}^{(N)} = \left|(\alpha_{\rm m}^{(N)} - \alpha_{\rm m})/\alpha_{\rm m}\right|$ of the numerical result from various order approximations $\alpha_{\rm m}^{(N)}$. It is apparent from the straight lines on the logarithmic plot that the error of the N-th order approximation $\alpha_{\rm m}^{(N)}$ decreases as ε^{2N+2}. The lines only break for $\varepsilon < 2^{-7}$ when the precision of the numerical results start decreasing. This is due to the large number of necessary collocation points and very long computation times when the oscillating tail becomes extremely small. The extremely good agreement of the numerical and analytic expansion results for $\alpha_{\rm m}$ shows that both methods are reliable and the coefficients ξ_n have been obtained correctly.

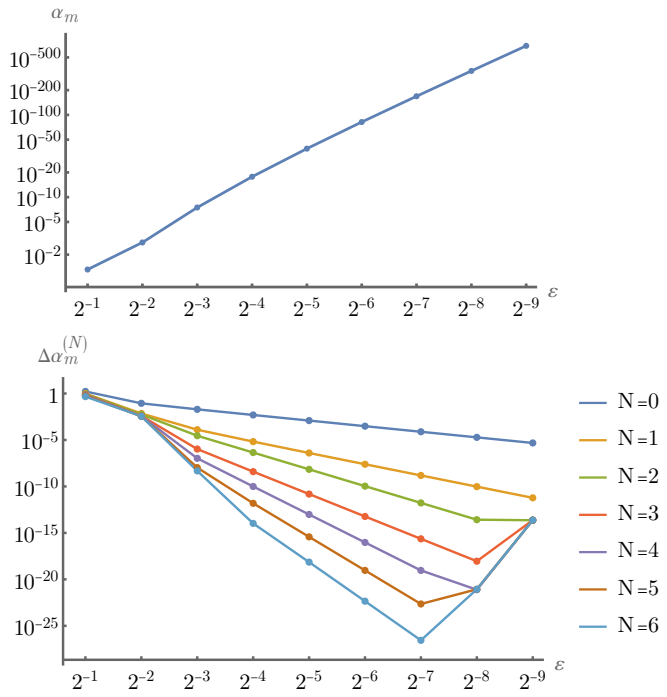

Figure 15: The upper panel shows the numerically calculated minimal amplitude $\alpha_{\rm m}$ as a function of ε for $c = 1$. The lower figure gives the relative difference $\Delta\alpha_{\rm m}^{(N)} = \left|(\alpha_{\rm m}^{(N)} - \alpha_{\rm m})/\alpha_{\rm m}\right|$ of the numerically calculated amplitude from various Nth order approximations as given in (128) and (130).

4 Scalar field oscillons

4.1 Nonlinear scalar fields on Minkowski background

We consider spherically symmetric time evolution of a massive self-interacting scalar field ϕ on $d+1$ dimensional Minkowski background. The equation describing the field can be written as

$$-\frac{\partial^2\phi}{\partial t^2}+\frac{\partial^2\phi}{\partial r^2}+\frac{d-1}{r}\frac{\partial\phi}{\partial r}=U'(\phi)\ , \tag{140}$$

where $U'(\phi)$ is the ϕ derivative of the potential $U(\phi)$ determining the self-interaction of the scalar field.

We are interested in long-lived localized states. The simplest such configurations are the well known breather solutions of the $1+1$ dimensional sine-Gordon equations, when the potential is $U(\phi)=1-\cos\phi$. There is a one-parameter family of *sine-Gordon breather* solutions,

$$\phi(r,t)=4\arctan\left[\frac{\varepsilon\cos(\omega t)}{\omega\cosh(\varepsilon r)}\right]\ , \tag{141}$$

where the parameter ε determines the amplitude. The parameter can take any value in the $0<\varepsilon<1$ interval, and the frequency is connected to it by the relation $\omega^2=1-\varepsilon^2$.

For $1+1$ dimensions the only analytic potential is the sine-Gordon potential which allows the existence of truly localized breather solutions [13, 14, 15]. If $d>1$, then for $d+1$ dimensional flat background no analytic potential is known for which exactly periodically oscillating localized breather solutions exist. Although there are no other breather solutions, still there exist very long living localized oscillating configurations which slowly lose energy by emitting scalar radiation to infinity. The possibility of these type of solutions for $1+1$ dimensional theories has been studied first by using perturbational methods [75, 55]. In 1975 it was shown using numerical methods by Kudryavtsev that by the collision of two $1+1$ dimensional soliton states (ϕ^4 kinks) such long-lived localized structures can really form [20]. These states are not completely periodic, since they lose energy by emitting scalar radiation to infinity. At the same time, their frequency and amplitude slowly changes.

Spherically symmetric long-lived oscillating states in $3+1$ dimensions have been found first by Bogolyubskii and Makhan'kov in Dubna in 1977, using a numerical time-evolution code [16, 17, 154]. The solutions were originally called pulsons, but later the naming oscillon became widespread. These configurations are only approximately time-periodic. Taking into account a longer time period, the amplitude clearly decreases, since the scalar slowly radiates energy out to infinity. For $d\geq 3$ spatial dimensions spherically symmetric oscillons oscillate several times with slowly decreasing amplitude. However, after having their amplitude decreased below a certain value, entering the unstable domain they suddenly decay. On the contrary, for $1+1$ and $2+1$ dimensional oscillons no such sudden decay can be

observed. These oscillons keep on existing for arbitrarily long time, with more and more slowly decreasing amplitudes.

The interest about oscillons began to grow more quickly after 1994, following the work of Marcelo Gleiser, who studied the formation of oscillons by numerical methods for symmetric and asymmetric double well ϕ^4 potentials [18, 19]. It was already apparent from the initial investigations that similar oscillons evolve from several different spherically symmetric initial data, which indicates the stability of oscillons with respect to spherically symmetric perturbations. Later investigations have also shown that oscillons are stable with respect to general perturbations, since non-symmetric initial configurations also develop quickly into spherically symmetric oscillon states, quickly radiating out the non-symmetric component to infinity.

For a more detailed presentation of the history and physical application of oscillons we refer the reader to an earlier review of the present author [155]. Oscillons are likely to appear in cosmological phase transitions, and also may have evolved during the inflationary period of the early universe from the inflaton or from coupled scalar fields, and may have influenced the dynamics of inflation. They may form by the collapse or collision of domain walls or cosmic vacuum bubbles. Oscillons also appear in the bosonic sector of the standard model, in Abelian Higgs models, in supersymmetric theories, and in various Bose-Einstein condensates. During the preheating epoch scalar fields are likely to form oscillons, which may even provide a detectable peak on the spectrum of gravitational waves.

There have been a large number of papers studying the formation and time evolution of oscillons by numerical methods, mostly considering spherically symmetric systems. Regularity at the center can be ensured by requiring that the field ϕ is reflection symmetric at $r = 0$. The outer boundary condition is much more problematic, because of the small amplitude radiation carrying out energy to infinity. One also has to ensure that there is no incoming radiation from infinity. Since a numerical grid can only reach out to finite distances, one has to impose some kind of non-reflecting boundary conditions at the outer boundary. This may be achieved by introducing a dissipative or damping term in a distant region.

In our numerical calculations we have treated the problem of the outer boundary by the compactification of space. For details please see our papers [60, 61, 62, 63] or the review [155]. Spatial derivatives are calculated using symmetric fourth-order stencils. Time integration is performed by the "method of lines", using a fourth-order Runge-Kutta method. In order to ensure the stability of the code, we have added a dissipation term that is proportional to the sixth derivative of the field.

The energy density of the scalar field is

$$\mathcal{E} = \frac{1}{2}\left(\frac{\partial\phi}{\partial t}\right)^2 + \frac{1}{2}\left(\frac{\partial\phi}{\partial r}\right)^2 + U(\phi) \ , \tag{142}$$

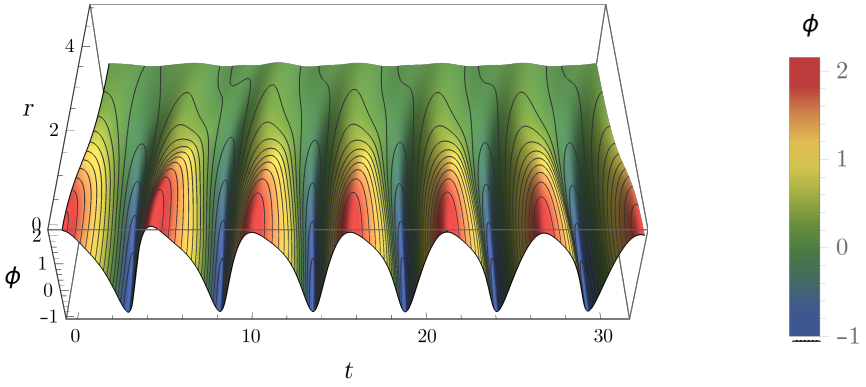

Figure 16: Typical evolution of the scalar field ϕ. The time increases to the right.

and the energy inside a sphere of radius $\bar{r}$ can be calculated as

$$E(\bar{r}) = \frac{2\pi^{\frac{d}{2}}}{\Gamma\left(\frac{d}{2}\right)} \int_0^{\bar{r}} r^{d-1} \mathcal{E} \mathrm{d}r \ . \tag{143}$$

The outward directed energy current density is

$$\mathcal{S} = -\frac{\partial \phi}{\partial t} \frac{\partial \phi}{\partial r} \ , \tag{144}$$

and the energy current going out through the sphere of radius $\bar{r}$ is

$$\mathrm{S}(\bar{r}) = -\frac{\mathrm{d}E(\bar{r})}{\mathrm{d}t} = \frac{2\pi^{\frac{d}{2}}}{\Gamma\left(\frac{d}{2}\right)} \bar{r}^{\,d-1} \mathcal{S}_{r=\bar{r}} \ . \tag{145}$$

4.2 Quasibreathers and nanopterons

Every oscillon loses energy slowly by radiating out the scalar field in a spherically symmetric way. The amplitude of the outgoing radiation is generally extremely small in comparison to the amplitude of the oscillations in the central domain. If we compensate the outgoing radiation by an exactly identical amplitude incoming radiation, then a time-periodic state is formed. Because of the incoming radiation, in the faraway domain a spherically symmetric standing wave forms, that we call *tail*. At the same time, in the inner *core* domain the larger amplitude oscillations remain essentially unchanged. We call these time-periodic solutions *weakly nonlocal* states [156, 5].

The study of time-periodic weakly nonlocal solutions is considerably easier, both by analytical and numerical methods, than the direct study of oscillons that slowly change frequency. For a fixed frequency, still there are many different weakly nonlocal solutions, with different tail-amplitudes and phases. Obviously, the oscillon is best approximated by the weakly nonlocal solution that has the minimal tail-amplitude. We denote this solution as ϕ_{m}. It is unique for a given frequency, and we name it *quasibreather* [60].

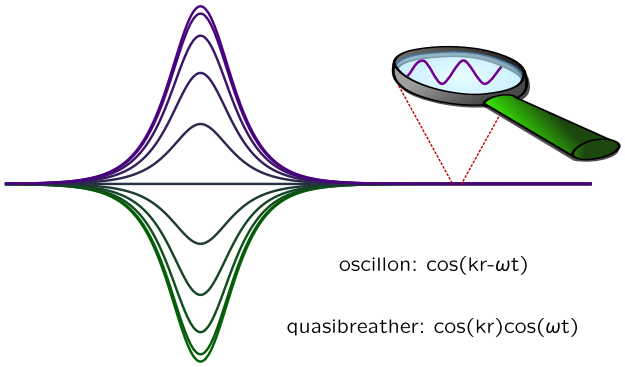

A closely related concept to quasibreathers is the notion of *nanopterons* introduced by John P. Boyd [156, 157, 5]. The naming comes from the Greek expression "dwarf-wing". Nanopteron solutions appear in various hydrodynamic, meteorological, oceanographic, plasma physical and particle physics models. According to Boyd's definition, nanopterons are weakly nonlocal states for which reducing the core amplitude the amplitude of the wing decreases exponentially. As we will see, this is always satisfied for quasibreathers associated to oscillons. The quasibreather solution can be considered as the minimal tail-amplitude nanopteron.

As numerical calculations show, the amplitude of the outgoing radiating wave tail of oscillons agree to high precision with the amplitude of the standing wave tail of the identical frequency quasibreather. Denoting the mass of the scalar field by m, for $d+1$ dimensional spacetimes the asymptotic form of the ω_f frequency part of the quasibreather's tail is

$$\phi = \frac{\alpha}{r^{\frac{d-1}{2}}} \cos(\lambda_f r + \delta) \cos(\omega_f t) \ , \tag{146}$$

where $\lambda_f = \sqrt{\omega_f^2 - m^2}$, and the constants α and δ are a constants giving the amplitude and phase. Violating the time-reflection symmetry by adding a term with asymptotics $\frac{\alpha}{r^{(d-1)/2}} \sin(\lambda_f r + \delta) \sin(\omega_f t)$, we obtain a wave carrying energy outwards, with identical α amplitude,

$$\phi = \frac{\alpha}{r^{\frac{d-1}{2}}} \cos(\lambda_f r + \delta - \omega_f t) \ . \tag{147}$$

Based on (145), the outgoing energy current S provided by this wave through a sphere of radius r, averaged for an oscillation period $2\pi/\omega_f$, is

$$\bar{S} = \frac{\pi^{\frac{d}{2}}}{\Gamma\left(\frac{d}{2}\right)} \lambda_f \omega_f \alpha^2 \ . \tag{148}$$

In the following, to obtain the energy loss rate of oscillons we will calculate the amplitude α of the quasibreather's tail.

We search for quasibreather solutions with frequency ω in a Fourier series form

$$\phi = \sum_{n=0}^{\infty} \Phi_n \cos(n\omega t) \ , \tag{149}$$

where the functions Φ_n are time-independent. In general, the frequency ω of the quasibreather's core is below the mass threshold m, and only the $n \geq 2$ order modes can have standing wave tails. The scalar field ϕ expanded in the form (149) is time-reflection symmetric at the moment $t = 0$. The existence of these type of solutions follows from the invariance of the system with respect to time-reflection. The choice is also motivated by the observation that according to numerical simulations weakly radiating oscillons also possess this symmetry to a very good approximation. For those type of potentials that are mirror symmetric around their minimum, such as the $U(\phi) = 1 - \cos\phi$ sine-Gordon potential, there are only odd indexed terms in the expansion (149), which makes the analysis significantly easier.

We write the expansion of the interaction potential around its minimum in the form

$$U(\phi) = \frac{1}{2}m^2\phi^2 + \sum_{k=2}^{\infty} \frac{1}{k+1} g_k \phi^{k+1} \ , \tag{150}$$

in terms of the mass of the scalar field m and the expansion coefficients g_k. The derivative of the potential with respect to ϕ can be written as

$$U'(\phi) = m^2\phi + \sum_{k=2}^{\infty} g_k \phi^k \ . \tag{151}$$

Substituting the expansion (149) into the field equation (140), for the functions Φ_n we obtain the following coupled differential equations,

$$\frac{\mathrm{d}^2\Phi_n}{\mathrm{d}r^2} + \frac{d-1}{r}\frac{\mathrm{d}\Phi_n}{\mathrm{d}r} + (n^2\omega^2 - m^2)\Phi_n = F_n \ , \tag{152}$$

where the terms F_n are nonlinear functions of $\Phi_0, \Phi_1, \Phi_2, \ldots$. The nonlinear terms on the right-hand side of equation (152) can be obtained in the following way,

$$\begin{aligned} F_n = \left(1 - \frac{1}{2}\delta_{n,0}\right) \Bigg[& \frac{g_2}{2} \sum_{p,q=0}^{\infty} \Phi_p\Phi_q\delta_{n,\pm p\pm q} + \frac{g_3}{4} \sum_{p,q,r=0}^{\infty} \Phi_p\Phi_q\Phi_r\delta_{n,\pm p\pm q\pm r} \\ & + \frac{g_4}{8} \sum_{p,q,r,s=0}^{\infty} \Phi_p\Phi_q\Phi_r\Phi_s\delta_{n,\pm p\pm q\pm r\pm s} \\ & + \frac{g_5}{16} \sum_{p,q,r,s,t=0}^{\infty} \Phi_p\Phi_q\Phi_r\Phi_s\Phi_t\delta_{n,\pm p\pm q\pm r\pm s\pm t} + \cdots \Bigg], \end{aligned} \tag{153}$$

where

$$\delta_{n,\pm p\pm q} = \delta_{n,p+q} + \delta_{n,p-q} + \delta_{n,-p+q} + \delta_{n,-p-q} \ , \tag{154}$$

and we define similarly the other δ expressions, by adding all possible variations for the signatures. If the potential is chosen to be the symmetric ϕ^4 potential in the form $U(\phi) = \frac{1}{4}\phi^2\left(\phi-2\right)^2$, then the mass of the scalar field is $m=\sqrt{2}$, and the nonvanishing expansion coefficients are $g_2=-3$ and $g_3=1$. Equations (152) can be used for the numerical construction of the time-periodic quasibreather solutions [157, 158, 64].

For $d \geq 2$ space dimensions the regularity at the center implies that the functions has to be mirror symmetric, $\Phi_n(x) = \Phi_n(-x)$. For one spatial dimension we also impose these conditions to make the solution unique. The appropriate behavior at the center implies one condition for each Fourier mode Φ_n.

At large distances from the quasibreather's core the functions Φ_n become small, they decouple, and satisfy the linear left-hand sides of equations (152). The behavior at large distances depends on the signature of the factor $n^2\omega^2 - m^2$. If n is below a certain value then $n^2\omega^2 - m^2 < 0$, and the solutions of the homogeneous equation asymptotically has the form

$$\Phi_n \approx \frac{1}{r^{\frac{d-1}{2}}}\left[\hat{\alpha}_n \exp(-\hat{\lambda}_n r) + \hat{\beta}_n \exp(\hat{\lambda}_n r)\right] \ , \tag{155}$$

where $\hat{\lambda}_n = \sqrt{m^2 - n^2\omega^2}$. The condition for the existence of at least weakly nonlocal solutions is that $\hat{\beta}_n = 0$, with arbitrary $\hat{\alpha}_n$. For each mode satisfying the condition $n^2\omega^2 - m^2 < 0$ we have one condition at the origin and one at infinity, which considering a second-order equation can be satisfied generally.

In general, for any frequency there exists an integer n_ω such that for $n \geq n_\omega$ the inequality $n^2\omega^2 - m^2 > 0$ holds. Introducing the notation $\lambda_n = \sqrt{n^2\omega^2 - m^2}$, the asymptotic behavior of the modes can be written as

$$\Phi_n \approx \frac{1}{r^{\frac{d-1}{2}}}\left[\tilde{\alpha}_n \sin(\lambda_n r) + \tilde{\beta}_n \cos(\lambda_n r)\right] \ . \tag{156}$$

Although for $d \geq 2$ the function Φ_n tends to zero for arbitrary $\tilde{\alpha}_n$ and $\tilde{\beta}_n$, the energy $E(r)$ contained in a sphere of radius r diverges linearly when $r \to \infty$ for any d when $\tilde{\alpha}_n$ or $\tilde{\beta}_n$ is nonzero. Truly localized, finite energy, time-periodic breather solution can only exist if for every $n \geq n_\omega$ modes $\tilde{\alpha}_n = \tilde{\beta}_n = 0$, and the central symmetry condition also holds. Three conditions for each mode for coupled second-order equations are generally too much. This argument shows that genuine breather solutions can only exist in some very exceptional cases, such as for the $1+1$ dimensional sine-Gordon potential, when the system is integrable. In other cases we can find the solution most similar to a localized configuration if we look for the minimal tail-amplitude weakly nonlocal solution, i.e. the quasibreather ϕ_{m}.

The frequency of the observed oscillons is always in the range $\omega < m$, where m is the scalar field mass. Most numerical simulations in the literature have been carried out for the ϕ^4 potential choosing $m=\sqrt{2}$. In later sections, in order to make the comparison easier with the small-amplitude expansion results, we will also use the scaling that makes $m=1$.

The amplitude of the quasibreather's tail can be extremely small for frequencies that are only a little smaller than m, but decreasing the frequency the tail-amplitude grows very quickly. When ω decreases close to the value $m/2$, the tail generally grows so large that we cannot talk about a localized state anymore. Hence in the following we only investigate quasibreathers in the frequency domain $\frac{1}{2}m < \omega < m$. In this case the linearized asymptotic behavior of the modes Φ_0 and Φ_1 is exponentially decaying, according to the first term of equation (155). The other Φ_n modes with $n \geq 2$ have standing wave tails according to (156).

For the numerical construction of the minimal standing wave tail quasibreathers in case of $d = 3$ spatial dimensions we have applied the LORENE numerical library [159]. The library was created at Paris Observatory in Meudon, and we carried out our research in collaboration with Philippe Grandclément, one of the developers of the code [60]. The LORENE library applies spectral methods and multi-domain decomposition of space. We divide the space into concentric spherically symmetric shell shaped domains, and for the radial dependences we employ expansion in terms of Chebyshev polynomials. By this method the solution of the differential equations is reduced into inversion of matrices on the coefficient space in each domain. We solve the nonlinear system by an iterative method. We also have to use numerical minimization to find the quasibreather solution with the minimal tail-amplitude. For more details on our numerical method please see our paper [60] or the review [155].

In Figure 17 we show the radial behavior of the first few Φ_n modes of the minimized tail quasibreather for the ϕ^4 potential with $m = \sqrt{2}$ and frequency $\omega = 1.365$. For potentials

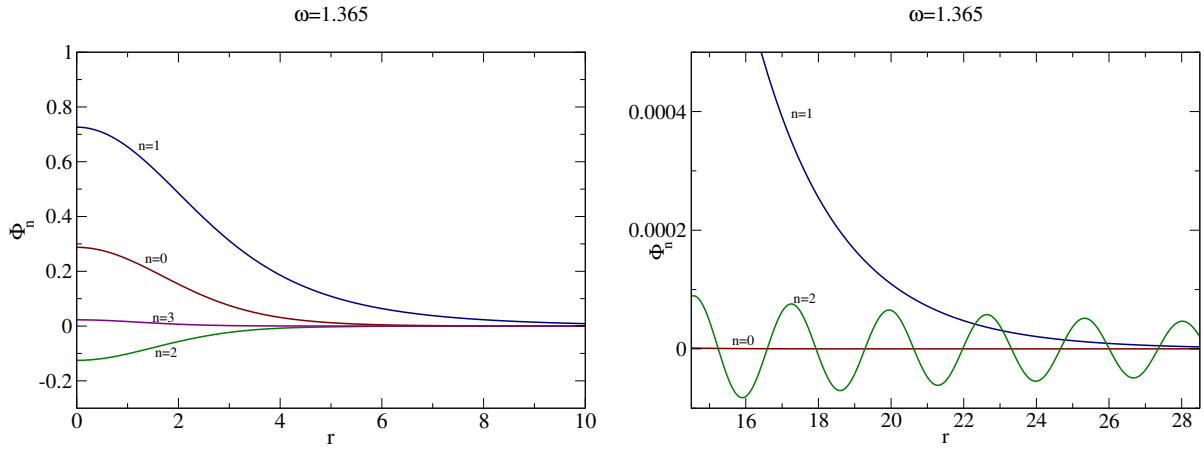

Figure 17: The r dependence of the Fourier modes Φ_n of the quasibreather near the core and in the transitional region where the tail starts to appear.

that are asymmetric around the minimum always the Φ_2 mode dominates the tail. The asymptotic tail in the higher modes have such small amplitude that their oscillations could not be seen in Figure 17. Since the magnitude of the Fourier component functions Φ_n decreases exponentially with growing n, it is usually sufficient to consider relatively few

components only. During our spectral calculations the use of the first 7 modes already gave results precise for three or four digits.

In the tail region of the quasibreather the tendency of the decrease of the energy density is according to $1/r^2$, from which it follows that the energy $E(r)$ inside a sphere diverges linearly with increasing r. Although the quasibreathers are not finite energy states, still in a large region they approximate with high precision the finite energy but radiating oscillon states. In the outer part of the core domain the energy density decreases approximately exponentially, until it reaches the value of the energy density of the tail. The energy density of the tail is essentially proportional to the square of the tail-amplitude α_2 of the mode Φ_2, because of the relative smallness of the other modes. We define the radius of the core as the value $r = R_{\rm trans}$ where the dominant mode Φ_1 first decreases to the local tail-amplitude of the oscillating mode Φ_2,

$$\Phi_1\Big|_{r=R_{\rm trans}} = \frac{|\alpha_2|}{R_{\rm trans}} \ . \tag{157}$$

This is the distance beyond which the oscillating standing wave tail becomes dominant.

We consider the total energy of the quasibreather as the $E(R_{\rm trans})$ energy inside the core radius $R_{\rm trans}$, calculated using (143). The ω dependence of this total energy can be seen in Figure 18. The energy is not a monotonic function, it takes a minimal value at the critical

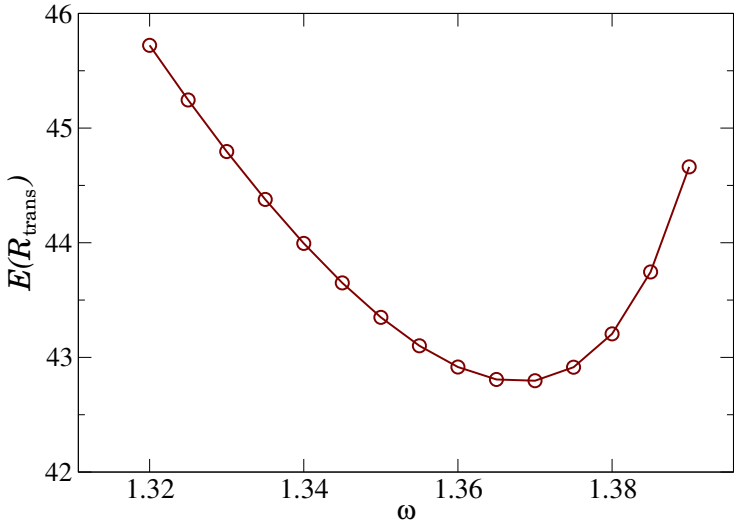

Figure 18: The energy $E(R_{\rm trans})$ of the quasibreather's core as a function of the frequency.

frequency $\omega_c \approx 1.368$. The nontrivial behavior is due to two competing effects. Increasing the frequency the core amplitude decreases, but the core size increases.

The critical frequency ω_c is crucial, since numerical simulations show that $3+1$ dimensional oscillons with frequencies $\omega < \omega_c$ are stable, while they are unstable in case of $\omega > \omega_c$. This stability change corresponds to the generally valid astrophysical experience with localized objects similar to stars. If by the increase of the central energy density the full

mass-energy is increasing then the configuration is stable, while in the opposite case it is unstable. In case of oscillons and quasibreathers the the central amplitude and central energy density increases monotonically with the decrease of the frequency. This argument also explain how $3+1$ dimensional oscillons can generally make hundreds of oscillations before a sudden decay, reaching into the unstable domain.

4.3 Small-amplitude expansion

In this subsection we describe an expansion procedure in terms of a parameter ε that represent the amplitude of the oscillons. The expansion gives a very good description of the core region of oscillons and quasibreathers, even for relatively large amplitudes. Originally, the expansion with respect to the amplitude was applied together with a Fourier expansion with respect to the time coordinate t, and the analysis was for one-dimensional space [75, 55, 160, 10, 157]. The method can be easily generalized for higher dimensions as well [76, 77, 154, 161]. Kichenassamy [14] have realized that it is not necessary to apply Fourier expansion together with the small-amplitude expansion. Time-periodicity follows from the weaker assumption that the solution must remain bounded during the whole time evolution. In our paper on the expansion of oscillons we have generalized and worked out in detail this method for $d+1$ dimensional spacetimes [61]. This expansion will play the role of outer expansion in the asymptotic matching procedure in later subsections.

We expand the scalar field ϕ with respect to powers of the parameter ε in the form,

$$\phi = \sum_{k=1}^{\infty} \varepsilon^k \phi_k \ , \tag{158}$$

introducing the ϕ_k functions that are parameter independent. We solve the field equation (140), which is valid for spherical symmetry. In case of one spatial dimension we assume that the scalar ϕ is mirror symmetric at $r=0$, which also implies that we choose a system moving together with the center of mass.

We specify the self-interaction potential $U(\phi)$ by the coefficients g_k in (150). In order to make the expressions simpler we rescale the coordinates t and r so that the mass of the scalar field is $m=1$. For the ϕ^4 potential we use the form $U(\phi) = \frac{1}{8}\phi^2\left(\phi-2\right)^2$, when the nonvanishing expansion coefficients are $g_2 = -3/2$ are $g_3 = 1/2$. The results presented in this subsection are valid for any analytic potential. We will only choose a specific potential when comparing with numerical computations.

We can only obtain long-lived localized solutions of the field equation (140) if we choose the characteristic size of the solutions ε dependent. According to numerical experience, the size of oscillons grows with decreasing ε amplitude. Because of this, it is advantageous to

introduce a new rescaled radial coordinate ρ by the expression

$$\rho = \varepsilon r \ . \tag{159}$$

Because of the use of the new coordinate the spatial variation of the obtained solutions will be much slower than their change with respect to time. This is always a valid assumption in the core region of the quasibreathers, but in the tail region the derivatives with respect to t and r have the same order, hence the formalism is not able to describe the standing wave tail region. This is not a severe problem, since the amplitude of the tail is $\exp(-1/\varepsilon)$ order small.

The frequency of oscillons increases slowly when their amplitude decreases due to the energy loss. If the amplitude ε of oscillons or quasibreathers approaches zero, their frequency tends to the $\omega_0 = m = 1$ value. The change in the time-scale can be taken into account most easily if we introduce a rescaled time coordinate

$$\tau = \omega t \ , \tag{160}$$

where ω is a function of ε. Since during our procedure we keep the frequency of the state at the constant 1 value with respect to the time coordinate τ, the function $\omega \equiv \omega(\varepsilon)$ gives the physical frequency of the oscillon. We can expand the square of the frequency in the following form:

$$\omega^2 = 1 + \sum_{k=1}^{\infty} \varepsilon^k \omega_k \ . \tag{161}$$

Carrying out the general expansion procedure [61, 155], it can be shown, that it is a natural and valid choice to take $\omega_2 = -1$ and $\omega_n = 0$ for all $n \neq 2$. Hence in the following we assume that the relation between the parameter ε and the frequency is

$$\omega^2 = 1 - \varepsilon^2 \ . \tag{162}$$

This can be always achieved by a reparametrization $\varepsilon \to \tilde{\varepsilon}(\varepsilon)$, which does not change the initial assumption that ε is proportional to the central amplitude of the oscillons in the small-amplitude limit.

From (162) also follows that small amplitude oscillons can only exist with frequency ω below the $m \equiv 1$ mass threshold. This is physically reasonable, since if the frequency ω is above the base frequency 1, then there is an oscillating tail associated to the dominating mode Φ_1 according to (156), which necessarily implies large energy loss. We can expect the existence of long-lived localized states if only the 2ω, 3ω and higher harmonics are able to radiate.

Using the Laplacian

$$\tilde{\Delta}\phi = \frac{\partial^2 \phi}{\partial \rho^2} + \frac{d-1}{\rho} \frac{\partial \phi}{\partial \rho} \ , \tag{163}$$

with respect to the rescaled coordinate, and taking the expanded form of the potential (150) with $m = 1$, the field equation (140) can be written into the form

$$-\omega^2 \frac{\partial^2 \phi}{\partial \tau^2} + \varepsilon^2 \tilde{\Delta}\phi = \phi + \sum_{k=2}^{\infty} g_k \phi^k \ . \tag{164}$$

Substituting the expansion (158) of ϕ, the identical ε power terms determine equations that has to be satisfied separately. The general form of these equations is

$$\frac{\partial^2 \phi_k}{\partial \tau^2} + \phi_k = f_k \ , \tag{165}$$

where the structure of the left-hand side homogeneous part is always the same, and the inhomogeneous source terms f_k are nonlinear functions of the lower order ϕ_l components with $l < k$. The expressions for f_k depend on the constants g_l for $l \leq k$. In the first equation obviously $f_1 = 0$, and the next two source terms are:

$$f_2 = -g_2 \phi_1^2 \ , \tag{166}$$

$$f_3 = \ddot{\phi}_1 + \tilde{\Delta}\phi_1 - 2g_2 \phi_1 \phi_2 - g_3 \phi_1^3 + \frac{\partial^2 \phi_1}{\partial \tau^2} \ . \tag{167}$$

The homogeneous part is always an expression describing a harmonic oscillator, so at the first glance it may appear that equations (165) only determine the time dependence of the ϕ_k functions. However, as we will see, the requirement that the solutions should not increase without bound with the evolution of time will fix the spatial dependence of the functions ϕ_k.

The general solution of the leading order equation (165) for $k = 1$ is of the form

$$\phi_1 = p_1 \cos(\tau + \delta_1) \ , \tag{168}$$

where the amplitude p_1 and the phase δ_1 are arbitrary functions of the radial coordinate ρ. All the other equations for ϕ_k from (165) are forced oscillator equations with base frequency $\tilde{\omega} = 1$. Continuing the expansion in a general way, it turns out that δ_1 must be a constant, and hence $\delta_1 = 0$ can be achieved by time-translation [61, 155]. This also implies that the states which are described by the expansion are time-reflection symmetric. To make the procedure more transparent, here we continue by setting $\delta_1 = 0$, and hence

$$\phi_1 = p_1 \cos \tau \ . \tag{169}$$

The inhomogeneous source term f_k on the right-hand side always constitutes of sums of terms with time dependence $\cos(n\tau)$, where $n \geq 0$ integer. When $n \neq 1$ the $\cos(n\tau)$ term generates a solution which is time-periodic, and hence bounded. However, if there is a source term in f_k proportional to $\cos \tau$, then it generates a solution proportional to $\tau \sin \tau$, which is unbounded because of the linearly increasing amplitude. Since we are looking for solutions

that remain regular and bounded for a long time, we have to require that for all k, in the expressions for f_k the coefficient of the $\cos\tau$ term has to be zero.

The solution of equation (165) for $k = 2$ is bounded and periodic in time,

$$\phi_2 = p_2 \cos\tau + \frac{g_2}{6} p_1^2 [\cos(2\tau) - 3] \ , \tag{170}$$

where p_2 is a further arbitrary function of ρ. One could also include a term $q_2 \sin\tau$ in (170) with some arbitrary function q_2, but it can be shown that it would only provide a small shift in the time-coordinate τ [61, 155].

Substituting the obtained solutions for ϕ_1 and ϕ_2 into the expression (167) of f_3, we obtain the following expression,

$$f_3 = \left[\tilde{\Delta} p_1 - p_1 + \lambda p_1^3\right] \cos\tau - \frac{1}{12} p_1^3 (2g_2^2 + 3g_3) \cos(3\tau) - g_2 p_1 \left[p_2 \cos(2\tau) + p_2\right] \ , \tag{171}$$

where we have introduced the notation

$$\lambda = \frac{5}{6} g_2^2 - \frac{3}{4} g_3 \ . \tag{172}$$

For the ϕ^4 potential $\lambda = 3/2$, and for the sine-Gordon potential $\lambda = 1/8$.

The necessary condition on the boundedness of the function ϕ_3 is that in equation (171) the coefficient of $\cos\tau$ has to be zero,

$$\tilde{\Delta} p_1 - p_1 + \lambda p_1^3 = 0 \ . \tag{173}$$

Since we are looking for localized solutions that tend to zero, at large distances the cubic term can be neglected. One of the two possible asymptotic solutions of the equation decays exponentially at large distances.

Multiplying equation (173) by $\rho^{d-1} p_1$ and integrating between $\rho = 0$ and infinity, it can be seen that if $\lambda \leq 0$ then only the trivial solution $p_1 = 0$ exists [61, 155]. It follows that small-amplitude solutions can only exist for potentials for which the scalar λ defined in (172) is positive. In the following we assume that $\lambda > 0$. The coefficient g_2 makes the potential $U(\phi)$ asymmetric, and any value of it enhances nonlinearity and helps the appearance of oscillons. For potentials that are symmetric around their minimum, necessarily $g_2 = 0$, and then $g_3 < 0$ is the necessary condition for the existence of oscillons. In the symmetric case this negative term makes the potential shallower around its minimum than the Klein-Gordon potential, hence increases the oscillation time and decreases the frequency compared to that.

4.3.1 The base equation

Introducing the function $S = \sqrt{\lambda}\, p_1$, from (173) we obtain an equation which is independent of the parameters,

$$\tilde{\Delta} S - S + S^3 = 0 \ . \tag{174}$$

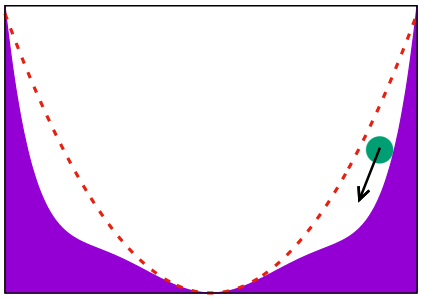

Since (174) is appropriate for the description of small amplitude oscillons for arbitrary potentials, following the nomenclature of Buslaev [76], we refer to it as the *base equation*.

In case of $d = 1$ spatial dimension the only bounded localized solution is

$$S = \sqrt{2}\,\mathrm{sech}\,\rho\ . \tag{175}$$

Obviously, this multiplied by -1 also solves the equation, but it is not necessary to deal with that, since even for potentials not symmetric around their minimum it leads to the same solution, just shifted by a half oscillation period. For one space dimension all functions appearing at the higher orders of the ε expansion can be expressed as linear combinations of various powers of $\mathrm{sech}\,\rho$, and hence the expansion can be technically much more easily performed for $d = 1$ than for higher dimensions [10, 14, 5].

For higher dimensions the solutions are only known in numerical form. The condition for central regularity is that at $\rho = 0$ the value of S is finite and its derivative is zero. For $d = 2$ and $d = 3$ spatial dimensions there are infinitely many localized regular solutions, characterized by an integer $n \geq 0$. The parameter n determines the number of nodes (zero crossings) of the solution denoted by $S \equiv S_n$. In Figure 19 we show the first few such functions. By physical intuition it appears reasonable that the solution S_0, which is nowhere zero, is the most important. It can be shown that the oscillon solutions corresponding to functions S with nodes have larger energy, are less stable, and have a shorter lifetime [61]. In the following we will focus on oscillons belonging to S_0, although the expansion procedure is valid for the general case as well. The central value of S_0 with nine digits precision is

$$S_0^{(\rho=0)} = \begin{cases} 2.20620086 & \text{if } d = 2\ , \\ 4.33738768 & \text{if } d = 3\ . \end{cases} \tag{176}$$

It can be shown that the base equation (174) has no regular localized solution for $d \geq 4$ spatial dimensions [61].

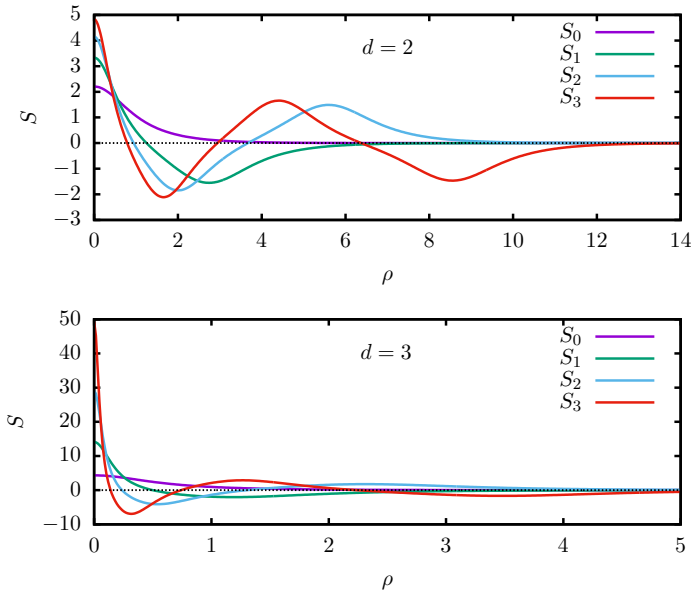

Figure 19: Localized regular solutions of the base equation (174) in case of $d = 2$ and $d = 3$ spatial dimensions.

4.3.2 Higher orders in the expansion

After the elimination of the resonance terms in (171), the solution of equation (165) for ϕ_3 is

$$\phi_3 = p_3 \cos\tau + \frac{p_1}{3}\left[\frac{1}{8}\left(\frac{4}{3}g_2^2 - \lambda\right)p_1^2\cos(3\tau) + g_2 p_2\left(\cos(2\tau) - 3\right)\right], \tag{177}$$

where p_3 is a new, yet unknown function of ρ. Similarly to this, at higher orders, when solving the equation for ϕ_k a new functions appear, p_k, which will be determined by the resonance condition at two orders higher.

As a next step, the source term f_4 can be calculated, and the vanishing of the $\cos\tau$ terms yields the resonance condition

$$\tilde{\Delta}p_2 - p_2 + 3S^2 p_2 = 0\ . \tag{178}$$

This equation corresponds to the linearization of the base equation (174) around S. Hence it is solved by $\frac{\mathrm{d}S}{\mathrm{d}r}$, which is not a symmetric function around $\rho = 0$. It can be shown that no other localized solution exist[76], hence we have to set $p_2 = 0$. Proceeding to higher orders in the expansion, at even orders the same simple equation determines the free functions, and hence it follows that $p_{2k} = 0$ for integer k. The odd indexed p_{2k+1} functions are determined by further second-order differential equations.

The ρ dependence of the function p_3 is determined at order ε^5 from the cancellation of the terms with time dependence $\cos\tau$. Let us introduce the function Z by the expression

$$p_3 = \frac{1}{\lambda^2\sqrt{\lambda}}\left[\sigma Z - \frac{1}{54}\lambda g_2^2 S(32 + 19S^2)\right]\ , \tag{179}$$

where

$$\sigma = \frac{1}{24}\lambda^2 - \frac{1}{6}\lambda g_2^2 + \frac{5}{8}g_5 - \frac{7}{4}g_2 g_4 + \frac{35}{27}g_2^4 \ . \tag{180}$$

Then the condition for p_3 can be written into the following much simpler form,

$$\tilde{\Delta} Z - Z + 3S^2 Z - S^5 = 0 \ , \tag{181}$$

which is a linear and inhomogeneous equation, independent of the potential $U(\phi)$. The equation is linear in Z, and for given S it has a unique regular and localized solution. For $d = 1$ spatial dimension this solution is

$$Z = S(4 - S^2)/3 \ , \tag{182}$$

where S has the form given in (175). In case of $d = 2$ or $d = 3$ spatial dimensions the function Z can be determined numerically. The value of the function Z in the center is

$$Z_0^{(\rho=0)} = \begin{cases} 1.4507606 & \text{if } d = 2 \ , \\ -16.174027 & \text{if } d = 3 \ . \end{cases} \tag{183}$$

We summarize the results of the expansion up to here. We have constructed the ε expansion of the solution of the field equation (140) up to fourth order. The solution is the sum of terms with harmonic time dependence, and the radial dependence is determined by two universal elliptic partial differential equations, (174) and (181). The result of the expansion for general potential $U(\phi)$ is

$$\phi_1 = p_1 \cos\tau \ , \tag{184}$$

$$\phi_2 = \frac{1}{6}g_2 p_1^2 \left[\cos(2\tau) - 3\right] \ , \tag{185}$$

$$\phi_3 = p_3 \cos\tau + \frac{1}{72}(4g_2^2 - 3\lambda)p_1^3 \cos(3\tau) \ , \tag{186}$$

$$\begin{aligned} \phi_4 = {} & \frac{1}{360}p_1^4 \left(3g_4 - 5g_2\lambda + 5g_2^3\right)\cos(4\tau) \\ & -\frac{1}{72}\left[8g_2\left(\frac{\mathrm{d}p_1}{\mathrm{d}\rho}\right)^2 - 12g_4 p_1^4 + 16g_2^3 p_1^4 - 24g_2 p_1 p_3 - 23g_2\lambda p_1^4 - 8g_2 p_1^2\right]\cos(2\tau) \\ & -g_2 p_1^2 - g_2 p_1 p_3 + \frac{1}{6}g_2\lambda p_1^4 - g_2\left(\frac{\mathrm{d}p_1}{\mathrm{d}\rho}\right)^2 + \frac{31}{72}g_2^3 p_1^4 - \frac{3}{8}g_4 p_1^4 \ . \end{aligned} \tag{187}$$

For potentials $U(\phi)$ which are symmetric around their minimum, the even coefficients are zero, $g_{2k} = 0$. In this case the resulting expressions become considerably simpler, and it is easier to proceed to higher orders with the expansion. Then the even indexed terms are zero in the ε expansion, namely $\phi_{2k} = 0$. Since in the general case ϕ_{2n} only contain $\cos(2k\tau)$ terms, and ϕ_{2n+1} only consist of $\cos((2k+1)\tau)$ terms, where $k = 0 \ldots n$, from this also follows that for symmetric potentials even indexed Φ_n terms do not appear in the Fourier

expansion (149). In this case, according to (179), the function p_3 is proportional to Z, and the equation determining the function p_5 becomes relatively simple,

$$\tilde{\Delta}p_5 - p_5 + 3S^2 p_5 + \frac{SZ}{576\sqrt{\lambda}}(3Z - 5S^3)\left(\frac{15g_5}{\lambda^2} + 1\right)^2 \tag{188}$$
$$+ \frac{S^3}{32\sqrt{\lambda}}\left[\left(\frac{\mathrm{d}S}{\mathrm{d}\rho}\right)^2 - S^2\right] - \frac{S^7}{576\sqrt{\lambda}}\left(\frac{315g_7}{\lambda^3} - \frac{60g_5}{\lambda^2} + 1\right) = 0 \ .$$

Hence for symmetric potentials the fifth order of the expansion is:

$$\phi_5 = p_5 \cos\tau + \frac{S^5}{1152\sqrt{\lambda}}\left(\frac{3g_5}{\lambda^2} + 2\right)\cos(5\tau) \tag{189}$$
$$- \frac{S}{384\sqrt{\lambda}}\left[\left(\frac{30g_5}{\lambda^2} + 2\right)SZ + 12S^2 - 12\left(\frac{\mathrm{d}S}{\mathrm{d}\rho}\right)^2 - \left(\frac{15g_5}{\lambda^2} - 2\right)S^4\right]\cos(3\tau) \ .$$

4.4 One-dimensional space with symmetric potential

Because of the technical complexity of the complex plane asymptotic matching method for oscillons, we first present the procedure for a special case when the calculation of the radiation is the simplest. In case of a $U(\phi)$ potential that is symmetric around its minimum, in the Fourier expansion (149) there are only odd indexed Φ_n components, and the equations that have to be solved are also easier to analyze. As we will see later, for $d > 1$ spatial dimensions the leading order tail-amplitude of spherically symmetric quasibreathers can be calculated by the same expression as the tail-amplitude of the $d = 1$ dimensional states. Because of this, it is necessary to investigate the one-dimensional case first.

Applying the notation of the expansion (150), the simplest potential which is symmetric around its minimum is $U(\phi) = \frac{1}{2}\phi^2 + \frac{g_3}{4}\phi^4$. In this subsection we still keep the mass of the scalar field at $m = 1$. Small-amplitude oscillons can only exist if the constant $\lambda = \frac{5}{6}g_2^2 - \frac{3}{4}g_3$ defined in (172) is positive. Since now $g_2 = 0$, necessarily g_3 must be negative. Because of this, by the rescaling of the scalar field ϕ, for an arbitrary symmetric potential we can set $g_3 = -1$, and then $\lambda = 3/4$. To ensure the stability of the system we intend to keep the potential bounded from below, hence we add a sixth degree term to the potential,

$$U(\phi) = \frac{1}{2}\phi^2 - \frac{1}{4}\phi^4 + \frac{g_5}{6}\phi^6 \ , \tag{190}$$

where we assume that $g_5 > 0$. During the following calculations we will use this general symmetric sixth-order potential. We will see that the amplitude of the tail depends strongly on the value of g_5.

4.4.1 Outer expansion

The ε expansion results discussed in Subsection 4.3 resulted in time-periodic solutions oscillating with frequency $\omega = \sqrt{1 - \varepsilon^2}$. Hence these solutions can be Fourier expanded according

to (149), in terms of the coefficient functions Φ_n. The ε expansion becomes significantly simpler for $d = 1$ spatial dimension, since in that case the differential equations determining the functions p_{2k+1} can be solved analytically. For $d = 1$ the solutions of these equations can be given as polynomials in $\operatorname{sech}\rho$. There is further simplification for symmetric potentials, since in that case $g_k = 0$ when k is even. From this also follows that $\Phi_n = 0$ for even n. According to equations (184) - (187) and (189), for the symmetric potential (190) the ε expansion of the first three nonzero Fourier components can be written as

$$\begin{aligned}\Phi_1 =&\varepsilon\frac{2\sqrt{2}}{\sqrt{3}}\operatorname{sech}\rho+\varepsilon^3\frac{1}{27\sqrt{6}}(80g_5+3)(2\operatorname{sech}\rho-\operatorname{sech}^3\rho)\\&+\varepsilon^5\frac{1}{1458\sqrt{6}}\Big[5(6400g_5^2-96g_5+63)\operatorname{sech}\rho-(25600g_5^2+480g_5+171)\operatorname{sech}^3\rho\\&\qquad+3(1600g_5^2+240g_5-9)\operatorname{sech}^5\rho\Big]+\mathcal{O}(\varepsilon^7)\ ,\end{aligned}\tag{191}$$

$$\begin{aligned}\Phi_3 =&-\varepsilon^3\frac{1}{3\sqrt{6}}\operatorname{sech}^3\rho\\&+\varepsilon^5\frac{1}{108\sqrt{6}}\left[-2(80g_5+3)\operatorname{sech}^3\rho+(200g_5-33)\operatorname{sech}^5\rho\right]+\mathcal{O}(\varepsilon^7)\ ,\end{aligned}\tag{192}$$

$$\Phi_5 =\varepsilon^5\frac{1}{108\sqrt{6}}(8g_5+3)\operatorname{sech}^5\rho+\mathcal{O}(\varepsilon^7)\ .\tag{193}$$

At higher orders it is also true that for odd k the first term of the expansion of Φ_k is proportional to $\varepsilon^k\operatorname{sech}^k\rho$. For a general symmetric potential the leading order terms of the Fourier components would remain the same. The coefficient g_7 of the expansion of the potential would only appear in the third term of (191), which is proportional to ε^5.

4.4.2 Complex extension

As it can be seen from equations (191)-(193), the behavior of the Fourier mode functions on the complex ρ plane are determined by the function $\operatorname{sech}\rho$. The function $\operatorname{sech}\rho$ has first-order poles at the points $\rho = i\frac{\pi}{2} + ik\pi$, where k is arbitrary integer. The radiation rate will be determined by the poles at $\rho = \pm i\frac{\pi}{2}$, which are the closest ones to the real axis. Since our functions take real values on the real axis, because of their symmetry, it is sufficient to study the behavior near $\rho = i\frac{\pi}{2}$. In order to make the generalization for higher dimensions easier later, for the distance of the singularity from the real axis we introduce the notation P. In the presently discussed one spatial dimensional case $P = \frac{\pi}{2}$. Introducing the variable R by the equation

$$\rho = iP + R\ ,\tag{194}$$

the Laurent series expansion of the function $\operatorname{sech}\rho$ around the point $\rho = iP$ is

$$\operatorname{sech}\rho = -\frac{i}{R}+\frac{iR}{6}-\frac{7iR^3}{360}+\frac{31iR^5}{15120}+\mathcal{O}(R^7)\ .\tag{195}$$

In each term of the expansion the coefficient of R^k is purely imaginary.

For the Fourier modes Φ_k, as functions of the radial coordinate $r = \rho/\varepsilon$, the singularities closest to the real axis are at the points $r = \pm i\frac{P}{\varepsilon}$, hence they get further and further away when the amplitude ε is decreased. Let us introduce the variable y, which measures the distance from the real axis with respect to the scale corresponding to the original radial coordinate r, with the equation

$$r = i\frac{P}{\varepsilon} + y \ . \tag{196}$$

Obviously, then $R = \varepsilon y$. The important observation is, that of the expression $\varepsilon \operatorname{sech} \rho$, which appears at several places in (191)-(193), there is a nonvanishing ε independent part, since

$$\varepsilon \operatorname{sech} \rho = -\frac{i}{y} + \frac{iy}{6}\varepsilon^2 - \frac{7iy^3}{360}\varepsilon^4 + \frac{31iy^5}{15120}\varepsilon^6 + \mathcal{O}(\varepsilon^8) \ . \tag{197}$$

Because of this, in case of the (190) symmetric potential, the behavior of the Fourier modes near the singularity is

$$\Phi_1 = -\frac{2\sqrt{2}\,i}{\sqrt{3}\,y} - \frac{i}{27\sqrt{6}\,y^3}(80g_5 + 3) - \frac{i}{486\sqrt{6}\,y^5}(1600g_5^2 + 240g_5 - 9) + \mathcal{O}(\varepsilon^2) \ , \tag{198}$$

$$\Phi_3 = -\frac{i}{3\sqrt{6}\,y^3} - \frac{i}{108\sqrt{6}\,y^5}(200g_5 - 33) + \mathcal{O}(\varepsilon^2) \ , \tag{199}$$

$$\Phi_5 = -\frac{i}{108\sqrt{6}\,y^5}(8g_5 + 3) + \mathcal{O}(\varepsilon^2) \ . \tag{200}$$

The first terms of all higher Φ_k modes are also proportional to i/y^k. For a general symmetric potential with $g_3 = -1$ the only change in the expansions (198)-(200) would be that in the third term in (198) the constant g_7 also appears. Since the functions obtained by the ε expansion are mirror symmetric on the real axis around $r = 0$, in every term of the expansion the coefficient of y^{-k} is purely imaginary. Because of this, the contribution of all terms are real on the imaginary y axis.

Since it contains positive powers of $1/y$, the approximation (198)-(200) can be applied if $|y|$ is large. At first sight this might appear contradictory, since we are now considering places close to the singularity. However, if ε is small enough, it can be easily satisfied that y is large while the rescaled $R = \varepsilon y$ is still small. The inequality $1 \ll |y| \ll 1/\varepsilon$ describes the matching domain, which is the overlapping part of the inner and outer regions used in the procedure. The expressions (198)-(200) will provide outer boundary condition to the inner problem.

The *outer region* is the part of the complex r plane where the small-amplitude expansion is valid, giving improving approximation with decreasing ε. Obviously, the real r axis is part of this domain. However, the ε expansion fails close to the singularity, where $|y|$ is not large

compared to 1, because the second derivatives of the functions Φ_n are much larger there than the functions themselves.

In order to obtain the precise quasibreather solution that includes the tail, in both regions we have to solve the Fourier mode equations (152) for some frequency ω that is just a little smaller than 1. In our case, with the choice $m = 1$ and $d = 1$, these equations are

$$\frac{\mathrm{d}^2\Phi_n}{\mathrm{d}r^2} + (\omega^2 n^2 - 1)\Phi_n = F_n \ , \tag{201}$$

for odd n. These equations are also valid if we replace the r derivative by y derivative, since the two coordinates are just complex shifted versions of each other, according to (196).

4.4.3 Inner expansion

The *inner region* is the part of the complex plane in the vicinity of the singularity, where $|R| = \varepsilon|y|$ is small. Here we use the shifted, but not rescaled y coordinate. Substituting $\omega^2 = 1 - \varepsilon^2$, we can write (201) as

$$\frac{\mathrm{d}^2\Phi_n}{\mathrm{d}y^2} + (n^2 - \varepsilon^2 n^2 - 1)\Phi_n = F_n \ . \tag{202}$$

The *inner expansion* can be obtained by expanding the Fourier components in powers of ε as

$$\Phi_n = \sum_{j=0}^{\infty} \Phi_n^{(j)} \varepsilon^{2j} \ . \tag{203}$$

Substituting into (202) and considering the identical ε power terms we obtain differential equations for $\Phi_n^{(j)}$, which should be solved in increasing order in j. So far only the equations for $\Phi_n^{(0)}$ has been considered in the literature, which are sufficient for obtaining the leading order tail-amplitude of the quasibreather. The leading order result for the tail-amplitude is precise only for very small ε values, when the tail is so small that one cannot calculate it by spectral numerical methods. Hence it would be important to calculate corrections to the leading order results in the future.

4.4.4 Leading order inner equation

Since we use the y coordinate in the inner region, the $\varepsilon \to 0$ limit of Φ_n is the function $\Phi_n^{(0)}$. The important advantage of the complex extension method is that we obtain a meaningful $\varepsilon \to 0$ limit in the inner region, while in the outer region, especially on the real r axis, the small ε limit of all Φ_n are vanishing, even in the central core domain.

The leading order equation that we have to solve in the inner region can be obtained from (202) by the substitution $\varepsilon = 0$, yielding

$$\frac{\mathrm{d}^2\Phi_n^{(0)}}{\mathrm{d}y^2} + (n^2 - 1)\Phi_n^{(0)} = F_n^{(0)} \ , \tag{204}$$

where the nonlinear source terms $F_n^{(0)}$ are the $\varepsilon \to 0$ limits of F_n. These can be obtained by replacing Φ_n by $\Phi_n^{(0)}$ everywhere in (153). The crucial advantage of equations (204) is that in contrast to (201), it is not necessary to solve them for each ω frequency separately. However, they still determine the leading order tail-amplitude for any small ε.

Substituting the expansion

$$\Phi_{2n-1}^{(0)} = i \sum_{k=n}^{\infty} A_k^{(n)} \frac{1}{y^{2k-1}} \tag{205}$$

into the equations (204), apart from a global ± 1 factor, the constants $A_k^{(n)}$ become uniquely determined. In this way we can directly obtain expressions (198)-(200), and also their higher order generalizations for arbitrary symmetric potentials, without calculating the small-amplitude expansion. The ambiguity in the signature corresponds to the symmetry $\phi \to -\phi$, and related to the choice of the signature of S in (175). The calculation of the expansion in powers of $1/y$ is technically much easier in this direct way, and can be performed to quite high orders by a software package suitable for symbolic algebraic computations. We were able to proceed up to orders of several hundred in powers of $1/y$, even if we used the same large number of Φ_{2n-1} Fourier components. However, it turns out that the consideration of Fourier components higher than Φ_7 influences the magnitude of the radiating tail only extremely slightly. The essential information that comes from the ε expansion procedure is that in the inner region the expansion of all Φ_n Fourier components begin with $1/y^n$ term, and also that the power of $1/y$ increases in steps of two. An important property of the expansion (205) is that all $A_k^{(n)}$ coefficients are purely real.

4.4.5 Asymmetric solution along the imaginary axis

We separate the Fourier mode functions $\Phi_n^{(0)}$ into real and imaginary parts by the notation

$$\Phi_n^{(0)} = \Psi_n + i\Omega_n \ , \tag{206}$$

where Ψ_n and Ω_n are real valued functions, and substitute into equations (204) describing the leading order inner solution. As an alternative to y we introduce the coordinate $\tilde{y} = iy$, which takes increasing real values when coming downwards along the imaginary axis. The linear part of the equations can be written into the form

$$-\frac{\mathrm{d}^2\Omega_n}{\mathrm{d}\tilde{y}^2} + (n^2-1)\Omega_n = 0 \ . \tag{207}$$

The inner solution can only be matched to the exterior solution if in the limit $\tilde{y} \to \infty$ the functions Ω_n tends to zero. For $n \geq 2$ we have the exponentially decaying solutions

$$\Omega_n = \nu_n \exp\left(-\sqrt{n^2-1}\,\tilde{y}\right) \ , \tag{208}$$

where ν_n are constants that should be determined later.

However, to obtain the correct behavior of the functions Ω_n on the imaginary axis the linearized approximation is not enough. Nevertheless, we can get a very precise description if we substitute $\Phi_n^{(0)} = \Psi_n + i\Omega_n$ into (204), and from the terms of F_n given by (153) we only keep those terms that are linear in the exponentially small variables Ω_k. For all Ψ_n we can substitute the approximation of the Φ_n functions given by the expansion (205). In this way we get coupled linear differential equations for the functions Ω_n along the imaginary axis.

In each Ω_k the other Ω_n generate contributions that decay as $\exp(-\sqrt{n^2-1}\,\tilde{y})$. For large values of $\tilde{y}$ the less quickly decaying exponential mode will dominate, which is Φ_3 for symmetric potentials. Taking into account terms multiplied by powers of $1/\tilde{y}$, in case of the symmetric sixth-order potential (190) one can obtain the following result:

$$\Omega_1 = \nu_3 \exp\left(-\sqrt{8}\,\tilde{y}\right)\left(\frac{1}{4\tilde{y}^2} - \frac{1}{4\sqrt{2}\,\tilde{y}^3} + \dots\right), \tag{209}$$

$$\Omega_3 = \nu_3 \exp\left(-\sqrt{8}\,\tilde{y}\right)\left(1 + \frac{1}{\sqrt{2}\,\tilde{y}} + \frac{1}{8\tilde{y}^2} - \frac{260g_5+3}{162\sqrt{2}\,\tilde{y}^3} + \dots\right), \tag{210}$$

$$\Omega_5 = \nu_3 \exp\left(-\sqrt{8}\,\tilde{y}\right)\left(-\frac{1}{8\tilde{y}^2} - \frac{1}{4\sqrt{2}\,\tilde{y}^3} + \dots\right). \tag{211}$$

We will present two methods that can be used to calculate the coefficient ν_3. The first is a numerical method which has been developed by Segur and Kruskal [10]. We solve equations (204) for the functions $\Phi_n^{(0)} = \Psi_n + i\Omega_n$ by numerically integrating along a constant $\operatorname{Im} y = y_i$ line, where $y_i < 0$, starting from a large positive value of $\operatorname{Re} y = y_r$. Since we are dealing with second-order differential equations, as initial value at the point $y = y_r + iy_i$ we use the series (205) calculated up to some order in $1/y$, and also the derivative of the same truncated series expression. Reaching to the imaginary axis $\operatorname{Re} y = 0$ at the point $y = iy_i$, from the numerically obtained value of Ω_3 we calculate the coefficient ν_3 using (210).

This method is based on the assumption that the in the vicinity of the starting point $y = y_r + iy_i$ the series (205) gives good approximation to $\Phi_n^{(0)}$. Since we start with large positive y_r, this implies that the obtained solutions will have no oscillations on the right hand side, hence they correspond to the Fourier components of the *asymmetric breather* solution $\phi \equiv \phi_-$ which has no tail for $r > 0$. This solution has a core very similar to the minimal tail quasibreather solution ϕ_{m}, but on the left side it may have a double amplitude tail, or more likely a movable singularity. We are not aware of any numerical results up to now that could establish the behavior of ϕ_- for $r < 0$. However the important point for us is that for $r > 0$ the difference of the solutions ϕ_- and ϕ_{m} is exponentially small in terms of ε.

The numerical solution can be calculated by taking into account only a finite number of Φ_n modes. Keeping the Fourier modes up to Φ_7 already gives extremely precise results. For the initial values the expansion (205) up to order $1/y^{10}$ is appropriate. Typical place of the

line of integration is at $y_i = -7$ with starting point $y_r = 300$. The result for ν_3 depends on the parameter g_5 in the potential (190). For $g_5 = 1$ the result for seven digits is

$$\nu_3 = -0.9097496 \ . \tag{212}$$

4.4.6 Asymptotic behavior of the coefficients

The second method for the determination of the constant ν_3 in (210) requires the analysis of the large k behavior of the coefficients $A_k^{(n)}$ in the expansion (205) of the Fourier components $\Phi_{2n-1}^{(0)}$. This analytic method has been applied first to the fifth-order KdV equation in [11] using Borel summation. An equivalent procedure using Laplace transform has been presented in [140]. We have generalized the method for one-dimensional oscillons in [62].

The large k behavior of the coefficients will be controlled by the fastest increasing coefficients, $A_k^{(2)}$. The dominant behavior is governed by the linear left hand side of (204),

$$(2k-3)(2k-2)A_{k-1}^{(2)} + 8A_k^{(2)} = 0 \ . \tag{213}$$

This shows that the leading order behavior for large k is

$$A_k^{(2)} = K_2(-1)^k \frac{(2k-2)!}{8^{k-1/2}} \ , \tag{214}$$

where K_2 is a constant. Through the nonlinear terms this will determine the asymptotic behavior of the other coefficients as well.

To leading order the coefficients of Φ_1 are determined by the equation

$$(2k-3)(2k-2)A_{k-1}^{(1)} = -\frac{3g_3}{4}\left(A_1^{(1)}\right)^2 A_{k-1}^{(2)} \ , \tag{215}$$

where the right-hand side comes from the nonlinear term in (204) proportional to $\left(\Phi_1^{(0)}\right)^2\Phi_3^{(0)}$. The solution which is valid for large values of k is $A_k^{(1)} = \frac{1}{2}k^{-2}A_k^{(2)}$. Equations for all other $A_k^{(n)}$ can be constructed in a similar way. It turns out that for large k the coefficients $A_k^{(n)}$ grow proportionally to $k^{4-2n}A_k^{(2)}$ for $n \geq 3$.

The behavior of the dominant $A_k^{(2)}$ can be more precisely determined if we also take into account a nonlinear term proportional to $\left(\Phi_1^{(0)}\right)^2\Phi_2^{(0)}$. It turns out that

$$A_k^{(2)} = K_2(-1)^k \frac{(2k-2)!}{8^{k-1/2}}\left(1 + \frac{1}{k} + \frac{5}{4k^2}\right) \ , \tag{216}$$

apart from corrections of order $1/k^3$ and higher. Using this identity we can calculate rather precisely the value of the constant K_2, even from not too high order $A_k^{(2)}$ coefficients. For example, for the sixth-order symmetric potential (190) in case of $g_5 = 1$ we get

$$K_2 = 0.5791646 \ . \tag{217}$$

The value of the constant K_2 is important, because as we will see soon, a simple formula connects it with the coefficient ν_3.

4.4.7 Laplace transform

Our aim is to get the imaginary part of the dominant radiating mode $\Phi_3^{(0)}$ along the lower part of the imaginary y axis. The calculation using Borel transform has been already presented in [62, 155]. Here we apply a somewhat simpler but equivalent Laplace transform method, which has been already discussed for the linear model problem in Subsection 2.8, and also for the fKdV problem in Subsection 3.5. According to (205), the following series is asymptotic to the function $\Phi_3^{(0)}$,

$$\Phi_3^{(0)} = i \sum_{k=2}^{\infty} A_k^{(2)} \frac{1}{y^{2k-1}} \ . \tag{218}$$

Since all individual terms are real on the imaginary axis, the imaginary part will be determined by the large k behavior of the coefficients. Hence we assume that all $A_k^{(2)}$ coefficients are given by the expression (214).

We can now look for $\Phi_3^{(0)}$ as the Laplace transform of a function that we denote by $V'(s)$,

$$\Phi_3^{(0)} = \int_{\tilde{\gamma}} I(s) \mathrm{d}s \quad , \quad I(s) = \exp(-ys) V'(s) \ , \tag{219}$$

where the contour $\tilde{\gamma}$ can be any path from $s = 0$ to infinity, along which $\mathrm{Re}(ys) \to \infty$. Since the Laplace transform of s^n is $n! y^{-n-1}$, it follows that the function $V'(s)$ can be expanded as

$$V'(s) = \sum_{k=2}^{\infty} \frac{i A_k^{(2)}}{(2k-2)!} s^{2k-2} = i K_2 \sum_{k=2}^{\infty} \frac{(-1)^k}{8^{k-1/2}} s^{2k-2} \ . \tag{220}$$

The sum is convergent, and yields

$$V'(s) = \frac{i K_2 s^2}{\sqrt{8}(s^2+8)} \ . \tag{221}$$

It can be seen that the function $V'(s)$ has a pole at $s = i\sqrt{8}$, with residue $-\frac{1}{2}K_2$. The residue of the integrand $I(s)$ in (219) is then $-\frac{1}{2}K_2 \exp(-\sqrt{8}\, iy)$. As it has been discussed for the linear model problem and the fKdV equation, choosing the contour $\tilde{\gamma}$ of integral along the upper half of the imaginary s axis, avoiding the pole at $s = i\sqrt{8}$ in a small half-circle from the right, we obtain the asymmetric solution $\Phi_{3,-}^{(0)}$ that decays without any oscillations in the right hand side of the complex y plane. Consequently, it corresponds to the asymmetric breather solution ϕ_-, which has no tail for $r > 0$, but it is slightly asymmetric with respect to $r = 0$. Only the small half-circle gives contribution to the imaginary part of the integral, which is half of the value that can be obtained by the residue theorem. It follows that

$$\mathrm{Im}\, \Phi_{3,-}^{(0)} = -\frac{1}{2}\pi K_2 \exp(-\sqrt{8}\, iy) \quad \text{for} \quad \mathrm{Re}\, y = 0 \ \text{and} \ \mathrm{Im}\, y < 0 \ . \tag{222}$$

Comparing with (210), where $\tilde{y} = iy$, we obtain the result

$$\nu_3 = -\frac{K_2 \pi}{2} \ . \tag{223}$$

This relation is valid for any symmetric potential $U(\phi)$. In case of the sixth-order symmetric potential given in (190) and for the choice $g_5 = 1$, the value of K_2 given in (217) corresponds to $\nu_3 = -0.9097496$, which agrees with the value written earlier in (212). The good agreement of the results obtained by the two independent calculations gives strong support for the correctness of both the numerical and analytic methods. The calculation of ν_3 from the value of K_2 is technically much easier than the earlier presented numerical method. In Figure 20 we show the dependence of ν_3 on the parameter g_5.

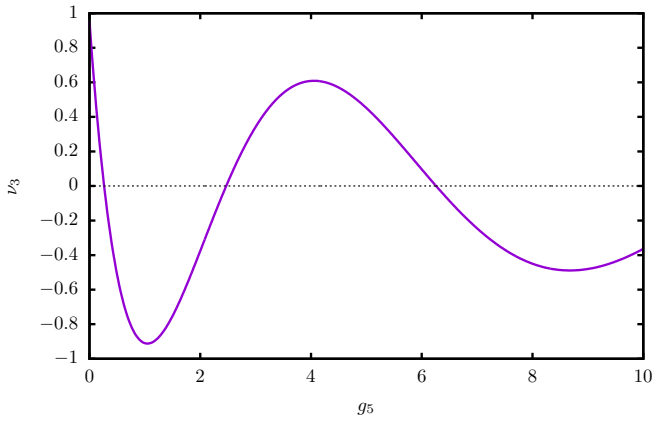

Figure 20: The coefficient ν_3 as a function of the parameter g_5 for the symmetric sixth-order potential (190).

4.4.8 Tail-amplitude

Similarly to our analysis of the fKdV problem, we use the property that the difference of the minimal tail-amplitude quasibreather $\phi_{\rm m}$ and asymmetric breather solution ϕ_- is very small. The function defined as $w = \phi_{\rm m} - \phi_-$ is small in the core region, on the right side of the core, and also in large regions of the complex r plane. For the $\cos(n\omega t)$ Fourier components of w we can write

$$w_n = \Phi_{n,{\rm m}} - \Phi_{n,-} \ , \tag{224}$$

where $\Phi_{n,{\rm m}}$ and and $\Phi_{n,-}$ are the Fourier components of $\phi_{\rm m}$ and ϕ_-. Substituting $\Phi_n \to \Phi_n + w_n$ into (201) and dropping terms containing products or powers of w_n, we obtain a system of equations linear in w_n. Then we can represent the background Φ_n by the outer expansion result (191)-(193). The solution of this system for w_n will approximate $\Phi_{n,{\rm m}} - \Phi_{n,-}$ extremely well, since this difference is exponentially small in terms of ε. Since we are interested in the result for small ε, we substitute $\omega = 1$. The originally nonlinear terms on the right hand side go to zero in the $\varepsilon \to 0$ limit, hence we can consider only the linear part on the left side. The leading order solution for the dominating $\cos(3t)$ radiative

mode turns out to be

$$w_3 = \beta \sin\left(\sqrt{8}\, r - \delta\right) \ , \tag{225}$$

where the amplitude β and the phase δ are constants. In a higher order version the amplitude and phase would include r dependent $\mathcal{O}(\varepsilon)$ contributions, similarly to the WKB result (69) in case of the fKdV problem.

If the Fourier component Φ_3 of a symmetric solution ϕ contains a tail component proportional to $\cos\left(\sqrt{8}\, r\right)$, then one can cancel it by adding the linearized solution w_3 with phase $\delta = \frac{\pi}{2}$, decreasing its tail-amplitude while keeping the symmetry. It follows that in the tail region the solution $\phi_{\rm m}$ has the Fourier component

$$\Phi_{3,{\rm m}} = \alpha_3 \sin\left(\sqrt{8}\, r\right) \ , \tag{226}$$

where α_3 is the minimal tail-amplitude that we intend to express in terms of the constant ν_3. Note that α_3 may turn out to be negative, which can be interpreted as a tail shifted by phase π. Canceling the tail in (226) by subtracting w_3 given by (225) with $\beta = \alpha_3$ and $\delta = 0$ we obtain a very good approximation of the asymmetric solution $\Phi_{3,-}$. Hence the difference $\Phi_{3,{\rm m}} - \Phi_{3,-}$ is given by

$$w_3 = \alpha_3 \sin\left(\sqrt{8}\, r\right) \ . \tag{227}$$

This is valid globally, including the core domain, not just in the tail region as (226).

We extend the linearized solution to the complex plane and consider the behavior close to the first singularity above the real axis by substituting $r = i\frac{P}{\varepsilon} + y$ according to (196). For the currently discussed one-dimensional case the distance to the singularity is $P = \frac{\pi}{2}$. Writing the result for w_3 in terms of the exponential function we can neglect the term proportional to $\exp\left(-\sqrt{8}\,\frac{P}{\varepsilon}\right)$. We obtain

$$w_3 = \frac{i}{2}\alpha_3 \exp\left(\sqrt{8}\,\frac{P}{\varepsilon}\right) \exp\left(-\sqrt{8}\, iy\right) \ . \tag{228}$$

Because of its symmetry, the Fourier component $\Phi_{3,{\rm m}}$ is purely real along the imaginary y axis. In the small ε limit the asymmetric solution $\Phi_{3,-}$ tends to the leading order inner solution $\Phi^{(0)}_{3,-}$, which has the imaginary part $\nu_3 \exp\left(-\sqrt{8}\, iy\right)$ according to (210). From (224) it follows that $\mathrm{Im}\, w_3 = -\,\mathrm{Im}\, \Phi^{(0)}_{3,-}$, which yields

$$\alpha_3 = -2\nu_3 \exp\left(-\sqrt{8}\,\frac{P}{\varepsilon}\right) \ . \tag{229}$$

The parameter ε is determined by the frequency of the state through the relation $\varepsilon = \sqrt{1-\omega^2}$.

The constant α_3 corresponds to the amplitude parameter in equation (146) that describes the general behavior of a standing wave tail. Hence the energy current averaged for an

oscillation period, $\bar{S}$, can be calculated by applying (148). In the one-dimensional case, for symmetric potentials $\bar{S} = 3\sqrt{8}\alpha^2$, and hence

$$\bar{S} = 24\sqrt{2}\,\nu_3^2 \exp\left(-\sqrt{8}\,\frac{\pi}{\varepsilon}\right) \ . \tag{230}$$

In Figure 21 we show the radiation rate for the ϕ^6 potential given in (190), for the case

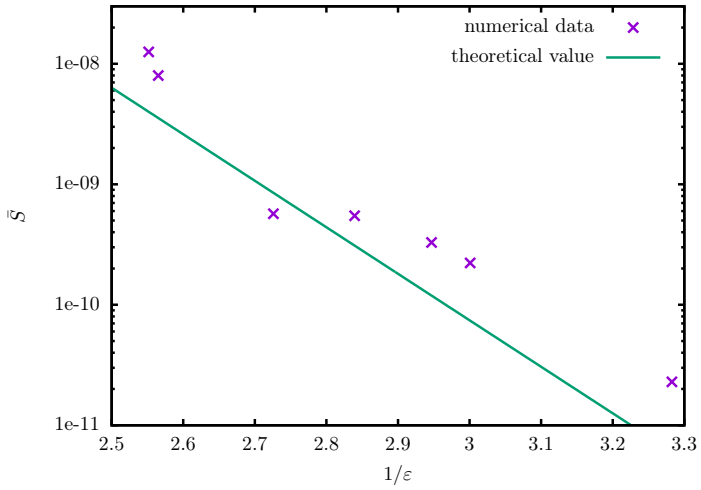

Figure 21: The value of the time averaged energy current $\bar{S}$ for the symmetric ϕ^6 potential in case of $g_5 = 1$, as a function of $1/\varepsilon$.

$g_5 = 1$. The analytical result for the time averaged energy current is given by (230), where according to (212) we have $\nu_3 = -0.9097496$. The numerical results have been obtained by our time-evolution code, using initial data provided by the small-amplitude expansion procedure. The agreement is reasonably good, but higher order expansion results and more efficient numerical codes should be worked out in the future.

4.5 Non-symmetric potentials

In case of $d = 1$ spatial dimension, if the potential $U(\phi)$ is not symmetric around its minimum, we can still calculate the magnitude of the radiation tail by a method similar to the one presented up to here. In the Fourier expansion (149) of the scalar field there are both even and odd indexed Φ_n terms in this case. We extend the functions, the equations and the small-amplitude expansion results into the complex r plane. In the vicinity of the singularity which is closest to the real axis we introduce the coordinate y by the relation (196), where $P = \frac{\pi}{2}$ in the one-dimensional case. In the outer region we still solve equations (201), while in the inner region we solve the leading order equations (204), where the nonlinear terms F_n are given by (153) in both cases.

Based on the complex extension of the small-amplitude expansion results (184) - (187), we look for the solution of the inner equations in the form

$$\Phi_n^{(0)} = \sum_{k=0}^{\infty} a_{n+2k}^{(n)} \frac{1}{y^{n+2k}} \ . \tag{231}$$

Substituting into the inner equations (204), we obtain

$$\begin{aligned}
\Phi_0^{(0)} &= \frac{g_2}{\lambda}\frac{1}{y^2} + \frac{169g_2^3\lambda + 144g_2\lambda^2 + 72g_2\sigma - 81g_4\lambda}{54\lambda^3}\frac{1}{y^4} + \dots \ , \\
\Phi_1^{(0)} &= -\frac{i\sqrt{2}}{\sqrt{\lambda}}\frac{1}{y} - \frac{i\sqrt{2}(19g_2^2\lambda + 18\sigma)}{27\lambda^2\sqrt{\lambda}}\frac{1}{y^3} + \dots \ , \\
\Phi_2^{(0)} &= -\frac{g_2}{3\lambda}\frac{1}{y^2} - \frac{220g_2^3\lambda - 243g_2\lambda^2 + 72g_2\sigma - 108g_4\lambda}{162\lambda^3}\frac{1}{y^4} + \dots \ , \\
\Phi_3^{(0)} &= \frac{i\sqrt{2}\,(4g_2^2 - 3\lambda)}{36\lambda\sqrt{\lambda}}\frac{1}{y^3} + \dots \ ,
\end{aligned} \tag{232}$$

where the definition of the constant λ is in (172), and σ is given in (180). The coefficients $a_{2k}^{(2n)}$ belonging to the Fourier components $\Phi_{2n}^{(0)}$ are always purely real, while the coefficients $a_{2k+1}^{(2n+1)}$ belonging to $\Phi_{2n+1}^{(0)}$ are purely imaginary.

In the same way as in (206), we decompose the Fourier components into real and imaginary parts, $\Phi_n^{(0)} = \Psi_n + i\Omega_n$. For the asymmetric potential the dominating radiating mode is Φ_2, which also dominates the imaginary part along the imaginary y axis. Into the nonlinear terms in (204) for the functions Ψ_n we substitute $\Phi_n^{(0)}$ given by the expansion (231), and we keep only linear terms in Ω_n. Solving the coupled linearized system along the imaginary axis using the coordinate $\tilde{y} = iy$, we obtain

$$\Omega_0 = \nu_2 \exp\left(-\sqrt{3}\,\tilde{y}\right)\left(-\frac{2g_2^2 - 3\lambda}{6\lambda\tilde{y}^2} + \frac{\sqrt{3}(16g_2^4 - 24g_2^2\lambda - 45\lambda^2)}{270\lambda^2\tilde{y}^3} + \dots\right) \ , \tag{233}$$

$$\Omega_1 = \nu_2 \exp\left(-\sqrt{3}\,\tilde{y}\right)\left(-\frac{\sqrt{2}g_2}{3\sqrt{\lambda}\tilde{y}} + \frac{8\sqrt{6}g_2^3}{135\sqrt{\lambda^3}\tilde{y}^2} + \dots\right) \ , \tag{234}$$

$$\Omega_2 = \nu_2 \exp\left(-\sqrt{3}\,\tilde{y}\right)\left(1 - \frac{2\sqrt{3}(4g_2^2 - 15\lambda)}{45\lambda\tilde{y}} + \frac{32g_2^4 - 282g_2^2\lambda + 255\lambda^2}{675\lambda^2\tilde{y}^2} + \dots\right) \ , \tag{235}$$

$$\Omega_3 = \nu_2 \exp\left(-\sqrt{3}\,\tilde{y}\right)\left(\frac{\sqrt{2}g_2}{5\sqrt{\lambda}\tilde{y}} - \frac{8\sqrt{6}g_2(g_2^2 - 6\lambda)}{225\sqrt{\lambda^3}\tilde{y}^2} + \dots\right) \ , \tag{236}$$

where ν_2 is a constant that will be used to calculate the radiation amplitude.

The coefficient ν_2 has been calculated first numerically by Segur and Kruskal [10] for the case of the ϕ^4 potential. We have improved the calculation by taking into account more Fourier modes in [62, 155]. We take the potential in the form $U(\phi) = \frac{1}{8}\phi^2\,(\phi - 2)^2$, in which

case $m = 1$ and the nonvanishing expansion coefficients are $g_2 = -3/2$ and $g_3 = 1/2$. Apart from a technical difficulty, the method for the numerical determination of ν_2 is similar to the technique that was described after equation (211). We solve numerically the differential equations (204) for the complex functions $\Phi_n^{(0)} = \Psi_n + i\Omega_n$ along a constant $\mathrm{Im}\, y = y_i$ line, starting from a large value of $\mathrm{Re}\, y = y_r$, until we reach the imaginary axis at $\mathrm{Re}\, y = 0$. As initial value, we use at the point $y = y_r + iy_i$ the series (232) calculated up to a certain $1/y^n$ order, and its derivative. Reaching the imaginary axis, from the value of Ω_2 we intend to calculate the coefficient ν_2 using (235). However, the determination of the numerical solution as an initial value problem from the point $y = y_r + iy_i$ is problematic, because of the exponential behavior of $\Phi_0^{(0)}$. Hence, following the method of Segur and Kruskal [10], at the point $y = y_r + iy_i$ we only fix the value of $\Phi_0^{(0)} = \Psi_0 + i\Omega_0$, but not its derivative. We exchange the missing two requirements by the boundary conditions $\Omega_0 = 0$ and $\frac{\mathrm{d}}{\mathrm{d}y}\Psi_0 = 0$ at the point $y = iy_i$ on the imaginary axis. For the other $\Phi_n^{(0)}$ components we still give their values and derivatives at the point $y = y_r + iy_i$. We used the Maple software package to solve the coupled differential equations as boundary value problems. We have obtained the result [62, 155]

$$\nu_2 = 8.38866 \cdot 10^{-3} \pm 1 \cdot 10^{-7} \ . \tag{237}$$

Using our notation the result of Segur and Kruskal [10] has been $\nu_2 = (9.0 \pm 2.0) \cdot 10^{-3}$. Their main aim was to show that ν_2 is nonzero, hence no ϕ^4 breather can exist. No analytical method is known for the calculation of the coefficient ν_2 in case of asymmetric potentials.

The tail-amplitude amplitude α_2 of the quasibreather solution can be determined in an analogous way as for the symmetric potential in Subsection 4.4.8. The difference $\Phi_{2,\mathrm{m}} - \Phi_{2,-}$ is given by

$$w_2 = \alpha_2 \sin\left(\sqrt{3}\, r\right) \ . \tag{238}$$

Extending the linearized solution to the complex plane and neglecting an exponentially small term above the real axis, in the matching region we obtain

$$w_2 = \frac{i}{2}\alpha_2 \exp\left(\sqrt{3}\,\frac{P}{\varepsilon}\right) \exp\left(-\sqrt{3}\, iy\right) \ . \tag{239}$$

Because of its symmetry, the Fourier component $\Phi_{2,\mathrm{m}}$ is purely real along the imaginary y axis. Hence $\mathrm{Im}\, w_2 = -\,\mathrm{Im}\, \Phi_{2,-}^{(0)}$ for $\mathrm{Re}\, y = 0$ and $\mathrm{Im}\, y < 0$. According to (235), to leading order $\mathrm{Im}\, \Phi_{2,-}^{(0)} = \nu_2 \exp\left(-\sqrt{3}\, iy\right)$, hence for the minimal tail-amplitude we obtain

$$\alpha_2 = -2\nu_2 \exp\left(-\sqrt{3}\,\frac{P}{\varepsilon}\right) \ , \tag{240}$$

where $P = \frac{\pi}{2}$. Using (148), for the radiated energy current averaged to an oscillation period we obtain

$$\bar{S} = 8\sqrt{3}\,\nu_2^2 \exp\left(-\frac{\sqrt{3}\,\pi}{\varepsilon}\right) . \tag{241}$$

For one-dimensional ϕ^4 oscillons, in Figure 22 we show the numerically calculated energy

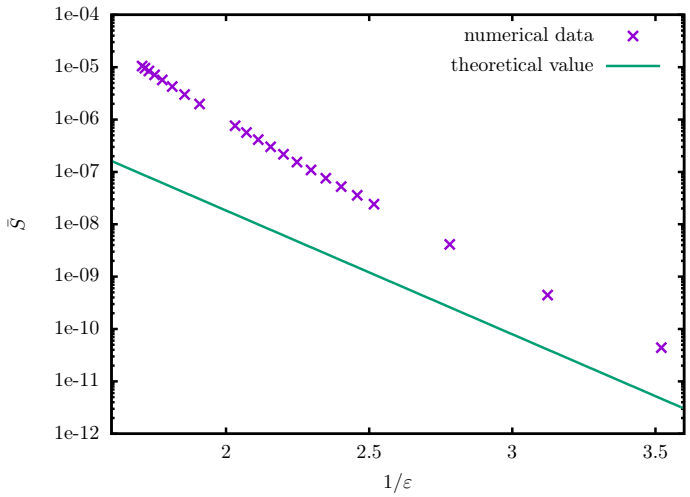

Figure 22: The time averaged energy current $\bar{S}$ for ϕ^4 oscillons as a function of the reciprocal of the parameter ε calculated from the frequency.

current averaged over an oscillation period, and compare it to the theoretical result given by (237) and (241). It can be seen that for those relatively large amplitude oscillons for which we were able to determine the energy loss numerically, the radiation is one or two magnitude larger than the theoretically predicted value. The obvious reason for this is that our analytic results are valid only to leading order, for small enough ε values. Nevertheless, it can be seen that by the decrease of the parameter ε the numerical data gets closer to the theoretical value. For the ϕ^4 potential the value of the radiation coefficient is very small, $\nu_2 = 8.38866 \cdot 10^{-3}$, which makes the numerical checking of the analytical result especially difficult.

4.6 Spherically symmetric oscillons

The radiation of higher dimensional spherically symmetric oscillon states can be calculated similarly to the one-dimensional case, but the procedure is technically more complicated [63]. We look for time-periodic quasibreather solutions with frequency ω, and we intend to determine their tail-amplitude. The components Φ_n of the Fourier expansion (149) satisfy the equations (152), which for a scalar field with mass $m = 1$ can be written as

$$\frac{\mathrm{d}^2\Phi_n}{\mathrm{d}r^2} + \frac{d-1}{r}\frac{\mathrm{d}\Phi_n}{\mathrm{d}r} + (n^2\omega^2 - 1)\Phi_n = F_n \ . \tag{242}$$

The F_n expressions on the right-hand side are given by (153). The frequency ω is related to the amplitude parameter ε by $\varepsilon^2 = 1 - \omega^2$. We extend equations (242) into the complex r plane, and investigate the behavior of the solutions around the singularity which is closest to

the real axis. In order to achieve this, we first need to study the small-amplitude expansion results, which has been presented in Section 4.3 for arbitrary dimensions.

Based on the expressions (184)-(187), the first few Fourier components are

$$\Phi_0 = -\varepsilon^2 \frac{1}{2} g_2 p_1^2 + \varepsilon^4 \left[-g_2 p_1^2 - g_2 p_1 p_3 + \frac{1}{6} g_2 \lambda p_1^4 - g_2 \left(\frac{\mathrm{d}p_1}{\mathrm{d}\rho} \right)^2 + \frac{31}{72} g_2^3 p_1^4 - \frac{3}{8} g_4 p_1^4 \right] + \cdots , \tag{243}$$

$$\Phi_1 = \varepsilon p_1 + \varepsilon^3 p_3 + \cdots , \tag{244}$$

$$\Phi_2 = \varepsilon^2 \frac{1}{6} g_2 p_1^2 - \varepsilon^4 \frac{1}{72} \left[8 g_2 \left(\frac{\mathrm{d}p_1}{\mathrm{d}\rho} \right)^2 - 12 g_4 p_1^4 + 16 g_2^3 p_1^4 - 24 g_2 p_1 p_3 - 23 g_2 \lambda p_1^4 - 8 g_2 p_1^2 \right] + \cdots , \tag{245}$$

$$\Phi_3 = \varepsilon^3 \frac{1}{72} (4 g_2^2 - 3\lambda) p_1^3 + \cdots , \tag{246}$$

$$\Phi_4 = \varepsilon^4 \frac{1}{360} p_1^4 \left(3 g_4 - 5 g_2 \lambda + 5 g_2^3 \right) + \cdots . \tag{247}$$

The function p_1 is connected to S by the relation $S = \sqrt{\lambda}\, p_1$. The function S is determined by the base equation (174), where $\tilde{\Delta}$ is the Laplacian belonging to the coordinate $\rho = \varepsilon r$, given by (163). The solution S determines the Fourier components Φ_n up to order ε^2.

The important difference with respect to the one-dimensional case is that for higher dimensions the asymptotically decaying regular, nodeless solution for S is only known in a numerical form. As we have seen, for one spatial dimension $S = \sqrt{2}\,\mathrm{sech}\,\rho$. From the study of the base equation (174) it also follows that small-amplitude oscillons exist only for $d \leq 3$ spatial dimensions [61]. The numerical value of the solution S at the central point was given in (176) for $d = 2$ and $d = 3$ spatial dimensions. The position $\rho = iP$ of the singularity closest to the real axis can be found by numerical solution of the differential equation along the imaginary axis, yielding

$$P = \begin{cases} 1.0925562 & \text{for } \; d = 2 \; , \\ 0.6021836 & \text{for } \; d = 3 \; . \end{cases} \tag{248}$$

For $d = 1$ spatial dimension $P = \frac{\pi}{2} \approx 1.5707963$.

In the more than one dimensional case the singularity is not a simple pole as in (195), but because of the appearing logarithmic terms it is a branch point. Introducing R by $\rho = iP + R$, the expansion of S contains the following terms:

$$S = \sum_{k=0}^{\infty} \sum_{j=4k-1}^{\infty} S_{j,k}\, R^j \left[\ln(iR) \right]^k \; . \tag{249}$$

The constants $S_{j,k}$ are real for even j, and purely imaginary for odd j, hence S takes real

values on the imaginary axis. The first few orders of the expansion are:

$$\begin{aligned} S = &-\frac{i\sqrt{2}}{R} + \frac{\sqrt{2}(d-1)}{6P} - \frac{i\sqrt{2}(d^2-6P^2-8d+7)}{36P^2}R \\ &- \frac{\sqrt{2}(d-1)(4d^2-18P^2-35d+85)}{216P^3}R^2 \\ &- \frac{i\sqrt{2}(d-1)(2d^3-9dP^2-21d^2+18P^2+72d-80)}{135P^4}R^3\ln(iR) + \cdots \ . \end{aligned} \tag{250}$$

In order to calculate the Fourier components Φ_n up to order ε^4 using equations (243)-(247), it is necessary to know the function p_3. This function is related by the expression (179) to the potential independent function Z, which can be obtained by the solution of (181). For one space dimension Z can be obtained by the equations (182) and (175). For $d \geq 2$ the behavior of the function Z on the imaginary axis can be studied by the numerical solution of the differential equation, using the central values given in (183). The first few terms of the expansion of Z are:

$$\begin{aligned} Z = &-\frac{i2\sqrt{2}}{3R^3} - \frac{8\sqrt{2}(d-1)}{15P}\frac{\ln(iR)}{R^2} + Z_{-2,0}\frac{1}{R^2} + \frac{i\sqrt{2}(d^2-45P^2-32d+31)}{45P^2}\frac{1}{R} \\ &+ \frac{2\sqrt{2}(d-1)(d^2-6P^2+2d+1)}{135P^3}\ln(iR) + \cdots \ , \end{aligned} \tag{251}$$

where the constant $Z_{-2,0}$ can be obtained by numerical methods.

4.6.1 Inner solution

In the expressions (243)-(247) the function p_1 always appears with at least one ε factor. Similarly, p_3 has at least ε^3 factor. According to (196) we introduce the $y = R/\varepsilon$ inner coordinate for more than one dimensions as well. Hence up to order ε,

$$\varepsilon S = \frac{-i\sqrt{2}}{y} + \varepsilon\frac{\sqrt{2}(d-1)}{6P} \ , \tag{252}$$

$$\varepsilon^3 Z = -\frac{i2\sqrt{2}}{3}\frac{1}{y^3} - \varepsilon\ln\varepsilon\,\frac{8\sqrt{2}(d-1)}{15P}\frac{1}{y^2} - \varepsilon\,\frac{8\sqrt{2}\,(d-1)}{15\,P}\frac{\ln(iy)}{y^2} + \varepsilon\,Z_{-2,0}\frac{1}{y^2} \ . \tag{253}$$

Based on these considerations, substituting into (243)-(247), the *inner expansion* of the Fourier components Φ_n in terms of ε starts in the following way:

$$\Phi_n = \Phi_n^{(0)} + \varepsilon\ln\varepsilon\,\Phi_n^{(1)} + \varepsilon\,\Phi_n^{(2)} + \mathcal{O}(\varepsilon^2\ln\varepsilon) \ , \tag{254}$$

where the functions $\Phi_n^{(k)}$ are already ε independent.

Using the coordinate y in the inner region, the first terms of the expressions (252) and (253), which are ε independent, are also independent of the dimension d. Since the parameter d does not appear in (243)-(247) either, the functions $\Phi_n^{(0)}$ will be the same as in the earlier

discussed one-dimensional case. Hence the first terms of the expansion of $\Phi_n^{(0)}$ are given by (232). By this we have shown that the leading order behavior of the Fourier modes in the inner region are dimension independent, and we can apply the one-dimensional results that were presented in detail earlier. Only the position of the singularity is changing for different dimensions, according to (248). Since it is relatively easy to calculate the next order correction for small ε, we continue with the study of the $\varepsilon \ln \varepsilon$ term in (254).

The terms of the functions $\Phi_n^{(1)}$ which can be obtained from equations (243)-(247) are

$$\begin{aligned} \Phi_0^{(1)} &= -\frac{16ig_2(d-1)\sigma}{15\lambda^3 P}\,\frac{1}{y^3} + \dots \ , \\ \Phi_1^{(1)} &= -\frac{8\sqrt{2}(d-1)\sigma}{15\lambda^2\sqrt{\lambda}\,P}\,\frac{1}{y^2} + \dots \ , \\ \Phi_2^{(1)} &= \frac{16ig_2(d-1)\sigma}{45\lambda^3 P}\,\frac{1}{y^3} + \dots \ , \end{aligned} \tag{255}$$

where the definition of the constant σ was given in (180). These and the values of $\Phi_n^{(0)}$ given by (232) are consistent with the relation

$$\Phi_n^{(1)} = C\frac{\mathrm{d}}{\mathrm{d}y}\Phi_n^{(0)} \ , \tag{256}$$

where the constant C is given by

$$C = \frac{8i(d-1)\sigma}{15\lambda^2 P} \ . \tag{257}$$

It can be checked that $\Phi_n^{(1)}$ given by (256) is really the appropriate solution of the $\varepsilon \ln \varepsilon$ part of the inner Fourier mode equations [63, 155]. However, the value of the constant C can be obtained only from the small-amplitude expansion.

For a potential $U(\phi)$ which is not symmetric around its minimum, the imaginary part along the imaginary y axis is dominated by the second Fourier mode, which is also the main radiating mode. The imaginary part of the asymmetric solution $\Phi_{2,-}^{(0)}$ is still given by (235). For a symmetric potential the imaginary part and the radiation is dominated by the third mode, and $\mathrm{Im}\,\Phi_{3,-}^{(0)}$ is given by (210). We can write the leading order behavior along the lower half of the imaginary y axis for both cases in the following unified way:

$$\mathrm{Im}\,\Phi_{k,-}^{(0)} = \nu_k \exp(-i\sqrt{k^2-1}\,y) \ , \tag{258}$$

where now and in the rest of this subsection we set $k = 3$ for potentials symmetric around their minimum, and $k = 2$ for asymmetric potentials. The value of ν_k is exactly the same as for one-dimension, we can use the numerical or Laplace transform results obtained there.

From (256) it follows that the $\varepsilon \ln \varepsilon$ component along the imaginary axis behaves as

$$\mathrm{Im}\,\Phi_{k,-}^{(1)} = \sqrt{k^2-1}\,C\nu_k \exp(-i\sqrt{k^2-1}\,y) \ , \tag{259}$$

where the constant C is given in (257). Taking into account the order $\varepsilon \ln \varepsilon$ contributions but neglecting order ε and higher order terms, the imaginary part of the full kth Fourier component behaves as

$$\mathrm{Im}\, \Phi_{k,-} = i\nu_k \left(1 + \widetilde{C}\, \varepsilon \ln \varepsilon\right) \exp(-i\sqrt{k^2-1}\, y) \tag{260}$$

for $\mathrm{Re}\, y = 0$, $\mathrm{Im}\, y < 0$, where $\widetilde{C} = -i\sqrt{k^2-1}\, C$ is a constant. It is a real number,

$$\widetilde{C} = \sqrt{k^2-1}\, \frac{8(d-1)\sigma}{15\lambda^2 P} \ . \tag{261}$$

4.6.2 Linearized solution

We write the small difference of the minimal tail and the asymmetric Fourier component solutions as

$$w_k = \Phi_{k,\mathrm{m}} - \Phi_{k,-} \ . \tag{262}$$

Note that although the asymmetric solution is singular at $r = 0$, the differences w_k are small in the tail region and in most of the core region, also including the complex extension.

Similarly to the one-dimensional case, w_k can be well approximated by the solution of the linearized version of equation (242). The linearized equation can be obtained by dropping the terms on the right-hand side, and since ε is small we can take $\omega = 1$. For d spatial dimensions the general solution can be written in terms of Bessel functions,

$$w_k = \sqrt[4]{k^2-1}\sqrt{\frac{\pi}{2}}\, r^{1-\frac{d}{2}} \left[\alpha_k Y_{\frac{d}{2}-1}\left(\sqrt{k^2-1}\, r\right) + \beta_k J_{\frac{d}{2}-1}\left(\sqrt{k^2-1}\, r\right)\right] \ , \tag{263}$$

where α_k and β_k are real constants. The $x \to \infty$ asymptotic behavior of the Bessel functions are

$$J_\nu(x) \approx \sqrt{\frac{2}{\pi x}}\, \cos\left(x - \frac{\nu\pi}{2} - \frac{\pi}{4}\right) \ , \tag{264}$$

$$Y_\nu(x) \approx \sqrt{\frac{2}{\pi x}}\, \sin\left(x - \frac{\nu\,\pi}{2} - \frac{\pi}{4}\right) \ . \tag{265}$$

Setting $\alpha_k = 0$, the function w_k becomes symmetric and regular at the center, hence the minimal tail solution cannot have the $J_{\frac{d}{2}-1}$ component. It follows that (262) holds with $\beta = 0$. Hence for large $|r|$,

$$w_k = \frac{\alpha_k}{r^{\frac{d-1}{2}}} \sin\left[\sqrt{k^2-1}\, r - \frac{\pi}{4}(d-1)\right] . \tag{266}$$

Writing it in terms of exponential functions,

$$w_k = \frac{i\alpha_k}{2r^{\frac{d-1}{2}}} \left[i^{\frac{d-1}{2}} \exp(-i\sqrt{k^2-1}\, r) - (-i)^{\frac{d-1}{2}} \exp(i\sqrt{k^2-1}\, r)\right] . \tag{267}$$

In the vicinity of the singularity above the real r axis, making the substitution $r = i\frac{P}{\varepsilon} + y$, because of the factor $\exp(-P/\varepsilon)$ the second term of (267) becomes negligible, and since in the matching region $|y| \ll P/\varepsilon$, to leading order in ε we obtain

$$w_k = \frac{1}{2} i\alpha_k \left(\frac{\varepsilon}{P}\right)^{\frac{d-1}{2}} \exp\left(\sqrt{k^2-1}\,\frac{P}{\varepsilon}\right) \exp(-i\sqrt{k^2-1}\,y) \ . \tag{268}$$

4.6.3 Tail-amplitude

Since $\Phi_{k,\mathrm{m}}$ is symmetric, it is purely real along the imaginary y axis. Hence from (262) it follows that $\operatorname{Im}\Phi_{k,-} = -\operatorname{Im} w_k$ for $\operatorname{Re} y = 0$ and $\operatorname{Im} y < 0$. Hence comparing (268) with (260) we obtain the tail-amplitude

$$\alpha_k = -2\nu_k \left(1 + \widetilde{C}\,\varepsilon \ln\varepsilon\right) \left(\frac{P}{\varepsilon}\right)^{\frac{d-1}{2}} \exp\left(-\sqrt{k^2-1}\,\frac{P}{\varepsilon}\right) \ , \tag{269}$$

where $\widetilde{C}$ is the constant given in (261). For $d = 1$ spatial dimension $\widetilde{C} = 0$, and the expression yields (229) and (240) for symmetric and asymmetric potentials.

In the expression (269) giving the radiation amplitude α_k the coefficient ν_k is independent of the number of spatial dimensions, hence one can apply the methods presented for the one-dimensional case. For symmetric potentials it is advisable to use the Laplace transform method presented in Subsection 4.4.7, applying the identity $\nu_3 = -K_2\pi/2$. For potentials that are not symmetric around their minimum only the numerical integration method works, which has been discussed in Subsection 4.5. Although ν_k agrees, but the expression (269) for the tail-amplitude differs in several ways from the one-dimensional result, which generally results in larger radiation amplitude for higher dimensions. According to (248), the distance P of the singularity from the real axis becomes smaller when increasing the number d of space dimensions, which makes the exponential term less small in (269). The factor $\varepsilon^{(d-1)/2}$ in the denominator also increases the radiation amplitude α_k for the case of $d > 1$. Since for $0 < \varepsilon < 1$ the value of $\varepsilon \ln\varepsilon$ is negative, according to (261), the logarithmic correction for $\sigma > 0$ decreases, and for $\sigma < 0$ increases the radiation with respect to the leading order result. The constant σ has been defined in (180) in terms of the expansion constants g_k that determine the potential.

The parameter α_k corresponds to the amplitude parameter in equation (146) that describes a general tail. Hence the energy current averaged for an oscillation period, $\bar{S}$, can be calculated using (148), where $\omega_f = k$ and $\lambda_f = \sqrt{k^2-1}$, yielding

$$\bar{S} = \frac{\pi^{\frac{d}{2}}}{\Gamma\left(\frac{d}{2}\right)} 4\nu_k^2\, k\sqrt{k^2-1}\, \left(1 + \widetilde{C}\,\varepsilon\ln\varepsilon\right)^2 \left(\frac{P}{\varepsilon}\right)^{d-1} \exp\left(-2\sqrt{k^2-1}\,\frac{P}{\varepsilon}\right) \ . \tag{270}$$

For a symmetric potential $k = 3$, otherwise $k = 2$. The constant $\widetilde{C}$ is defined in (261). The

dimension dependent factor is:

$$\frac{\pi^{\frac{d}{2}}}{\Gamma\left(\frac{d}{2}\right)} = \begin{cases} 1 & \text{for } d = 1 \ , \\ \pi & \text{for } d = 2 \ , \\ 2\pi & \text{for } d = 3 \ . \end{cases} \tag{271}$$

In Figure 23 we show the radiation rate for the ϕ^6 potential given in (190) with $g_5 = 1$,

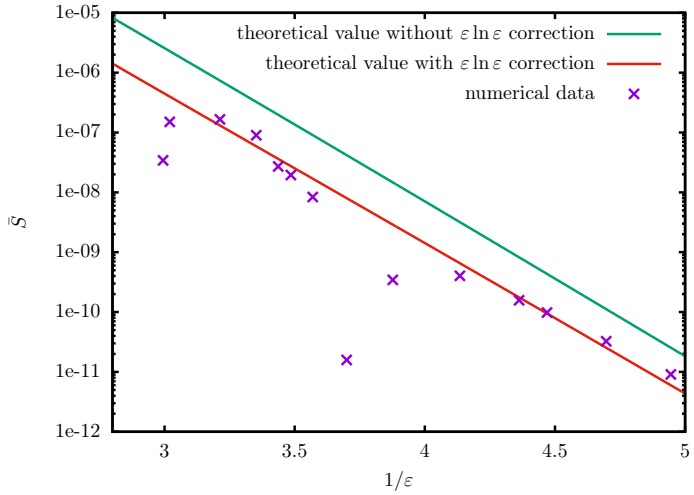

Figure 23: The time averaged energy current $\bar{S}$ for the ϕ^6 potential with $g_5 = 1$ in case of $d = 2$ spatial dimensions.

for $d = 2$ spatial dimensions. The analytical result is given by (270). We also show the leading order result which can be obtained by dropping the $\varepsilon \ln \varepsilon$ order correction. The $\varepsilon \ln \varepsilon$ contribution takes us closer to the numerical results.

5 Self-gravitating scalar fields – oscillatons

5.1 History and physical significance of oscillatons

The discovery of localized states formed by self-gravitating real scalar fields happened completely independently from the studies of flat background oscillons. A possible reason for this might be that in the gravitational case, because of the nonlinearity of the Einstein equations, a non-self-interacting massive Klein-Gordon field is already able to form long-lived localized states, while for flat background a nontrivial $U(\phi)$ potential is necessary for this.

It was first shown by Seidel and Suen in 1991, that coupling the Einstein equations to a real Klein-Gordon field localized states can form, which appear time-periodic [78]. In their first paper they called these objects oscillating soliton stars. Looking for time-periodic solutions, they have solved the system of ordinary differential equations for the first few Fourier modes, and up to the reached precision they have found localized solutions. Using these as initial data in a numerical code developed for the spherically symmetric system, they have indeed obtained very closely periodically evolving states. This has also indicated the stability of the oscillating soliton stars. They have also shown that from general spherically symmetric initial data similar long-lived solutions can evolve, which supported the physical significance of the solutions. Although by the applied numerical precision the solutions appeared to be completely time-periodic, the authors have commented that it is possible that still there is a very slow change in the amplitude and frequency.

Soliton stars can be formed from both real and complex scalar fields. In case of a complex field the forming objects are known as boson stars [162, 163, 164, 165, 166, 128]. For boson stars only the argument of the complex scalar field ϕ depends on time, in the form $e^{i\omega t}$, the metric of the spacetime remains time-independent. For a real scalar field soliton star both the scalar and the metric oscillate in time, which makes the investigation technically much more complicated. For the oscillating soliton stars formed from real scalar fields in a second paper Seidel and Suen [79] have introduced the name *oscillaton*. The use of this name became generally accepted in the literature.

Similarly to flat background oscillons and to complex scalar boson stars, oscillatons are members of a one-parameter family of solutions. Increasing the central amplitude, the size of the oscillatons becomes smaller, and their frequency also decreases. Initially the mass of the oscillaton grows, but with the decrease of the size we get to an $\mathrm{M_{crit}}$ maximal mass state. Further decreasing the size the oscillaton becomes unstable as the mass decreases.

Oscillatons formed from scalar fields in various cosmological models has been considered as dark matter in galaxies [85, 167]. The smaller the amplitude of the oscillaton is, the less important are the higher order Fourier components, and the more similar the oscillaton becomes to the same mass boson star configuration. We can find detailed numerical results

obtained by using the Fourier expansion up to the tenth order in the paper of Ureña-López, Matos and Becerril [168]. However, the numerical precision used there did not make possible the detection of the necessarily existing standing wave tail, which is many orders of magnitude smaller than the typical amplitude in the inner core domain. In the same paper, it was shown that for small amplitudes, i.e. for large size and weak gravitation, the time-periodic oscillatons and boson stars can be described by a specific system of two coupled second-order ordinary differential equations. These are known as Schrödinger-Newton equations in the literature.

Applying a numerical code developed for the time-evolution of a spherically symmetric general relativistic real scalar field, Alcubierre at al. [169] have studied in detail the behavior of deformed oscillatons. If one applies a relatively small perturbation on oscillatons, they perform low frequency quasinormal oscillations with decreasing amplitude, and they tend to another nearby oscillaton state. However, if as a result of the deformation the mass of the system becomes larger than the M_{crit} maximal oscillaton mass, then the end result can be a black hole. These investigations not only show that the oscillatons are stable, but also that they correspond to one of the general end states of the system.

Most studies of oscillatons have been restricted to the case of the non-self-interacting massive Klein-Gordon potential $U(\phi) = \frac{1}{2}m^2\phi^2$. Not only because this is the simplest and most natural choice, but also because it can be shown that for small amplitudes and large sizes the gravitational interaction dominates above the self-interaction of the scalar field. For other potentials the maximal mass M_{crit} can become larger, similarly to boson stars [170, 171].

There are one-parameter families of time-periodic oscillaton solutions, which are indexed by the number of nodes (crossings of zero) of the scalar field as a function of the radial coordinate [168]. Balakrishna at al. [172] have constructed time-periodic excited states with nodes, and by a time-evolution code they have demonstrated that the excited states are unstable. Relatively small amplitude excited states evolve into ground state oscillatons, while large amplitude ones collapse to black holes. In the same paper the first results about non spherically symmetric oscillatons can be found, obtained by the use of a 3+1 dimensional time-evolution code. According to the simulations, non spherically symmetric perturbations quickly decay by the emission of gravitational radiation. A $3 + 1$ dimensional code is used in [173] for studying the time-evolution of spherically symmetric oscillaton initial data with physically motivated $U(\phi)$ interaction potentials.

The real scalar field necessary for the formation of oscillatons may be provided most naturally by axions and similar low mass weakly interacting hypothetical bosonic particles. If the self-interaction is determined by a potential $U(\phi)$ describing an axion field, then in several articles the forming oscillatons are named axion stars. When an axion star and a

neutron star is collided, the end result is an axion cloud around a black hole or a neutron star [174]. Scalar dark matter may be accumulated in the center of stars, and form an oscillaton-like core there. Contrary to initial expectations, the accumulation of dark matter does not enhance the collapse of stars into black holes [121]. At the collision of oscillatons the emitted gravitational waves may be quite different from the waves emitted by the collision of black holes [175]. Boson stars and oscillatons are both members of a larger family of more complicated scalar field localized solutions [176, 177]. For more detailed review on the history and physical applications of oscillatons please see [155, 166, 128].

Although in their 1991 paper showing the existence of oscillatons Seidel and Suen [78] have pointed out that it is possible that oscillatons lose energy very slowly by radiating out scalar field, the authors of many subsequent papers could not find any indication supporting this in their numerical simulations. Generally, it was implicitly assumed that oscillatons are really exponentially localized and time-periodic. It was first pointed out by Don Page in 2003 that oscillatons must necessarily radiate, giving the first results for their classical and quantum radiation rate [80]. That no indication of mass-energy loss was observed in several papers is understandable in view of how much smaller is the amplitude of the tail responsible for the radiation in comparison to the amplitude of the core. The most favorable case to observe the tail is the maximal mass stable oscillaton, when the central amplitude is near 0.5. For this oscillaton the amplitude of the scalar field decreases exponentially when going outwards, until the oscillating tail appears with magnitude of the order 10^{-8}. For smaller mass smaller amplitude oscillatons the ratio of the tail and core amplitudes become even smaller, since the magnitude of the tail decreases exponentially as a function of the central amplitude.

5.2 Scalar fields in general relativity

We investigate a real scalar field ϕ coupled to gravity in the framework of general relativity. The self-interaction of the scalar is determined by the potential $U(\phi)$. In our papers [81, 155] we have considered $d+1$ dimensional spherically symmetric spacetimes, showing that small amplitude localized oscillatons only exist for $3 \leq d \leq 5$ spatial dimensions. For ease of understanding, here we only deal with the physically important $3+1$ dimensional case. We denote the coordinates by x^a, and assume that the signature of the metric g_{ab} is $(-+++)$. We use $G = c = \hbar = 1$ Planck units.

We have to solve the Einstein equations

$$G_{ab} = 8\pi T_{ab} \ , \tag{272}$$

where the stress-energy tensor of the scalar field is

$$T_{ab} = \nabla_a \phi \nabla_b \phi - g_{ab} \left[\frac{1}{2} \nabla^c \phi \nabla_c \phi + U(\phi) \right] . \tag{273}$$

The Klein-Gordon equation can be written as

$$\nabla^a \nabla_a \phi = U'(\phi) \ , \tag{274}$$

This wave equation is not independent from the Einstein equations, since it can also be obtained by taking the divergence of (272) and using the twice contracted Bianchi identity $\nabla^a G_{ab} = 0$.

Considering them as functions of the coordinates x^c, if the scalar $\phi(x^c)$ and metric $g_{ab}(x^c)$ solves the Einstein equations with potential U, then for arbitrary positive constant γ

$$\hat{\phi}(x^c) = \phi(\gamma x^c) \ , \qquad \hat{g}_{ab}(x^c) = g_{ab}(\gamma x^c) \tag{275}$$

is also a solution, with rescaled potential $\gamma^2 U$. We can use this freedom to set the value of the scalar field mass to an arbitrary positive value. In case of spherical symmetry and spherical coordinates the rescaling of the angular coordinates is of course not necessary, one only has to rescale the time t and radial r coordinates. The characteristic length scale of the system is determined by the scalar field mass m. Hence it is natural to make the choice $m = 1$, which we will assume in the following. At the application of the physically interesting results we can use the rescaling (275) to restore the m dependence.

We assume that the potential $U(\phi)$ has a minimum at the place $\phi = 0$, and its value there is $U(\phi) = 0$. We assume that the potential is analytic, and write the expansion around the minimum of the potential in the form (150), in terms of the mass m of the scalar field and the coefficients g_k. In the wave equation (274), which describes the evolution of the scalar field, the derivative of the potential, $U'(\phi)$, is given by (151).

In order to eliminate the 8π factors appearing at the terms containing the scalar field, we introduce a rescaled scalar field and a rescaled potential,

$$\tilde{\phi} = \sqrt{8\pi}\, \phi \ , \qquad \tilde{U}(\tilde{\phi}) = 8\pi U(\phi) \ . \tag{276}$$

Then, according to (273), the right-hand side of the Einstein equations is

$$8\pi T_{ab} = \nabla_a \tilde{\phi} \nabla_b \tilde{\phi} - g_{ab} \left[\frac{1}{2} \nabla^c \tilde{\phi} \nabla_c \tilde{\phi} + \tilde{U}(\tilde{\phi}) \right] \ . \tag{277}$$

The expansion of the rescaled potential is

$$\tilde{U}(\tilde{\phi}) = \frac{1}{2} m^2 \tilde{\phi}^2 + \sum_{k=2}^{\infty} \frac{1}{k+1} \tilde{g}_k \tilde{\phi}^{k+1} \ , \tag{278}$$

where the transformation of the constants determining the expansion are

$$\tilde{g}_k = \frac{g_k}{(8\pi)^{(k-1)/2}} \ . \tag{279}$$

Since $\tilde{U}'(\tilde{\phi}) = \sqrt{8\pi}\, U'(\phi)$, the form of the wave equation (274) is unchanged,

$$\nabla^a \nabla_a \tilde{\phi} = \tilde{U}'(\tilde{\phi}) \ . \tag{280}$$

5.3 Spatially conformally flat coordinates

We study spherically symmetric spacetimes using coordinates $x^a = (t, r, \theta, \varphi)$. We can choose the metric diagonal, and name the components in the following way,

$$g_{tt} = -A \ , \quad g_{rr} = B \ , \quad g_{\theta\theta} = C \ , \quad g_{\varphi\varphi} = C \sin^2\theta \ , \tag{281}$$

where A, B and C are functions of the time coordinate t and radial coordinate r. The spherically symmetric diagonal metric form (281) does not yet fixes uniquely the applied coordinate system. The Einstein equations only give sufficient conditions for two of the functions A, B and C, one function can be chosen freely. The most often applied method for fixing the diffeomorphism freedom is the choice of the radial coordinate $r = \sqrt{C}$, i.e. the use of Schwarzschild coordinates. The assumption that the metric is diagonal fixes the constant t hypersurfaces as well.

However, as it was pointed out first by Don N. Page [80], it is more reasonable to use a coordinate system in which the three-dimensional space is conformally flat. This is satisfied if $g_{\theta\theta} = r^2 g_{rr}$, which in our notation requires that

$$C = r^2 B \ . \tag{282}$$

This choice is motivated by the realization that in this case the oscillation of the metric component g_{tt} is smaller. In correlation to this, the oscillation sensed by observers moving on constant (r, θ, φ) coordinate lines is much larger in the Schwarzschild case. For small amplitude configurations, if the amplitude of the oscillaton is order ε^2, then the periodically oscillating part of the acceleration of these observers is order ε^3 in case of Schwarzschild coordinates, while it is order ε^5 small for the spatially conformally flat case. In the remaining part of this review we will only use the conformally flat coordinates determined by (282).

Using the conformally flat coordinate system, the nontrivial linearly independent components of the Einstein equations can be written in the following form:

$$\frac{3}{2B^2}\left(B_{,t}\right)^2 - \frac{2A}{r^2 B^{5/4}}\left(\frac{r^2 B_{,r}}{B^{3/4}}\right)_{,r} = \left(\tilde{\phi}_{,t}\right)^2 + \frac{A}{B}\left(\tilde{\phi}_{,r}\right)^2 + 2A\,\tilde{U}(\tilde{\phi}) \ , \tag{283}$$

$$\frac{\left(r^2 B\right)_{,r}}{2r^4 A^2 B^2}\left(r^2 A^2 B\right)_{,r} - \frac{2B^{1/4}}{A^{1/2}}\left(\frac{B_{,t}}{A^{1/2}B^{1/4}}\right)_{,t} - \frac{2}{r^2} = \left(\tilde{\phi}_{,r}\right)^2 + \frac{B}{A}\left(\tilde{\phi}_{,t}\right)^2 - 2B\,\tilde{U}(\tilde{\phi}) \ , \tag{284}$$

$$-A^{1/2}\left(\frac{B_{,t}}{A^{1/2}B}\right)_{,r} = \tilde{\phi}_{,t}\,\tilde{\phi}_{,r} \ , \tag{285}$$

$$\frac{rB}{A^{1/2}}\left(\frac{A_{,r}}{rA^{1/2}B}\right)_{,r} + rB^{1/2}\left(\frac{B_{,r}}{rB^{3/2}}\right)_{,r} = -2\left(\tilde{\phi}_{,r}\right)^2 \ . \tag{286}$$

We have chosen the components such that the right-hand sides of (283)-(286) should correspond to $16\pi T_{tt}$, $16\pi T_{rr}$, $8\pi T_{tr}$ and $16\pi(T_{\theta_1\theta_1}/r^2 - T_{rr})$, respectively. The wave equation

(280) in case of spatially conformally flat coordinates is

$$\frac{\tilde{\phi}_{,rr}}{B} - \frac{\tilde{\phi}_{,tt}}{A} + \frac{\tilde{\phi}_{,r}}{2r^4AB^2}\left(r^4AB\right)_{,r} - \frac{\tilde{\phi}_{,t}}{2B^3}\left(\frac{B^3}{A}\right)_{,t} - \tilde{U}'(\tilde{\phi}) = 0 \ . \tag{287}$$

Assuming that the scalar field tends to zero fast enough at infinity, the metric of the spacetime must tend to the vacuum Schwarzschild metric. In the spatially conformally flat system, when $C = r^2B$, the Schwarzschild metric can be written in the form

$$\mathrm{d}s^2 = -\left(\frac{2r-M}{2r+M}\right)^2 \mathrm{d}t^2 + \left(1+\frac{M}{2r}\right)^4 \left[\mathrm{d}r^2 + r^2\left(\mathrm{d}\theta^2 + \sin^2\theta \mathrm{d}\varphi^2\right)\right] \ , \tag{288}$$

where M is the total mass.

5.4 Time-periodic solutions

It is considerably simpler to examine exactly time-periodic solutions than radiating systems with slowly changing frequency. These time-periodic solutions have a large amplitude core and a small amplitude standing wave tail (or wing). They have been named nanopterons by Boyd [156, 5]. The nanopteron with the minimal amplitude tail is called *quasibreather*, and the amplitude of the quasibreather's tail determines the mass loss of the radiating state [60].

For the exactly time-periodic solutions oscillating with frequency ω we look for the scalar field and metric components in the following Fourier series form:

$$\tilde{\phi} = \sum_{n=0}^{N_F} \Phi_n \cos(n\omega t) \ , \tag{289}$$

$$A = 1 + \sum_{n=0}^{N_F} \tilde{A}_n \cos(n\omega t) \ , \tag{290}$$

$$B = 1 + \sum_{n=0}^{N_F} \tilde{B}_n \cos(n\omega t) \ , \tag{291}$$

where ϕ_n , $\tilde{A}_n$ and $\tilde{B}_n$ only depend on the radial coordinate r, and $N_F > 0$ is some integer. Although the exact expansion should consist of infinitely many components, due to the exponential convergence we can already get very good approximation by taking N_F moderately high. We assume that the frequency ω is somewhat lower than the mass threshold $m = 1$. We note that since the definition (289) contains $\tilde{\phi}$, there is a $\sqrt{8\pi}$ factor difference between the Φ_n functions used here and in Section 4.

The necessary and sufficient condition for the regularity at the center is that the functions Φ_n, $\tilde{A}_n$ and $\tilde{B}_n$ should be finite at the center $r = 0$, and that their derivative should be zero at that point. For the $r \to \infty$ asymptotic boundary condition the most natural assumption is that the metric should be asymptotically flat, and the coordinate t should tend to the

proper time. As we will see soon, this is a too restrictive condition, but if we do not go out to extreme large r radii, it can still be applied. The asymptotic flatness holds if $\tilde{A}_n \to 0$ and $\tilde{B}_n \to 0$ for all $n \geq 0$ when $r \to \infty$. The components of the wave equation (287) at large distances can be approximated by (152) which is valid on flat background. If the scalar field tends to zero, the nonlinear source terms F_n become negligible, and the Fourier equations decouple. In the frequency domain $\frac{1}{2} < \omega < 1$, which is relevant for the oscillatons, for $n \geq 2$ the asymptotic behavior of the functions Φ_n is still described by (156), in terms of the amplitude parameters $\tilde{\alpha}_n$ and $\tilde{\beta}_n$. In the same way as at the flat background calculations, the energy density tends to zero proportionally to r^{-2}. From this follows that if any of the amplitudes $\tilde{\alpha}_n$ or $\tilde{\beta}_n$ is nonzero for any $n \geq 2$, then the proper mass becomes infinite, and the spacetime cannot be asymptotically flat. The vanishing of all $\tilde{\alpha}_n$ and $\tilde{\beta}_n$ for all Fourier modes, together with the central regularity, obviously present too many boundary conditions for the second-order differential equations determining Φ_n. Generally, we cannot expect the existence of exactly time-periodic finite mass centrally regular solutions.

If we require that $\tilde{\alpha}_n = \tilde{\beta}_n = 0$ for all $n \geq 2$, then all Φ_n tend to zero exponentially, and we obtain a finite mass asymptotically flat solution. However, this solution will be singular at the center $r = 0$. This corresponds to the asymmetric solution we have used in Subsection 4.6. Based on counting the parameters, for any fixed ω frequency the asymmetric breather solution is unique. Apart from a small region around the center, the asymmetric solution is very close to the intended quasibreather solution, which has a regular center and a minimal amplitude tail.

It is important to clarify that the quasibreather description is only valid inside a very large but finite radius. However small is the energy density of the oscillating tail, if we consider large enough spheres the contribution of the tail to the total mass will not be negligible anymore. Consequently, the assumption that $\tilde{A}_n$ and $\tilde{B}_n$ tend to zero will not remain valid for arbitrarily large r values, and the form of the wave equation (152) will also change. For large enough r values the metric component A slowly becomes so large that the first radiating Fourier component, which is Φ_3 for symmetric potentials and Φ_2 otherwise, becomes a decaying mode instead of oscillating. Going out for even larger r, one by one all the other Φ_n stop being oscillating. In this way, we obtain exactly time-periodic but infinite mass breather solutions, which has been discussed in more detail in Chapter IX of the paper of Don N. Page [80]. The quasibreathers investigated in the present review can be considered as parts of these infinite mass breathers inside a sphere of large radius. The quasibreather contains the core region and also a considerable part of the tail region, where the first radiating mode oscillates, but inside the given radius the contribution of the tail to the mass is still negligible in comparison to the mass of the core.

For potentials $U(\phi)$ which are symmetric around their minimum, i.e. $\tilde{g}_{2k} = 0$ for integer

k, the Fourier expansion of the scalar contains only odd, while the metric only even indexed components, $\Phi_{2k} = 0$, $\tilde{A}_{2k+1} = 0$ and $\tilde{B}_{2k+1} = 0$. For symmetric potentials the first radiating mode is Φ_3. In the following, we will mainly study symmetric potentials. Obviously, the Klein-Gordon potential, for which $\tilde{g}_k = 0$ for $k > 1$, is symmetric as well.

5.5 Numerical results

We have used a high precision spectral numerical method to determine the structure of quasibreathers for a self-gravitating real Klein-Gordon field with mass $m = 1$. Our code uses the KADATH spectral library, which has been developed by Philippe Grandclément [178, 179]. The details of the method can be found in our paper [82] and in the review [155]. The current thesis is focused on asymptotic expansion methods, so here I only present the main results obtained by the code.

In Figure 24 we show the change of the scalar field and the metric functions during

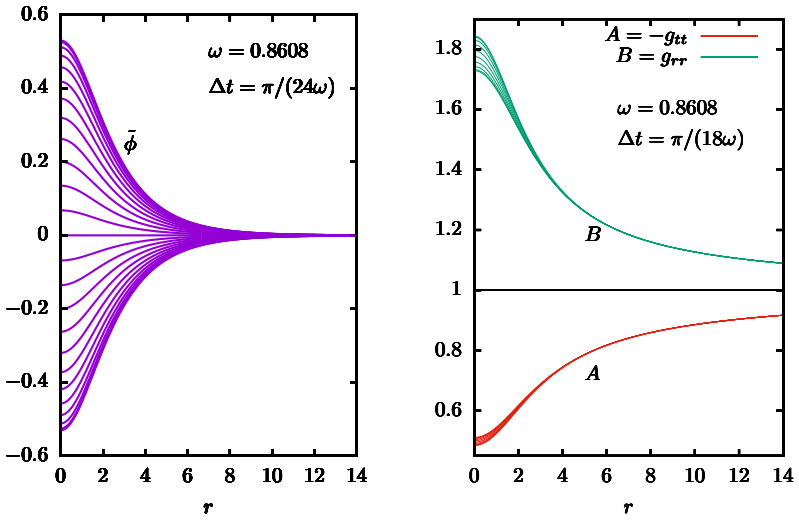

Figure 24: Time evolution of the scalar field $\tilde{\phi}$ and the metric components A and B during one oscillation period for an oscillaton with frequency $\omega = \omega_c = 0.8608$.

one oscillation period in the core domain for the Klein-Gordon oscillaton with the critical frequency $\omega = \omega_c = 0.8608$. Oscillatons with lower than the critical frequency are unstable, while for $\omega_c < \omega < 1$ they are stable. It can be seen that for A and B the oscillations around the static component $1 + \tilde{A}_0$ and $1 + \tilde{B}_0$ in (290)-(291) are relatively small. Studying higher frequency states, it turns out that approaching the value 1 with the frequency ω the relative magnitude of the oscillation in A and B becomes even smaller, and the state becomes more similar to the complex field boson star configuration.

In Figure 25, for the same critical frequency oscillaton, we give the radial dependence of the first few Fourier modes of the scalar field. Because of the several magnitude variation

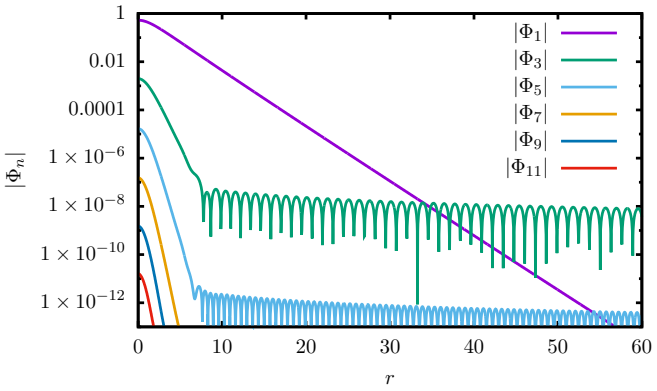

Figure 25: The Fourier components Φ_n of the scalar field $\tilde{\phi}$ at the frequency $\omega = 0.8608$.

of the functions we show their absolute value in logarithmic scale. The downwards pointing peaks correspond to zero crossings. In Figure 26 we can see the components of the metric

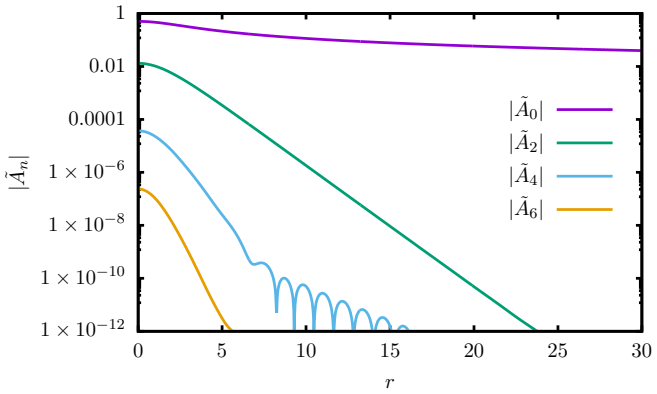

Figure 26: The Fourier components $\tilde{A}_n$ of the metric function A, in case of $\omega = 0.8608$.

function A, while in Figure 27 we show the components of B. We can obtain similar figures

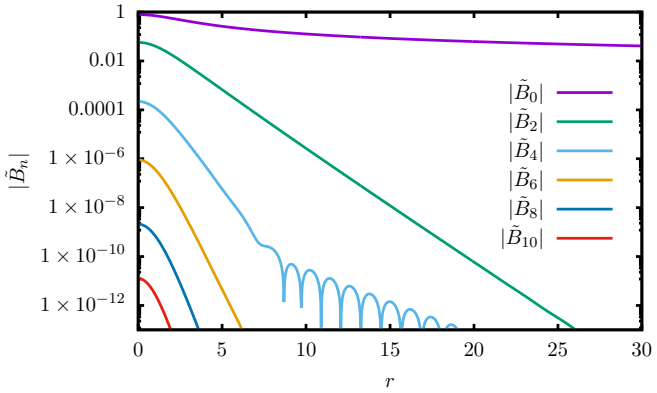

Figure 27: The Fourier components $\tilde{B}_n$ of the function B, for $\omega = 0.8608$.

for other frequencies as well. With the increase of the frequency the tail-amplitude decreases very quickly. As the frequency approaches the threshold value 1, the relative magnitude of the higher Fourier modes with respect to the base mode also decreases, and hence in those cases we can already get precise approximation by taking into account fewer Fourier modes.

A crucial result of our numerical simulations is the demonstration that there is no such frequency ω for which the oscillating tail responsible for the radiation vanishes. The dominant part of the tail is in the third mode, having the form $\Phi_3 \approx \alpha_3 \frac{1}{r}\cos(\lambda_3 r + \delta_3)$, where $\lambda_3 = \sqrt{9\omega^2 - 1}$. In the upper panel of Figure 28 we give the frequency dependence of the minimized

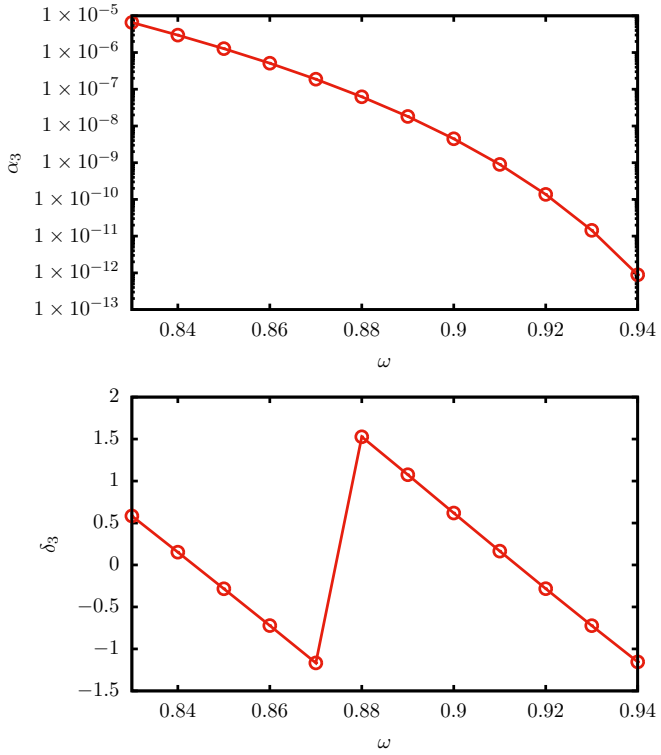

Figure 28: Frequency dependence of the minimized amplitude α_3 and phase δ_3.

amplitude α_3 in the domain where the tail is large enough so that we were able to compute it numerically. In the lower panel of the figure we also give the phase δ_3 belonging to the minimal tail-amplitude. The observation that there is no such ω for which $\alpha_3 = 0$ shows that there is no exactly periodic localized breather solution of the system.

In Figure 29 we plot the total mass M belonging to the core part of the oscillatons. The mass is maximal at the frequency $\omega_c = 0.8608$, with value $M_c = 0.60535$. This critical state separates from each other the domain of the stable and the unstable oscillatons. Although the mass has a maximum, the central values of the Fourier modes Φ_1 and Φ_3, and hence also the central energy density, are all monotonically decreasing functions of the frequency ω.

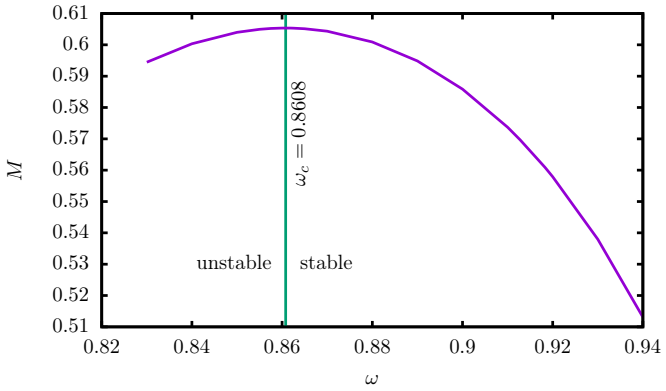

Figure 29: The mass of Klein-Gordon oscillatons as a function of their frequency.

5.6 Small-amplitude expansion of oscillatons

The method described in Section 4.3 for the description of small amplitude oscillons can be generalized for self-gravitating scalar fields as well. The leading order of the expansion, usually derived by less systematic methods, has been already known in the literature [168, 80, 180], and leads to the Schrödinger-Newton equations. At first, we have generalized our method for a coupled dilaton-scalar system on flat background [181]. This theory also leads to the Schrödinger-Newton equations at leading order, and it behaves very similarly to the gravitational system. In the rest of this subsection we present our results about the expansion of $3+1$ dimensional spherically symmetric oscillatons in general relativity, published in [81]. This asymptotic expansion gives a very good approximation to the core domain, but it is unable to describe the tail region which is responsible for the radiation. According to this approximation the scalar field ϕ tends to zero at large distances exponentially at each order of the expansion.

We look for a family of localized spherically symmetric solutions of the (272) Einstein equations and the (280) wave equation, which are characterized by a parameter ε related to the amplitude of the states. We use the coordinate system determined by (282), in which case the spatial part of the metric is conformally flat. Similarly to flat background oscillons, we expect that the smaller the central amplitude of an oscillaton is, the larger its size becomes. Numerical simulations clearly support this expectation. Hence we introduce a new rescaled radial coordinate ρ by

$$\rho = \varepsilon r \ . \tag{292}$$

This also implies that we are looking for solutions which are slowly varying in space.

We expand the scalar field $\tilde{\phi}$ and the metric components in terms of the powers of ε,

$$\tilde{\phi} = \sum_{k=1}^{\infty} \epsilon^{2k} \phi_{2k} \ , \tag{293}$$

$$A = 1 + \sum_{k=1}^{\infty} \epsilon^{2k} A_{2k} \ , \tag{294}$$

$$B = 1 + \sum_{k=1}^{\infty} \epsilon^{2k} B_{2k} \ . \tag{295}$$

Since we intend to use asymptotically Minkowskian coordinates, where far from the oscillaton the coordinate t measures the proper time and r measures the radial distance, we search for such ϕ_{2k}, A_{2k} and B_{2k} functions which tend to zero if $\rho \to \infty$.

The largest difference with respect to flat background oscillons is that in (293)-(295) there are only even powers of ε. For small amplitude configurations, if we assume that with the increase of the parameter ε the spatial size decreases as $1/\varepsilon$, then for flat background oscillons the amplitude of the core grows proportionally to ε, while for self-gravitating oscillatons the growth is proportional to ε^2. This is a fundamental difference between the scaling properties of the two kind of objects.

The oscillation frequency also depends on the amplitude of the oscillatons. Similarly to the flat background case, the smaller the amplitude is the closer the frequency gets to the value $m = 1$. In view of this, we introduce a rescaled time coordinate τ by

$$\tau = \omega t \ , \tag{296}$$

where ω is a function of the parameter ε. We choose the coordinate τ in such a way, that in terms of that, the frequency should be exactly 1, independently of ε. Since we have already set the scalar field mass to $m = 1$, the value of ω gives the oscillation frequency of the oscillaton. Similarly to flat background oscillons, it can be shown that a natural way to choose the relation between the frequency and the amplitude parameter is

$$\omega^2 = 1 - \varepsilon^2 \ . \tag{297}$$

5.6.1 Leading order results

The field equations that we have to solve are the (283)-(286) Einstein equations and the (287) wave equation. In the equations only the even powers of the frequency ω appear, of which we can substitute by the help of (297). After this, we can separately solve the parts of the equations proportional to ε^n, in increasing orders of n.

We get the first conditions at order ε^2. From the Einstein equations follow that $\frac{\partial^2 B_2}{\partial \tau^2} = 0$ and $\frac{\partial^2 B_2}{\partial \tau \partial \rho} = 0$. Since we are looking for solutions that remain bounded as the time passes, we get

$$B_2 = -a_2 \ , \tag{298}$$

where a_2 is a new function that only depends on ρ. From the wave equation follows that $\frac{\partial^2 \phi_2}{\partial \tau^2} + \phi_2 = 0$. This has the solution $\phi_2 = p_2 \cos(\tau + \delta)$, where p_2 and δ are functions of ρ.

At higher order of the expansion it turns out that δ is constant, so it can be set to zero by a shift of the time coordinate τ. Hence

$$\phi_2 = p_2 \cos\tau \ . \tag{299}$$

The radial dependence of the new functions a_2 and p_2 will be determined at higher orders.

From the ε^4 part of the Einstein equation (283) follows that

$$\frac{\mathrm{d}^2 a_2}{\mathrm{d}\rho^2} + \frac{2}{\rho}\frac{\mathrm{d}a_2}{\mathrm{d}\rho} = \frac{1}{2}p_2^2 \ . \tag{300}$$

The ε^4 part of the equation (286) gives the condition

$$\frac{\partial}{\partial\rho}\left\{\frac{1}{\rho}\frac{\partial}{\partial\rho}\left[A_2 - a_2\right]\right\} = 0 \ . \tag{301}$$

The solution is $A_2 - a_2 = \rho f_1 + f_2$, where f_1 and f_2 are two functions of τ. Since we are looking for solutions such that both A_2 and a_2 tend to zero at infinity, necessarily $f_1 = f_2 = 0$, and hence A_2 is time independent,

$$A_2 = a_2 \ . \tag{302}$$

Using this, from the ε^4 part of the Einstein equation (284) follows the condition:

$$\frac{\partial^2 B_4}{\partial\tau^2} = \frac{p_2^2}{2}\cos(2\tau) \ . \tag{303}$$

The solution, which is not growing without bound as time increases, can be written as

$$B_4 = b_4 - \frac{p_2^2}{8}\cos(2\tau) \ , \tag{304}$$

where b_4 is a further arbitrary function of ρ.

The part of the wave equation (287) which is proportional to ε^4 gives

$$\frac{\partial^2\phi_4}{\partial\tau^2} + \phi_4 + \frac{\tilde{g}_2}{2}p_2^2\left[1+\cos(2\tau)\right] - \left[\frac{\mathrm{d}^2 p_2}{\mathrm{d}\rho^2} + \frac{2}{\rho}\frac{\mathrm{d}p_2}{\mathrm{d}\rho} - p_2 - p_2 a_2\right]\cos\tau = 0 \ . \tag{305}$$

The structure of this equation is the same as that of (165) written at the flat background case. Solution that remains bounded in time can only exist for ϕ_4 if the coefficient of the resonant $\cos\tau$ term vanishes, from which it follows that

$$\frac{\mathrm{d}^2 p_2}{\mathrm{d}\rho^2} + \frac{2}{\rho}\frac{\mathrm{d}p_2}{\mathrm{d}\rho} = p_2(a_2+1) \ . \tag{306}$$

This equation and (300) form a coupled system for a_2 and p_2, of which localized solution may exist. The solution of this system determines the leading ε^2 order behavior of the functions $\tilde{\phi}$, A and B for small amplitude oscillatons. Up to this order the functions are the same for

arbitrary scalar potential, assuming that the mass of the scalar field has been set to the value $m = 1$. This means that small amplitude, and hence large sized, oscillatons always behave in the same way as in the Klein-Gordon case. In other words, the gravitational interaction dominates over the self-interaction of the scalar for small-amplitude configurations.

If the resonance condition (306) is satisfied then (305) determines the time dependence of ϕ_4,

$$\phi_4 = p_4 \cos\tau + \frac{\tilde{g}_2}{6} p_2^2 \left[\cos(2\tau) - 3\right] \ , \tag{307}$$

where p_4 is a function of ρ. The ϕ_4 given in (307) still remains a solution if we add a further $q_4 \sin\tau$ term, where q_4 is an arbitrary function of ρ. However, from the equations at higher orders in ε follows that by a small shift in τ it is always possible to set $q_4 = 0$. Similarly, at all higher orders of ε it can be shown that only terms with time dependence $\cos(k\tau)$ appear in the expansions, and hence the oscillaton must be time-reflection symmetric at the moment $\tau = 0$. The time dependence of the B_4 function is given by (304), while the time dependence of A_4 and the spatial dependences will be determined at order ε^6.

5.6.2 Schrödinger-Newton equations

Introducing the functions s and S by the relations

$$s = -a_2 - 1 \ , \quad S = \frac{1}{\sqrt{2}} p_2 \ , \tag{308}$$

equations (306) and (300) can be written into the following form:

$$\frac{\mathrm{d}^2 S}{\mathrm{d}\rho^2} + \frac{2}{\rho}\frac{\mathrm{d}S}{\mathrm{d}\rho} + sS = 0 \ , \tag{309}$$

$$\frac{\mathrm{d}^2 s}{\mathrm{d}\rho^2} + \frac{2}{\rho}\frac{\mathrm{d}s}{\mathrm{d}\rho} + S^2 = 0 \ , \tag{310}$$

which are known as the time-independent Schrödinger-Newton (SN) equations [182, 183]. It is also possible to obtain these equations by the study of the collapse of the quantum mechanical wave function resulting from gravitational interaction [184, 185]. The near-Newtonian behavior of a small-amplitude boson star is also described by the SN equations [163, 186]. From any solution of the SN equations (309)-(310), using the scale invariance

$$(S(\rho), s(\rho)) \to (\lambda^2 S(\lambda\rho), \lambda^2 s(\lambda\rho)) \tag{311}$$

we can obtain another solution for any $\lambda > 0$.

For any $n \geq 0$ integer there exist a localized regular solution of the SN equations, for which S has exactly n nodes (zero crossings). The nodeless solution with $n = 0$ corresponds to the lowest mass most stable oscillaton, hence in the following we will only study that case.

For the solutions of the system, if $\rho \to \infty$ the function S tends to zero exponentially, and s tends to a constant $s_0 < 0$ in the following way:

$$s \approx s_0 + \frac{s_1}{\rho} \ . \tag{312}$$

We use the scaling freedom (311) to set $s_0 = -1$. According to (308) this ensures that a_2 tends to zero asymptotically. Then the asymptotic behavior of the function is $a_2 \approx -\frac{1}{\rho}s_1$, which is only modified by exponentially decaying contributions. For the case when S is nodeless, the numerical results for the central values of the functions are $s = 0.938323$, $S = 1.021493$, and the constant is $s_1 = 3.505330$.

5.6.3 Higher orders of the expansion

From the order ε^6 components of the field equations follows the time dependence of A_4,

$$A_4 = a_4^{(0)} + a_4^{(2)} \cos(2\tau) \ , \tag{313}$$

where $a_4^{(0)}$ and $a_4^{(2)}$ are functions of the radial coordinate ρ. The functions p_4 and $a_4^{(0)}$ are determined by the following coupled differential equations:

$$\frac{\mathrm{d}^2 a_4^{(0)}}{\mathrm{d}\rho^2} + \frac{2}{\rho}\frac{\mathrm{d}a_4^{(0)}}{\mathrm{d}\rho} = p_2 p_4 + \left(\frac{\mathrm{d}a_2}{\mathrm{d}\rho}\right)^2 - p_2^2(a_2+1) \ , \tag{314}$$

$$\frac{\mathrm{d}^2 p_4}{\mathrm{d}\rho^2} + \frac{2}{\rho}\frac{\mathrm{d}p_4}{\mathrm{d}\rho} = p_4(a_2+1) + a_4^{(0)}p_2 - 2a_2p_2(a_2+1) - \frac{3p_2^3}{16} - \left(\frac{5}{6}\tilde{g}_2^2 - \frac{3}{4}\tilde{g}_3\right)p_2^3 \ . \tag{315}$$

We look for the unique solution for which both $a_4^{(0)}$ and p_4 tend to zero if $\rho \to \infty$. The function p_4 tends to zero exponentially, while for large ρ values

$$a_4^{(0)} \approx \frac{s_1^2}{2\rho^2} + \frac{s_2}{\rho} + s_3 \ , \tag{316}$$

where s_1 is the constant defined in equation (312), moreover s_2 and s_3 are further constants. If $a_4^{(0)}$ and p_4 are solutions of (314)-(315), then for any constant c

$$\tilde{a}_4^{(0)} = a_4^{(0)} + c\left[2(a_2+1) + \rho\frac{\mathrm{d}a_2}{\mathrm{d}\rho}\right], \tag{317}$$

$$\tilde{p}_4 = p_4 + c\left(2p_2 + \rho\frac{\mathrm{d}p_2}{\mathrm{d}\rho}\right), \tag{318}$$

are also solutions. This family of solutions is generated by the scale invariance (311) of the SN equations. If we have an arbitrary solution of the equations (314)-(315), then by the appropriate choice of c we can obtain another solution for which $s_3 = 0$ holds in (316).

The equation determining the function b_4 is

$$\frac{\mathrm{d}b_4}{\mathrm{d}\rho} = -\frac{\mathrm{d}a_4^{(0)}}{\mathrm{d}\rho} + \frac{1}{4}\frac{\mathrm{d}a_2}{\mathrm{d}\rho}\left(\rho\frac{\mathrm{d}a_2}{\mathrm{d}\rho} + 8a_2\right) + \frac{\rho}{4}\left[\left(\frac{\mathrm{d}p_2}{\mathrm{d}\rho}\right)^2 - p_2^2(a_2-1)\right] \ . \tag{319}$$

For large ρ values b_4 tends to zero according to

$$b_4 \approx \frac{3}{8\rho^2} s_1^2 + \frac{s_2}{\rho} \ . \tag{320}$$

The equation determining the $\cos(2\tau)$ part of the function A_4 is

$$\frac{\mathrm{d}^2 a_4^{(2)}}{\mathrm{d}\rho^2} - \frac{1}{\rho}\frac{\mathrm{d}a_4^{(2)}}{\mathrm{d}\rho} = \frac{1}{4}(a_2+1)p_2^2 - \frac{3}{4}\frac{\mathrm{d}p_2}{\mathrm{d}\rho}\left(\frac{\mathrm{d}p_2}{\mathrm{d}\rho} + \frac{1}{\rho}p_2\right) \ . \tag{321}$$

Summarizing our results so far, up to ε^4 order the components of the scalar field and of the metric are

$$\tilde{\phi} = \varepsilon^2 p_2 \cos\tau + \varepsilon^4 \left\{ p_4 \cos\tau + \frac{\tilde{g}_2 p_2^2}{6}\left[\cos(2\tau) - 3\right] \right\} + \mathcal{O}(\varepsilon^6) \ , \tag{322}$$

$$A = 1 + \varepsilon^2 a_2 + \varepsilon^4 \left[a_4^{(0)} + a_4^{(2)} \cos(2\tau) \right] + \mathcal{O}(\varepsilon^6) \ , \tag{323}$$

$$B = 1 - \varepsilon^2 a_2 + \varepsilon^4 \left[b_4 - \frac{p_2^2}{8}\cos(2\tau) \right] + \mathcal{O}(\varepsilon^6) \ . \tag{324}$$

Proceeding to higher orders, the expressions become considerably longer and more complicated. However, it can be shown that for symmetric potentials, in which case $\tilde{g}_{2k} = 0$, the scalar field $\tilde{\phi}$ only contains $\cos(k\tau)$ terms with odd k, while A and B has only even Fourier components.

The higher order expressions become considerably simpler for symmetric potentials, when $\tilde{g}_{2k} = 0$. Since for symmetric potentials the first radiating mode in $\tilde{\phi}$, which is proportional to $\cos(3\tau)$, appears at order ε^6, we give its higher order expansion in this case,

$$\tilde{\phi} = \left(\varepsilon^2 p_2 + \varepsilon^4 p_4 + \varepsilon^6 p_6\right)\cos\tau + \varepsilon^6 \left(\frac{3p_2^3}{128} + \frac{\tilde{g}_3 p_2^3}{32} + \frac{p_2 a_4^{(2)}}{8} \right)\cos(3\tau) + \mathcal{O}(\varepsilon^8) \ , \tag{325}$$

where p_6 is a function of ρ, which is determined by a long differential equation appearing at higher orders.

In Figures 30 and 31 we show the numerically calculated p_2, a_2, p_4, $a_4^{(0)}$, $a_4^{(2)}$ and b_4 functions for the Klein-Gordon potential. Equations (322)-(324) determine a one-parameter family of solutions, which depends on the parameter ε. This family solves the field equations up to order ε^4 for a self-interacting, self-gravitating scalar field with mass $m = 1$. By the rescaling (275) of the t and r coordinates we can obtain one-parameter families for arbitrary scalar field mass m.

5.7 Radiation law of oscillatons

The method presented in Section 4 for the determination of the radiation of flat background oscillons can also be generalized for self-gravitating oscillatons. The extension into the complex plane of the Fourier mode equations and the small-amplitude expansion was first applied

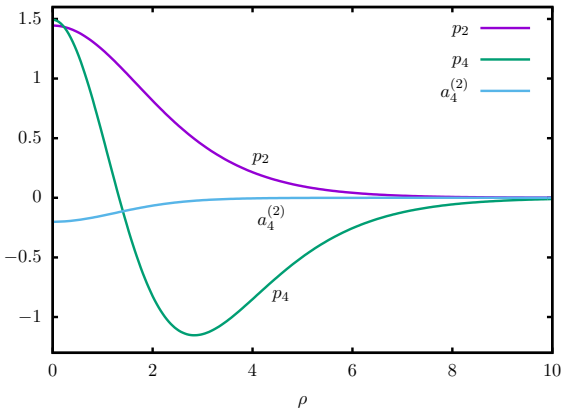

Figure 30: The exponentially decaying p_2, p_4 and $a_4^{(2)}$ functions for the Klein-Gordon oscillaton.

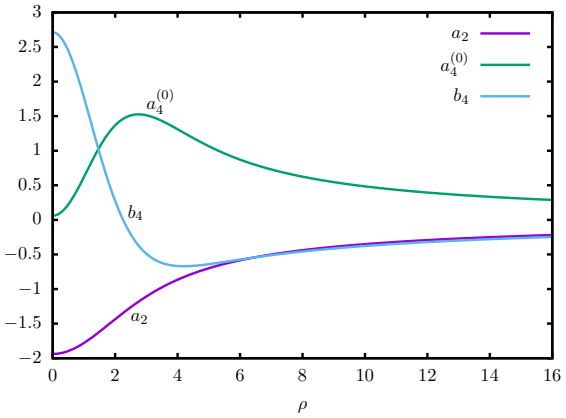

Figure 31: The functions a_2, $a_4^{(0)}$ and b_4 for the Klein-Gordon system. They tend to zero according to a power law when $\rho \to \infty$.

by Segur and Kruskal for radiation of one-dimensional ϕ^4 oscillons [10]. The Borel summation method for the calculation of the small correction near the singularity was introduced by Pomeau, Ramani and Grammaticos [11]. The results in this subsection have been published in our paper [81]. We only consider symmetric potentials here.

For a small amplitude quasibreather or asymmetric breather we can get the relation between the (289)-(291) Fourier expansion and the (293)-(295) small-amplitude expansion by using the expressions (322)-(325). The expansion of the Fourier components are

$$\Phi_1 = \varepsilon^2 p_2 + \varepsilon^4 p_4 + \mathcal{O}(\varepsilon^6) \ , \tag{326}$$

$$\Phi_3 = \varepsilon^6 \left(\frac{3p_2^3}{128} + \frac{\tilde{g}_3 p_2^3}{32} + \frac{p_2 a_4^{(2)}}{8} \right) + \mathcal{O}(\varepsilon^8) \ , \tag{327}$$

$$\tilde{A}_0 = \varepsilon^2 a_2 + \varepsilon^4 a_4^{(0)} + \mathcal{O}(\varepsilon^6) \ , \tag{328}$$

$$\tilde{A}_2 = \varepsilon^4 a_4^{(2)} + \mathcal{O}(\varepsilon^6) \ , \tag{329}$$

$$\tilde{B}_0 = -\varepsilon^2 a_2 + \varepsilon^4 b_4 + \mathcal{O}(\varepsilon^6) \ , \tag{330}$$

$$\tilde{B}_2 = -\frac{1}{8}\varepsilon^4 p_2^2 + \mathcal{O}(\varepsilon^6) \ . \tag{331}$$

5.7.1 Singularities on the complex plane

We have to extend to the complex r plane both the small-amplitude expansion and the Fourier expansion. For the case of the ε expansion, the functions ϕ_k, A_k and B_k have symmetrically positioned singularities on the imaginary axis, corresponding to the singularities of the (309)-(310) Schrödinger-Newton (SN) equations. Since their contribution to the radiation decreases exponentially with their distance from the real axis, we only need to consider the nearest pair of singularities.

Introducing the new variables

$$z = \frac{1}{2}(s+S) \quad , \qquad Z = \frac{1}{2}(s-S) \ , \tag{332}$$

the two SN equations will have the same structure,

$$\frac{\mathrm{d}^2 Z}{\mathrm{d}\rho^2} + \frac{2}{\rho}\frac{\mathrm{d}Z}{\mathrm{d}\rho} + Z^2 - zZ = 0 \ , \tag{333}$$

$$\frac{\mathrm{d}^2 z}{\mathrm{d}\rho^2} + \frac{2}{\rho}\frac{\mathrm{d}z}{\mathrm{d}\rho} + z^2 - Zz = 0 \ . \tag{334}$$

Using the central initial values given after Eq. (312), and numerically integrating the differential equations along the imaginary axis, it can be observed that z becomes singular at the points $\rho = \pm iP$, where $P \approx 3.97736$, while Z tends to zero oscillating at the same places.

We introduce the complex R coordinate defined by $\rho = iP + R$. It turns out that the leading order behavior near the singularity is necessarily $z = -6/R^2$. Then to leading order, the differential equation for Z is

$$\frac{\mathrm{d}^2 Z}{\mathrm{d}R^2} + \frac{6}{R^2} Z = 0 \ . \tag{335}$$

The solution along the negative half of the imaginary R axis is then

$$Z = c_1 \sqrt{iR}\, \sin\left(\frac{\sqrt{23}}{2}\ln(iR) + c_2\right) \ , \tag{336}$$

where c_1 and c_2 are some real constants. The function Z tends to zero performing increasing frequency oscillations when approaching $\rho = iP$ from below. The expansion of the function z to higher orders is

$$z = -\frac{6}{R^2} - \frac{12i}{5PR} + \frac{48}{25P^2} \ , \tag{337}$$

to which there is also a correction of the form (336). It follows from (332) that the leading terms in the behavior of the functions s and S near the singularity has the same form, given by the right-hand side of (337). Continuing the expansion without taking into account the non-analytic terms, logarithmic terms appear, the first having the form $R^4 \ln R$. Knowing the behavior of s and S according to (337), equations (308) determines the order ε^2 parts of the functions ϕ, A and B near the singularity.

Substituting into (314), (315), (319) and (321), the order ε^4 contributions, i.e. $a_4^{(0)}$, p_4, b_4 and $a_4^{(2)}$, can also be determined in the neighborhood of the singularity. In the Klein-Gordon case, when $\tilde{g}_k = 0$ for $k \geq 2$ we get

$$a_4^{(0)} = -\frac{2547}{52R^4} + \frac{1944\, i \ln(iR)}{35PR^3} + \frac{ia_{-3}}{R^3} + \mathcal{O}\left(\frac{\ln R}{R^2}\right) , \tag{338}$$

$$\frac{1}{\sqrt{2}} p_4 + a_4^{(0)} = \frac{225}{26R^4} + \frac{18\, i}{5PR^3} + \mathcal{O}\left(\frac{1}{R^2}\right) , \tag{339}$$

$$b_4 = \frac{16479}{260R^4} - \frac{1944\, i \ln(iR)}{35PR^3} - \frac{ia_{-3}}{R^3} + \frac{36\, i}{5PR^3} + \mathcal{O}\left(\frac{\ln R}{R^2}\right) , \tag{340}$$

$$a_4^{(2)} = -\frac{27}{5R^4} - \frac{36\, i}{5PR^3} + \mathcal{O}\left(\frac{1}{R^2}\right) . \tag{341}$$

The value of the constant a_{-3} is fixed by the behavior of the functions on the real axis, namely by the requirement of the exponential decay of p_4 for large real ρ.

5.7.2 Inner region

Since the rescaled radial coordinate is $\rho = \varepsilon r$, the singularities closest the the real axis are located at the points $r = \pm iP/\varepsilon$. As ε tends to zero, the singularities get further from the real axis, but in their neighborhood the Fourier components Φ_n, $\tilde{A}_n$ and $\tilde{B}_n$ will not be small, they have ε independent parts. In agreement with (196) we introduce the shifted radial coordinate y by

$$r = \frac{iP}{\varepsilon} + y . \tag{342}$$

The coordinate y is valid in the *inner region*, and obviously $R = \varepsilon y$. In the neighborhood of the upper singularity we can obtain the leading order behavior of the Fourier modes, if we substitute the results (337)-(341) of the small-amplitude expansion into the equations (326)-(331), and take the $\varepsilon \to 0$ limit. By this procedure we get the first leading order terms of the inner ϵ expansion. We denote these by upper index (0), similarly as in (254)

for oscillons. For the case of the Klein-Gordon potential the results are

$$\Phi_1^{(0)} = \left(-\frac{6}{y^2} + \frac{2997}{52y^4} + ...\right)\sqrt{2} \ , \tag{343}$$

$$\Phi_3^{(0)} = \left(-\frac{243}{40y^4} + ...\right)\sqrt{2} \ , \tag{344}$$

$$\tilde{A}_0^{(0)} = \frac{6}{y^2} - \frac{2547}{52y^4} + ... \ , \tag{345}$$

$$\tilde{A}_2^{(0)} = -\frac{27}{5y^4} + ... \ , \tag{346}$$

$$\tilde{B}_0^{(0)} = -\frac{6}{y^2} + \frac{16479}{260y^4} + ... \ , \tag{347}$$

$$\tilde{B}_2^{(0)} = -\frac{9}{y^4} + ... \ . \tag{348}$$

Since these expressions are obtained from the outer ϵ expansion, they are valid for large y values. They provide boundary conditions for the inner solution, being valid in the matching region, where y is large but $R = \varepsilon y$ is still small.

We can also obtain the expansion (343)-(348) if we look for the solution of the ε^0-th order inner Fourier mode equations in a series form with respect to $1/y^2$,

$$\Phi_{2n-1}^{(0)} = \sum_{k=n}^{\infty} \psi_k^{(n)} \frac{1}{y^{2k}} \ , \tag{349}$$

$$\tilde{A}_{2n}^{(0)} = \sum_{k=n+1}^{\infty} \alpha_k^{(n)} \frac{1}{y^{2k}} \ , \tag{350}$$

$$\tilde{B}_{2n}^{(0)} = \sum_{k=n+1}^{\infty} \beta_k^{(n)} \frac{1}{y^{2k}} \ , \tag{351}$$

where $\psi_k^{(n)}$, $\alpha_k^{(n)}$ and $\beta_k^{(n)}$ are constants. Substituting the definition (342) of the coordinate y into (283)-(287), and taking the limit $\varepsilon \to 0$, near the singularity certain lower order terms in r become negligible. After this, substituting the $1/y^2$ expansion in the form (349)-(351) into the mode equations, because of the absence of the odd powers of $1/y$, apart from the signature of $\psi_1^{(1)}$ the coefficients $\psi_k^{(n)}$, $\alpha_k^{(n)}$ and $\beta_k^{(n)}$ will be uniquely determined. The computation of the expansion (343)-(348) from the Fourier mode equations is technically much simpler than the small-amplitude expansion method, and by the use of an algebraic manipulation software it can be calculated to quite high orders in $1/y$.

The large k asymptotic behavior of the constants $\psi_k^{(n)}$, $\alpha_k^{(n)}$ and $\beta_k^{(n)}$ will determine the amplitude of the radiative tail of oscillatons. The leading order asymptotic behavior of these constants can be obtained by the study of the structure of the mode equations. It can be shown, that for large k the dominating coefficients are $\psi_k^{(2)}$, belonging to the third Fourier

mode. The result for the Klein-Gordon potential is

$$\psi_k^{(2)} = K_2(-1)^k \frac{(2k-1)!}{8^k}\left[1+\frac{51}{2k}+\frac{663}{2k^2}+\mathcal{O}\left(\frac{1}{k^3}\right)\right], \tag{352}$$

where K_2 is a constant. All other coefficients grow more slowly with k. Although the coefficients of the $1/k$ and $1/k^2$ correction terms may depend on the interaction potential of the scalar field, the leading order behavior for any symmetric potential is the same as in (352). The value of the constant factor K_2 is crucial for the determination of the mass loss rate of the oscillatons. Calculating the coefficients up to order $k = 100$, and using the Fourier mode equations up to order $N_F = 6$, in the Klein-Gordon case we obtain $K_2 \approx -0.301$.

5.7.3 The asymmetric breather solution

We can consider an appropriate higher order generalization of (343)-(348) as boundary conditions for the leading order inner Fourier mode equations for large $|y|$ in the directions $-\pi/2 < \arg y < 0$, ensuring a unique solution. This corresponds to the requirement that the scalar field ϕ tends to zero along the positive part of the real r axis for $r \to \infty$, without a standing wave tail. Similarly to the method described in Subsections 4.4 and 4.6, we look for the asymmetric breather solution described by the functions $\Phi_{n,-}^{(0)}$, $\tilde{A}_{n,-}^{(0)}$ and $\tilde{B}_{n,-}^{(0)}$.

The Fourier components of the wave equation (287) can be written in a form agreeing with (242) even in the self-gravitating case,

$$\frac{\mathrm{d}^2\Phi_n}{\mathrm{d}r^2}+\frac{2}{r}\frac{\mathrm{d}\Phi_n}{\mathrm{d}r}+(n^2\omega^2-1)\Phi_n = F_n\ , \tag{353}$$

where now the nonlinear source terms F_n are polynomial expressions containing Φ_k, $\tilde{A}_k$, $\tilde{B}_k$ and their derivatives, for $k \le N_F$. Using the coordinate y in the inner region and taking the $\varepsilon \to 0$ limit we obtain the leading order inner equation

$$\frac{\mathrm{d}^2\Phi_n^{(0)}}{\mathrm{d}y^2}+(n^2-1)\Phi_n^{(0)} = F_n^{(0)}\ , \tag{354}$$

where $F_n^{(0)}$ are the $\varepsilon \to 0$ limits of the nonlinear source terms F_n. Apart from the structure of the nonlinear source terms, this equation has the same form as (204), which describes one-dimensional oscillons in the inner domain. On the imaginary axis the $1/y^2$ expansion gives real valued functions at all orders. On the other hand, the asymmetric breather solution must necessarily have a small but nonzero imaginary part on the imaginary axis. Since we are considering symmetric $U(\phi)$ potentials, the dominant mode is Φ_3, both along the imaginary y axis and in the radiating tail. To leading order approximation, the imaginary part of $\Phi_3^{(0)}$ satisfies the linear left-hand side of equation (354). Consequently, in the same way as at

(210), the asymmetric solution has an imaginary part which is exponentially decaying when going down along the imaginary axis,

$$\mathrm{Im}\,\Phi^{(0)}_{3,-} = \nu_3 \exp\left(-i\sqrt{8}\,y\right) \qquad \text{for} \qquad \mathrm{Re}\,y = 0\ , \quad \mathrm{Im}\,y < 0\ , \tag{355}$$

where ν_3 is a constant. On the other hand, the inner solution $\Phi^{(0)}_{3,\mathrm{m}}$ that corresponds to the regular quasibreather solution has zero imaginary part on the imaginary axis.

5.7.4 Laplace transform

For symmetric potentials the value of the constant ν_3 can be calculated by the application of the Laplace transform method, which has been presented in detail for oscillons in Subsection 4.4.7. According to (349), the following series is asymptotic to the function $\Phi^{(0)}_3$,

$$\Phi^{(0)}_3 = \sum_{k=2}^{\infty} \psi^{(2)}_k \frac{1}{y^{2k}}\ . \tag{356}$$

Since all individual terms are real on the imaginary axis, the imaginary part will be determined by the large k behavior of the coefficients. Hence we can assume that all $\psi^{(2)}_k$ coefficients are given by the leading order part of expression (352),

$$\psi^{(2)}_k = K_2(-1)^k \frac{(2k-1)!}{8^k}\ . \tag{357}$$

We look for $\Phi^{(0)}_3$ as the Laplace transform of a function denoted by $V'(s)$,

$$\Phi^{(0)}_3 = \int_{\tilde\gamma} I(s)\mathrm{d}s \quad , \quad I(s) = \exp(-ys)V'(s)\ , \tag{358}$$

where the contour $\tilde\gamma$ goes from $s = 0$ to infinity, such that $\mathrm{Re}(ys) \to \infty$. Since the Laplace transform of s^n is $n!y^{-n-1}$, it follows that the function $V'(s)$ can be expanded in the following form, which can be summed,

$$V'(s) = \sum_{k=2}^{\infty} \frac{\psi^{(2)}_k}{(2k-1)!} s^{2k-1} = K_2 \sum_{k=2}^{\infty} \frac{(-1)^k}{8^k} s^{2k-1} = \frac{K_2 s^3}{8(s^2+8)}\ . \tag{359}$$

The function $V'(s)$ has a pole at $s = i\sqrt{8}$, with residue $-\frac{1}{2}K_2$. The residue of $I(s)$ is then $-\frac{1}{2}K_2 \exp(-\sqrt{8}\,iy)$. As it has been discussed for the linear model problem, for the fKdV equation, and also for flat background oscillons, it is natural to choose the contour $\tilde\gamma$ along the upper half of the imaginary s axis, going around the pole at $s = i\sqrt{8}$ in a small half-circle, as shown in the middle panel of Fig 10. Then we obtain the asymmetric solution $\Phi^{(0)}_{3,-}$ that decays without oscillations in the right side of the complex y plane. Consequently, it corresponds to the asymmetric breather solution ϕ_-, which has no tail for $r > 0$, but it is

singular at $r = 0$. Only the small half-circle gives contribution to the imaginary part of the integral, which is half of the value that can be obtained by the residue theorem. It follows that

$$\mathrm{Im}\,\Phi^{(0)}_{3,-} = -\frac{1}{2}\pi K_2 \exp(-\sqrt{8}\,iy) \quad \text{for} \quad \mathrm{Re}\,y = 0 \text{ and } \mathrm{Im}\,y < 0\ . \tag{360}$$

Comparing with (355), we obtain the result for the constant ν_3,

$$\nu_3 = -\frac{K_2\pi}{2}\ . \tag{361}$$

For the Klein-Gordon potential the earlier calculated $K_2 \approx -0.301$ yields $\nu_3 \approx 0.473$.

5.7.5 Tail-amplitude

The tail-amplitude of the quasibreather solution can be obtained essentially in the same way as in Subsections 4.6.2 - 4.6.3. We denote the difference of the third Fourier mode of the minimal tail quasibreather and the asymmetric breather solutions by $w_3 = \Phi_{3,\mathrm{m}} - \Phi_{3,-}$. It is exponentially small apart from a small region around $r = 0$. Since in the $\varepsilon \to 0$ limit the core amplitude tends to zero and the metric approaches the Minkowski spacetime, the function w_3 can be approximated well by the solution of the linear left hand side of (353) with $n = 3$ and $\omega = 1$. The general solution for $d+1$ dimensional spacetimes has been given in (263). The minimal tail quasibreather cannot have a tail part corresponding to the phase of the centrally regular solution, hence $\beta_3 = 0$ in this case also. For the currently discussed 3-dimensional case the solution is

$$w_3 = \frac{\alpha_3}{r}\sin\left(\sqrt{8}\,r - \frac{\pi}{2}\right) = -\frac{\alpha_3}{r}\cos\left(\sqrt{8}\,r\right)\ , \tag{362}$$

where α_3 is the constant giving the tail-amplitude. Writing the result in terms of the exponential function and substituting $r = i\frac{P}{\varepsilon} + y$, close to the singularity the leading order behavior for small ε can be written as

$$w_3 = \frac{i\varepsilon}{2P}\alpha_3 \exp\left(\sqrt{8}\,\frac{P}{\varepsilon}\right)\exp(-i\sqrt{8}\,y)\ . \tag{363}$$

Since $\Phi_{3,\mathrm{m}}$ is purely real along the imaginary y axis, in the current case also true that $\mathrm{Im}\,\Phi_{3,-} = -\,\mathrm{Im}\,w_3$ for $\mathrm{Re}\,y = 0$ and $\mathrm{Im}\,y < 0$. Comparing with (355), for the tail-amplitude we get

$$\alpha_3 = \frac{2\nu_3 P}{\varepsilon}\exp\left(-\sqrt{8}\,\frac{P}{\varepsilon}\right)\ , \tag{364}$$

which is valid for any potential which is symmetric around its minimum. For 3 spatial dimensions $P \approx 3.97736$, and for the Klein-Gordon potential $\nu_3 \approx 0.473$. Hence for the tail-amplitude of the Klein-Gordon oscillaton we get

$$\alpha_3 = \frac{3.761}{\varepsilon}\exp\left(-\frac{11.2497}{\varepsilon}\right)\ . \tag{365}$$

This is only the tail-amplitude of the first radiating Fourier mode Φ_3, but the tail in the higher modes are much smaller than this, as it can also be seen in Fig. 25. According to (362), the scalar field in the tail region can be described by the expression

$$\phi = \frac{1}{\sqrt{8\pi}}\tilde{\phi} = -\frac{\alpha_3}{r\sqrt{8\pi}}\cos\left(\sqrt{8}\,r\right)\cos(3t)\ . \tag{366}$$

In Figure 32 we compare the leading order analytical result (365) for the tail-amplitude α_3

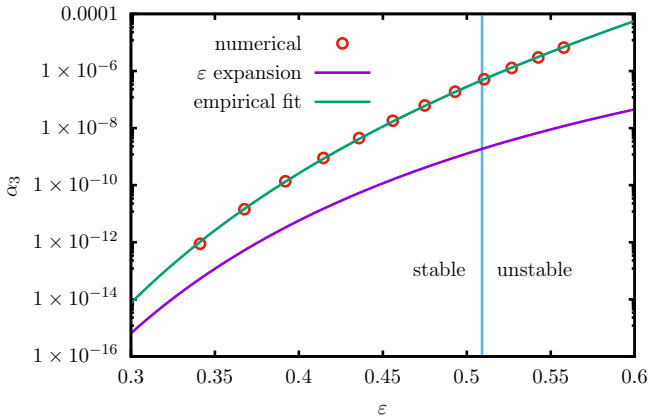

Figure 32: Comparison of the numerically obtained values of the tail-amplitude α_3 of the Fourier mode Φ_3 to the leading order theoretical result shown by the purple curve. The green curve was obtained by a fit to the data points.

to the numerical results already presented in Fig. 28, but now as a function of the amplitude parameter $\varepsilon = \sqrt{1-\omega^2}$.

For these large values of the parameter ε the theoretical curve lies much below the data points. The following empirical function,

$$\alpha_3^{\mathrm{emp}} = \frac{3.761}{\varepsilon}\left(1+\varepsilon^2\right)^{16.63}\exp\left[-\frac{11.2497}{\varepsilon}\left(1-0.2990\,\varepsilon^2\right)\right]\ , \tag{367}$$

fits well the numerical results, furthermore at small ε values it approaches the theoretical result (365). We can expect that in the whole stable domain (367) gives a good estimate for the amplitude of the tail, and hence for the strength of the radiation. For the largest ε values the numerical results shown in Fig. 32 are several hundred times larger than the analytical results, but with the decrease of ε the relative difference decreases exponentially. The smallest ε for which we could numerically calculate the tail is $\varepsilon = 0.341$, where the magnitude of the tail-amplitude α_3 is 10^{-12}. In this case the reliable numerical result is still twenty times larger than the leading order theoretical one. The parameter $\varepsilon = 0.341$ in a power series expansion generally cannot be considered small. However, because of the exponential decrease of the relative difference it appears convincing that the two approaches would give more and more agreeing results for smaller ε values.

5.7.6 Mass loss rate

In order to obtain results which are also precise for large amplitude oscillatons, we do not assume now that $\omega = 1$. We have to calculate the energy carried out by the following spherical wave,

$$\phi = \frac{\alpha_3}{r\sqrt{8\pi}} \cos\left(\lambda_3 r - 3\omega t\right) \ , \tag{368}$$

where $\lambda_3 = \sqrt{9\omega^2 - 1}$. Equation (148) giving the radiated energy current averaged for an oscillation period can also be applied now, where $\omega_f = 3\omega$, $\lambda_f = \lambda_3$ and $\alpha = \alpha_3/\sqrt{8\pi}$. As a result of this, the time averaged mass loss rate of oscillatons is

$$\bar{S} = -\overline{\frac{\mathrm{d}M}{\mathrm{d}t}} = \frac{3}{4}\alpha_3^2 \omega \sqrt{9\omega^2 - 1} \ . \tag{369}$$

Substituting the empirical expression (367) for α_3, we can obtain a result for the radiation rate, which according to our numerical calculations is valid for large amplitude states as well:

$$\bar{S} = 10.61 \frac{\omega\sqrt{9\omega^2 - 1}}{\varepsilon^2} \left(1 + \varepsilon^2\right)^{33.26} \exp\left[-\frac{22.4993}{\varepsilon}\left(1 - 0.2990\,\varepsilon^2\right)\right] \ , \tag{370}$$

where $\omega = \sqrt{1 - \varepsilon^2}$. Using only the small-amplitude expansion results, we would obtain

$$\bar{S} = \frac{30.0}{\varepsilon^2} \exp\left(-\frac{22.4993}{\varepsilon}\right) \ , \tag{371}$$

which is indeed the small ε appropriation of (370).

According to the numerical calculations discussed in Sec. 5.5, the the maximal oscillaton mass is $M_c = 0.60535$, which belongs to the amplitude parameter $\varepsilon_c = 0.509$. From (370) follows that the relative mass loss rate of the largest mass stable oscillaton is

$$\left(\frac{1}{M}\overline{\frac{\mathrm{d}M}{\mathrm{d}t}}\right)_{M=M_c} = -5.917 \times 10^{-13} m \ , \tag{372}$$

where m is the scalar field mass in Planck units. In Figure 33 we show how the mass of an initially maximal mass oscillaton changes in time, giving the ratio M/M_c. Because of the extremely slow decrease we take the product $t\,m$ logarithmically on the horizontal axis. The plot was made using the more precise numerical results.

In Figure 34 we show that during one oscillation period an oscillaton loses how small part of its mass. This quantity is independent on the scalar field mass m,

$$\frac{\Delta M}{M} = -\frac{2\pi}{\omega}\frac{1}{M}\overline{\frac{\mathrm{d}M}{\mathrm{d}t}} \ . \tag{373}$$

From the figure it can be seen that the relative mass loss rate is so small that every stable oscillaton can be considered as time-periodic to a very good approximation. The leading

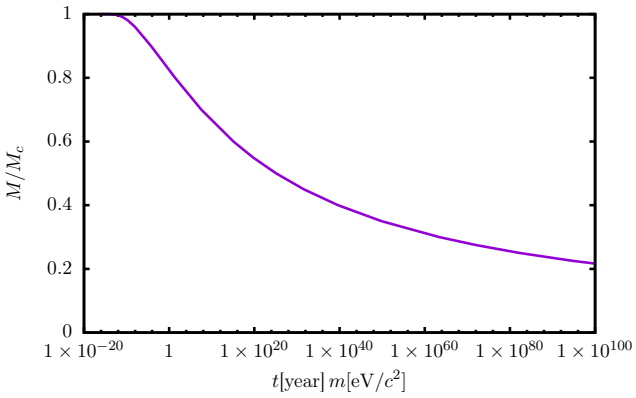

Figure 33: The mass change of the initially M_c maximal mass oscillaton as a function of the product of the scalar mass m and the elapsed time t, using ordinary units.

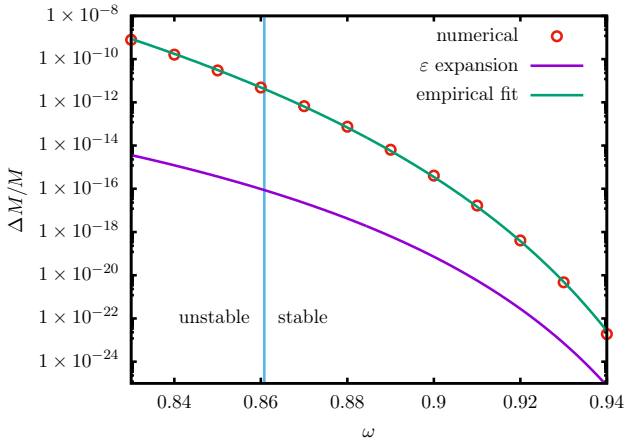

Figure 34: Relative mass loss of oscillatons during one oscillation period.

order theoretical result gives several orders of magnitude too small results in the domain where the tail is not too small for numerical simulations. This shows that it would be important to obtain higher order corrections to the available leading order ε expansion results. Such contributions have been only calculated yet for the case of the fifth-order KdV problem, which is technically simpler because of the stationarity of the solutions. We plan to apply the knowledge acquired during the detailed analysis of the fKdV problem to oscillons and oscillatons in the near future. More advanced numerical methods that could be used for the calculation of even smaller tail-amplitudes would be also useful for the scalar field case.

6 Summary and outlook

Although static or exactly time-periodic localized regular solutions do not exist in real scalar field theories, according to numerical simulations a large class of the possible initial data evolve into long-lived localized states. The frequency of these objects increases very slowly because of the weak energy loss resulting from the radiation of the scalar field. If the nonlinearity of the theory defined on a fixed background is provided by the self-interaction potential of the scalar field, then the formed object is generally called oscillon. The localized state formed from a self-gravitating scalar field in the framework of general relativity is known as oscillaton. In our papers on which this review is based, we have determined the shape and other properties of oscillons and oscillatons considerably more precisely than it was known earlier. Our numerical and analytical results consistently support each other. The extreme precision is mainly needed for the reliable and precise determination of the radiation loss of oscillons and oscillatons.

For the calculation of the outgoing radiation the necessary first step is the definition and study of the exactly time-periodic quasibreather state, which has a minimal amplitude standing wave tail. The periodicity in time makes it possible not only the application of precise spectral numerical codes, but also allows analytical methods by the extension of the equations into the complex plane. It can be shown relatively easily, that the radiation is exponentially small in terms of the parameter ε determining the oscillation amplitude of the core region. However, the concrete determination of the factor before the exponential term is only possible by a rather complicated method consisting of several steps. The main aim of this review is to present the analytical method for the calculation of the radiation rate in a comprehensible and easily reproducible way. During our work it became apparent, that the analytical results based on the ε expansion give precise results for small and intermediate amplitude states, while for the large amplitude states only the spectral numerical method is able to determine the radiation in a reliable way.

Because of the long lifetime of these configurations, various physical applications become feasible in cosmology and astrophysics. The radiation of $3+1$ dimensional oscillons is so small that several thousands of oscillation periods may happen before they move into the unstable domain and suddenly decay. The oscillatons coupled to gravity radiate so weakly, that even during a time period corresponding to the lifetime of the universe they do not lose more than half of their original mass. Oscillons and oscillatons can be expected to form in any theory containing several fields, if among them at least one real massive scalar field is included. But in case of appropriate nonlinearity, even the existence of the scalar is not necessarily needed, as it is shown by the existence of the oscillating localized states forming from self-gravitating Proca fields [122, 121].

It is important to clarify how a nonzero cosmological constant Λ influences the formation,

structure and radiation of localized states. A negative cosmological constant, acting as an effective attractive force, enhances the formation of oscillons and oscillatons, and decreases their radiation. The influence of a positive cosmological constant is just the opposite. The effect of a positive Λ for oscillons has been investigated in papers [187, 188, 189]. For oscillatons in our paper [83] we have presented in detail how a small $\Lambda > 0$ induces a small mass loss rate. By a positive cosmological constant we can model the accelerated expansion of the current universe, or describe the early inflationary period.

The negative cosmological constant have indirect physical significance because of the AdS/CFT correspondence. Researchers began to study more extensively the behavior of self-gravitating scalar fields for the $\Lambda < 0$ case after Bizoń and Rostworowski demonstrated by numerical methods in 2011 the instability of the anti-de Sitter spacetime [190]. They have investigated the time evolution of spherically symmetric wave packets formed by a massless real Klein-Gordon field in general relativity, for $\Lambda < 0$. According to their results, black holes can form from arbitrarily small amplitude initial data, by repeated bouncings of the wave packet through the center to infinity and back, becoming more and more concentrated in the meantime. However, not all type of initial data evolve into black holes.

If the cosmological constant is negative, there exist exactly time-periodic localized solutions, which do not radiate at all, and hence they can be considered as breathers [191]. For not too large perturbations, the deformed versions of these solutions remain near the time-periodic solution for all time, and no black hole formation occurs during their evolution. In this way, "stability islands" are formed around the breather solutions in the space of the possible initial data [192, 193]. We have studied spherically symmetric scalar breather solutions on fixed AdS background in our paper [194] for various self-interaction potentials. Breather solutions with AdS asymptotics exist even for zero mass fields, in which case their typical size is determined by the cosmological constant. For negative Λ we have studied spherically symmetric breather solutions formed by a self-gravitating real scalar field in our paper [195], by analytic and numerical methods, for d spatial dimensions. We have used a method, which contrary to earlier work, can be applied for odd d as well. For all $n \geq 0$ integers, a one-parameter family of breather solutions exists, where n gives the number of nodes of the scalar field. For the small amplitude limit the oscillation frequency tends to the integer value $\omega = d + 2n$.

The study of the scalar fields for $\Lambda < 0$ in general relativity was mainly motivated by the fact that in this case, even if we are restricted to spherical symmetry, the system has a nontrivial dynamics, which makes it possible that energy is radiated to infinity. In this way, instead of the complicated theory of gravitational waves and their radiation, we have to deal with a technically much simpler but in many respects analogously behaving model. The formation of small black holes in the scalar system makes it very likely that the system

consisting of only vacuum gravitational waves is also unstable for the $\Lambda < 0$ case. On the other hand, not all solutions evolve into black holes in this case either. When Λ is negative, there exist exactly time-periodic, but not spherically symmetric, localized breather solutions of the vacuum Einstein equations [196, 197, 198, 199]. These solutions are not losing energy by radiation, and for large distances they approach the anti-de Sitter spacetime. The vacuum AdS breather solutions are generally known by the name AdS geons. The concept of geons was introduced by John Archibald Wheeler in 1955 for long-lived localized states formed by electromagnetic or gravitational waves in the asymptotically flat case [200, 201, 202]. The structure of one-parameter families of AdS geons has been studied in our papers [203] and [204], by spectral numeric and high order expansion methods. Among these solutions there are axially symmetric ones, rotating solutions with helical symmetry, and surprisingly, also non-symmetric ones with zero angular momentum as well.

Acknowledgments

I would like to thank all my colleagues who have been co-authors in the papers [60, 61, 62, 63, 181, 81, 83, 82, 194, 195, 6, 7] that we have published on the topic of this review. I am especially grateful to Péter Forgács, who suggested me the topic of oscillons, oscillatons and similar geon-type configurations, and who has been working together with me enthusiastically for so many years since then. I would like to offer my special thanks to Philippe Grandclément, who has made much effort to teach us how to apply spectral numerical methods, and who created the numerical code for the calculation of the time-periodic quasibreather solutions presented in this review. I am also grateful to István Rácz for encouraging me to learn numerical time-evolution methods. We have developed together a fourth-order method of lines code for general spherically symmetric systems, which employs spatial compactification to deal with the problem of the outer boundary.

References

[1] J. K. Hunter and J. Scheurle, "Existence of perturbed solitary wave solutions to a model equation for water waves," *Physica D: Nonlinear Phenomena*, vol. 32, no. 2, pp. 253–268, 1988.

[2] E. Benilov, R. Grimshaw, and E. Kuznetsova, "The generation of radiating waves in a singularly-perturbed Korteweg-de Vries equation," *Physica D: Nonlinear Phenomena*, vol. 69, no. 3, pp. 270–278, 1993.

[3] J. P. Boyd, "A comparison of numerical and analytical methods for the reduced wave equation with multiple spatial scales," *Applied Numerical Mathematics*, vol. 7, no. 6, pp. 453–479, 1991. [Deep Blue Repositories].

[4] J. P. Boyd, "Radiative decay of weakly nonlocal solitary waves," *Wave Motion*, vol. 27, no. 3, pp. 211–221, 1998.

[5] J. P. Boyd, *Weakly Nonlocal Solitary Waves and Beyond-All-Orders Asymptotics*. Springer US, 1998.

[6] G. Fodor, P. Forgács, and M. Mushtaq, "Higher order corrections to beyond-all-order effects in a fifth order Korteweg–de Vries equation," *Phys. Rev. D*, vol. 107, p. 105002, 2023.

[7] G. Fodor, P. Forgács, and M. Mushtaq, "New derivation of the amplitude of asymptotic oscillatory tails of weakly delocalized solitons," *Phys. Rev. D*, vol. 109, p. 125011, 2024.

[8] V. L. Pokrovskii and I. M. Khalatnikov, "On the problem of above-barrier reflection of high-energy particles," *JETP*, vol. 13, p. 1207, 1961.

[9] M. D. Kruskal and H. Segur, "Asymptotics beyond all orders in a model of crystal growth," *Stud. Appl. Math.*, vol. 85, pp. 129–181, 1991. Original preprint: Tech. Rep. 85-25, Aeronautical Research Associates of Princeton, 1985.

[10] H. Segur and M. D. Kruskal, "Nonexistence of small-amplitude breather solutions in ϕ^4 theory," *Phys. Rev. Lett.*, vol. 58, pp. 747–750, 1987.

[11] Y. Pomeau, A. Ramani, and B. Grammaticos, "Structural stability of the Korteweg-de Vries solitons under a singular perturbation," *Phys. D: Nonlin. Phenom.*, vol. 31, no. 1, pp. 127–134, 1988.

[12] G. H. Derrick, "Comments on nonlinear wave equations as models for elementary particles," *Journal of Mathematical Physics*, vol. 5, no. 9, pp. 1252–1254, 1964.

[13] P. A. Vuillermot, "Nonexistence of spatially localized free vibrations for a class of nonlinear wave equations," *Commentarii Mathematici Helvetici*, vol. 62, no. 1, pp. 573–586, 1987.

[14] S. Kichenassamy, "Breather solutions of the nonlinear wave equation," *Communications on Pure and Applied Mathematics*, vol. 44, no. 7, pp. 789–818, 1991.

[15] J. Denzler, "Nonpersistence of breather families for the perturbed sine Gordon equation," *Communications in Mathematical Physics*, vol. 158, p. 397–430, 1993.

[16] I. L. Bogolubsky, "Cascade evolution of spherically symmetric pulsons in multivacuum field theory models," *Physics Letters A*, vol. 61, no. 4, pp. 205 – 206, 1977.

[17] I. L. Bogolyubskii and V. G. Makhan'kov, "Dynamics of spherically symmetrical pulsons of large amplitude," *JETP Letters*, vol. 25, p. 107, 1977.

[18] M. Gleiser, "Pseudostable bubbles," *Phys. Rev. D*, vol. 49, pp. 2978–2981, 1994.

[19] E. J. Copeland, M. Gleiser, and H.-R. Müller, "Oscillons: Resonant configurations during bubble collapse," *Phys. Rev. D*, vol. 52, pp. 1920–1933, 1995.

[20] A. E. Kudryavtsev, "Solitonlike solutions for a Higgs scalar field," *JETP Letters*, vol. 22, p. 82, 1975.

[21] A. B. Adib, M. Gleiser, and C. A. S. Almeida, "Long-lived oscillons from asymmetric bubbles: Existence and stability," *Phys. Rev. D*, vol. 66, p. 085011, 2002.

[22] E. W. Kolb and I. I. Tkachev, "Nonlinear axion dynamics and the formation of cosmological pseudosolitons," *Phys. Rev. D*, vol. 49, pp. 5040–5051, 1994.

[23] M. Hindmarsh and P. Salmi, "Numerical investigations of oscillons in 2 dimensions," *Phys. Rev. D*, vol. 74, p. 105005, 2006.

[24] M. Gleiser, "Oscillons in scalar field theories: Applications in higher dimensions and inflation," *International Journal of Modern Physics D*, vol. 16, no. 02n03, pp. 219–229, 2007.

[25] M. A. Amin, R. Easther, and H. Finkel, "Inflaton fragmentation and oscillon formation in three dimensions," *Journal of Cosmology and Astroparticle Physics*, vol. 2010, no. 12, pp. 001–001, 2010.

[26] M. A. Amin, R. Easther, H. Finkel, R. Flauger, and M. P. Hertzberg, "Oscillons after inflation," *Phys. Rev. Lett.*, vol. 108, p. 241302, 2012.

[27] J.-P. Hong, M. Kawasaki, and M. Yamazaki, "Oscillons from pure natural inflation," *Phys. Rev. D*, vol. 98, p. 043531, 2018.

[28] J. C. Aurrekoetxea, K. Clough, and F. Muia, "Oscillon formation during inflationary preheating with general relativity," *Phys. Rev. D*, vol. 108, p. 023501, 2023.

[29] R. Mahbub and S. S. Mishra, "Oscillon formation from preheating in asymmetric inflationary potentials," *Phys. Rev. D*, vol. 108, p. 063524, 2023.

[30] M. Piani and J. Rubio, "Preheating in Einstein-Cartan Higgs inflation: oscillon formation," *Journal of Cosmology and Astroparticle Physics*, vol. 2023, no. 12, p. 002, 2023.

[31] S.-Y. Zhou, E. J. Copeland, R. Easther, H. Finkel, Z.-G. Mou, and P. M. Saffin, "Gravitational waves from oscillon preheating," *Journal of High Energy Physics*, vol. 2013, no. 10, p. 26, 2013.

[32] S. Antusch, F. Cefalà, and S. Orani, "Gravitational waves from oscillons after inflation," *Phys. Rev. Lett.*, vol. 118, p. 011303, 2017.

[33] S. Antusch, F. Cefalà, and S. Orani, "What can we learn from the stochastic gravitational wave background produced by oscillons?," *Journal of Cosmology and Astroparticle Physics*, vol. 2018, no. 03, pp. 032–032, 2018.

[34] M. A. Amin, J. Braden, E. J. Copeland, J. T. Giblin, C. Solorio, Z. J. Weiner, and S.-Y. Zhou, "Gravitational waves from asymmetric oscillon dynamics?," *Phys. Rev. D*, vol. 98, p. 024040, 2018.

[35] N. Kitajima, J. Soda, and Y. Urakawa, "Gravitational wave forest from string axiverse," *Journal of Cosmology and Astroparticle Physics*, vol. 2018, no. 10, pp. 008–008, 2018.

[36] J. Liu, Z.-K. Guo, R.-G. Cai, and G. Shiu, "Gravitational wave production after inflation with cuspy potentials," *Phys. Rev. D*, vol. 99, p. 103506, 2019.

[37] Y. Sang and Q.-G. Huang, "Stochastic gravitational-wave background from axion-monodromy oscillons in string theory during preheating," *Phys. Rev. D*, vol. 100, p. 063516, 2019.

[38] K. D. Lozanov and M. A. Amin, "Gravitational perturbations from oscillons and transients after inflation," *Phys. Rev. D*, vol. 99, p. 123504, 2019.

[39] A. Bhoonah, J. Bramante, S. Nerval, and N. Song, "Gravitational waves from dark sectors, oscillating inflatons, and mass boosted dark matter," *Journal of Cosmology and Astroparticle Physics*, vol. 2021, no. 04, p. 043, 2021.

[40] T. Hiramatsu, E. I. Sfakianakis, and M. Yamaguchi, "Gravitational wave spectra from oscillon formation after inflation," *Journal of High Energy Physics*, vol. 2021, no. 3, pp. 1–35, 2021.

[41] Aggarwal *et al.*, "Challenges and opportunities of gravitational-wave searches at MHz to GHz frequencies," *Living reviews in relativity*, vol. 24, pp. 1–74, 2021.

[42] X.-X. Kou, J. B. Mertens, C. Tian, and S.-Y. Zhou, "Gravitational waves from fully general relativistic oscillon preheating," *Phys. Rev. D*, vol. 105, p. 123505, 2022.

[43] K. D. Lozanov, M. Sasaki, and V. Takhistov, "Universal gravitational waves from interacting and clustered solitons," *Physics Letters B*, vol. 848, p. 138392, 2024.

[44] E. Farhi, N. Graham, V. Khemani, R. Markov, and R. Rosales, "An oscillon in the $SU(2)$ gauged Higgs model," *Phys. Rev. D*, vol. 72, p. 101701, 2005.

[45] N. Graham, "An electroweak oscillon," *Phys. Rev. Lett.*, vol. 98, p. 101801, 2007.

[46] N. Graham, "Numerical simulation of an electroweak oscillon," *Phys. Rev. D*, vol. 76, p. 085017, 2007.

[47] P. Arnold and L. McLerran, "The sphaleron strikes back: A response to objections to the sphaleron approximation," *Phys. Rev. D*, vol. 37, pp. 1020–1029, 1988.

[48] C. Rebbi and R. Singleton, "Computational study of baryon number violation in high energy electroweak collisions," *Phys. Rev. D*, vol. 54, pp. 1020–1043, 1996.

[49] V. Achilleos, F. K. Diakonos, D. J. Frantzeskakis, G. C. Katsimiga, X. N. Maintas, E. Manousakis, C. E. Tsagkarakis, and A. Tsapalis, "Oscillons and oscillating kinks in the Abelian-Higgs model," *Phys. Rev. D*, vol. 88, p. 045015, 2013.

[50] F. K. Diakonos, G. C. Katsimiga, X. N. Maintas, and C. E. Tsagkarakis, "Symmetric solitonic excitations of the (1 + 1)-dimensional Abelian-Higgs classical vacuum," *Phys. Rev. E*, vol. 91, p. 023202, 2015.

[51] N. S. Manton and T. Romańczukiewicz, "Simplest oscillon and its sphaleron," *Phys. Rev. D*, vol. 107, p. 085012, 2023.

[52] M. Gleiser and J. Thorarinson, "Phase transition in U(1) configuration space: Oscillons as remnants of vortex-antivortex annihilation," *Phys. Rev. D*, vol. 76, p. 041701, 2007.

[53] M. Gleiser and J. Thorarinson, "Class of nonperturbative configurations in Abelian-Higgs models: Complexity from dynamical symmetry breaking," *Phys. Rev. D*, vol. 79, p. 025016, 2009.

[54] M. Gleiser and N. Stamatopoulos, "Information content of spontaneous symmetry breaking," *Phys. Rev. D*, vol. 86, p. 045004, 2012.

[55] R. F. Dashen, B. Hasslacher, and A. Neveu, "Particle spectrum in model field theories from semiclassical functional integral techniques," *Phys. Rev. D*, vol. 11, pp. 3424–3450, 1975.

[56] M. P. Hertzberg, "Quantum radiation of oscillons," *Phys. Rev. D*, vol. 82, p. 045022, 2010.

[57] J. Evslin, T. Romańczukiewicz, and A. Wereszczyński, "Quantum oscillons may be long-lived," *Journal of High Energy Physics*, vol. 2023, no. 8, pp. 1–18, 2023.

[58] P. M. Saffin, P. Tognarelli, and A. Tranberg, "Oscillon lifetime in the presence of quantum fluctuations," *Journal of High Energy Physics*, vol. 2014, no. 8, p. 125, 2014.

[59] J. Ollé, O. Pujolàs, T. Vachaspati, and G. Zahariade, "Quantum evaporation of classical breathers," *Phys. Rev. D*, vol. 100, p. 045011, 2019.

[60] G. Fodor, P. Forgács, P. Grandclément, and I. Rácz, "Oscillons and quasibreathers in the ϕ^4 Klein-Gordon model," *Phys. Rev. D*, vol. 74, p. 124003, 2006.

[61] G. Fodor, P. Forgács, Z. Horváth, and A. Lukács, "Small amplitude quasibreathers and oscillons," *Phys. Rev. D*, vol. 78, p. 025003, 2008.

[62] G. Fodor, P. Forgács, Z. Horváth, and M. Mezei, "Computation of the radiation amplitude of oscillons," *Phys. Rev. D*, vol. 79, p. 065002, 2009.

[63] G. Fodor, P. Forgács, Z. Horváth, and M. Mezei, "Radiation of scalar oscillons in 2 and 3 dimensions," *Physics Letters B*, vol. 674, no. 4, pp. 319 – 324, 2009.

[64] E. P. Honda and M. W. Choptuik, "Fine structure of oscillons in the spherically symmetric φ^4 Klein-Gordon model," *Phys. Rev. D*, vol. 65, p. 084037, 2002.

[65] P. M. Saffin and A. Tranberg, "Oscillons and quasi-breathers in D+1 dimensions," *Journal of High Energy Physics*, vol. 2007, no. 01, p. 030, 2007.

[66] P. Salmi and M. Hindmarsh, "Radiation and relaxation of oscillons," *Phys. Rev. D*, vol. 85, p. 085033, 2012.

[67] E. A. Andersen and A. Tranberg, "Four results on ϕ^4 oscillons in $D+1$ dimensions," *Journal of High Energy Physics*, vol. 2012, no. 12, p. 16, 2012.

[68] Y. M. Shnir, *Topological and Non-Topological Solitons in Scalar Field Theories*. Cambridge Monographs on Mathematical Physics, Cambridge University Press, 2018.

[69] J. Sakstein and M. Trodden, "Oscillons in higher-derivative effective field theories," *Phys. Rev. D*, vol. 98, p. 123512, 2018.

[70] M. Gleiser and M. Krackow, "Resonant configurations in scalar field theories: Can some oscillons live forever?," *Phys. Rev. D*, vol. 100, p. 116005, 2019.

[71] B. C. Nagy and G. Takács, "Collapse instability and staccato decay of oscillons in various dimensions," *Phys. Rev. D*, vol. 104, p. 056033, 2021.

[72] D. Cyncynates and T. Giurgica-Tiron, "Structure of the oscillon: The dynamics of attractive self-interaction," *Phys. Rev. D*, vol. 103, p. 116011, 2021.

[73] J. T. Gálvez Ghersi and J. Braden, "Dimensional deformation of sine-Gordon breathers into oscillons," *Phys. Rev. D*, vol. 108, p. 096017, 2023.

[74] F. van Dissel, O. Pujolàs, and E. I. Sfakianakis, "Oscillon spectroscopy," *Journal of High Energy Physics*, vol. 2023, no. 7, pp. 1–32, 2023.

[75] A. M. Kosevich and A. S. Kovalev, "Self-localization of vibrations in a one-dimensional anharmonic chain," *JETP*, vol. 40, p. 1973, 1975.

[76] V. S. Buslaev, "Solutions of "double soliton" type for the multidimensional equation $\Box u = F(u)$," *Theoretical and Mathematical Physics*, vol. 31, no. 1, pp. 293–299, 1977.

[77] I. L. Bogolyubskii, "Oscillating particle-like solutions of the nonlinear Klein-Gordon equation," *JETP Letters*, vol. 24, p. 535, 1976.

[78] E. Seidel and W.-M. Suen, "Oscillating soliton stars," *Phys. Rev. Lett.*, vol. 66, pp. 1659–1662, 1991.

[79] E. Seidel and W.-M. Suen, "Formation of solitonic stars through gravitational cooling," *Phys. Rev. Lett.*, vol. 72, pp. 2516–2519, 1994.

[80] D. N. Page, "Classical and quantum decay of oscillations: Oscillating self-gravitating real scalar field solitons," *Phys. Rev. D*, vol. 70, p. 023002, 2004.

[81] G. Fodor, P. Forgács, and M. Mezei, "Mass loss and longevity of gravitationally bound oscillating scalar lumps (oscillatons) in D dimensions," *Phys. Rev. D*, vol. 81, p. 064029, 2010.

[82] P. Grandclément, G. Fodor, and P. Forgács, "Numerical simulation of oscillatons: Extracting the radiating tail," *Phys. Rev. D*, vol. 84, p. 065037, 2011.

[83] G. Fodor, P. Forgács, and M. Mezei, "Boson stars and oscillatons in an inflationary universe," *Phys. Rev. D*, vol. 82, p. 044043, 2010.

[84] T. Matos and F. S. Guzmán, "On the spacetime of a galaxy," *Classical and Quantum Gravity*, vol. 18, no. 23, p. 5055, 2001.

[85] M. Alcubierre, F. S. Guzmán, T. Matos, D. Núñez, L. A. Ureña-López, and P. Wiederhold, "Galactic collapse of scalar field dark matter," *Classical and Quantum Gravity*, vol. 19, no. 19, p. 5017, 2002.

[86] M. Susperregi, "Dark energy and dark matter from an inhomogeneous dilaton," *Phys. Rev. D*, vol. 68, p. 123509, 2003.

[87] B. Malakolkalami and A. Mahmoodzadeh, "Time-dependent scalar fields as candidates for dark matter," *Phys. Rev. D*, vol. 94, p. 103505, 2016.

[88] L. A. Ureña-López, "Brief review on scalar field dark matter models," *Frontiers in Astronomy and Space Sciences*, vol. 6, 2019.

[89] L. Hui, "Wave dark matter," *Annual Review of Astronomy and Astrophysics*, vol. 59, no. Volume 59, 2021, pp. 247–289, 2021.

[90] V. A. Koutvitsky and E. M. Maslov, "Resonant phenomena in finite motions of test particles in oscillating dark matter configurations," *Phys. Rev. D*, vol. 109, p. 044024, 2024.

[91] I. I. Tkachev, "Coherent scalar-field oscillations forming compact astrophysical object," *Soviet Astronomy Letters*, vol. 12, pp. 305–308, 1986.

[92] C. Hogan and M. Rees, "Axion miniclusters," *Physics Letters B*, vol. 205, no. 2, pp. 228 – 230, 1988.

[93] E. W. Kolb and I. I. Tkachev, "Axion miniclusters and Bose stars," *Phys. Rev. Lett.*, vol. 71, pp. 3051–3054, 1993.

[94] A. Arvanitaki, S. Dimopoulos, S. Dubovsky, N. Kaloper, and J. March-Russell, "String axiverse," *Phys. Rev. D*, vol. 81, p. 123530, 2010.

[95] D. J. Marsh, "Axion cosmology," *Physics Reports*, vol. 643, pp. 1 – 79, 2016.

[96] D. J. E. Marsh, "Axions and ALPs: a very short introduction," in *Proceedings of the 13th "Patras" Workshop on Axions, WIMPs and WISPs, PATRAS 2017* (M. Maroudas, ed.), Verlag Deutsches Elektronen-Synchrotron, 2018.

[97] S. Krippendorf, F. Muia, and F. Quevedo, "Moduli stars," *Journal of High Energy Physics*, vol. 2018, no. 8, p. 70, 2018.

[98] F. Chadha-Day, J. Ellis, and D. J. E. Marsh, "Axion dark matter: What is it and why now?," *Science Advances*, vol. 8, no. 8, p. eabj3618, 2022.

[99] D. Cyncynates, O. Simon, J. O. Thompson, and Z. J. Weiner, "Nonperturbative structure in coupled axion sectors and implications for direct detection," *Phys. Rev. D*, vol. 106, p. 083503, 2022.

[100] K. Imagawa, M. Kawasaki, K. Murai, H. Nakatsuka, and E. Sonomoto, "Free streaming length of axion-like particle after oscillon/I-ball decays," *Journal of Cosmology and Astroparticle Physics*, vol. 2023, no. 02, p. 024, 2023.

[101] A. Chatrchyan, C. Eröncel, M. Koschnitzke, and G. Servant, "ALP dark matter with non-periodic potentials: parametric resonance, halo formation and gravitational signatures," *Journal of Cosmology and Astroparticle Physics*, vol. 2023, no. 10, p. 068, 2023.

[102] L. Visinelli, S. Baum, J. Redondo, K. Freese, and F. Wilczek, "Dilute and dense axion stars," *Physics Letters B*, vol. 777, pp. 64 – 72, 2018.

[103] P.-H. Chavanis, "Phase transitions between dilute and dense axion stars," *Phys. Rev. D*, vol. 98, p. 023009, 2018.

[104] E. Braaten and H. Zhang, "Colloquium: The physics of axion stars," *Rev. Mod. Phys.*, vol. 91, p. 041002, 2019.

[105] J. Eby, M. Leembruggen, L. Street, P. Suranyi, and L. C. R. Wijewardhana, "Global view of QCD axion stars," *Phys. Rev. D*, vol. 100, p. 063002, 2019.

[106] L. Chung-Jukko, E. A. Lim, and D. J. E. Marsh, "Multimessenger signals from compact axion star mergers," *Phys. Rev. D*, vol. 110, p. 063506, 2024.

[107] M. Escudero, C. K. Pooni, M. Fairbairn, D. Blas, X. Du, and D. J. E. Marsh, "Axion star explosions: A new source for axion indirect detection," *Phys. Rev. D*, vol. 109, p. 043018, 2024.

[108] H.-Y. Schive, T. Chiueh, and T. Broadhurst, "Cosmic structure as the quantum interference of a coherent dark wave," *Nature Physics*, vol. 10, p. 496, 2014.

[109] J. Veltmaat and J. C. Niemeyer, "Cosmological particle-in-cell simulations with ultralight axion dark matter," *Phys. Rev. D*, vol. 94, p. 123523, 2016.

[110] P. Mocz, A. Fialkov, M. Vogelsberger, M. Boylan-Kolchin, P.-H. Chavanis, M. A. Amin, S. Bose, T. Dome, L. Hernquist, L. Lancaster, M. Notis, C. Painter, V. H. Robles, and J. Zavala, "Cosmological structure formation and soliton phase transition in fuzzy dark matter with axion self-interactions," *Monthly Notices of the Royal Astronomical Society*, vol. 521, no. 2, pp. 2608–2615, 2023.

[111] X. Du, D. J. E. Marsh, M. Escudero, A. Benson, D. Blas, C. K. Pooni, and M. Fairbairn, "Soliton merger rates and enhanced axion dark matter decay," *Phys. Rev. D*, vol. 109, p. 043019, 2024.

[112] B. Eggemeier, P. Hayman, J. C. Niemeyer, and R. Easther, "Postinflationary structure formation boosted by parametric self-resonance," *Phys. Rev. D*, vol. 109, p. 043521, 2024.

[113] W. Hu, R. Barkana, and A. Gruzinov, "Fuzzy cold dark matter: The wave properties of ultralight particles," *Phys. Rev. Lett.*, vol. 85, pp. 1158–1161, 2000.

[114] D. J. E. Marsh and A.-R. Pop, "Axion dark matter, solitons and the cusp–core problem," *Monthly Notices of the Royal Astronomical Society*, vol. 451, no. 3, pp. 2479–2492, 2015.

[115] B. Schwabe, J. C. Niemeyer, and J. F. Engels, "Simulations of solitonic core mergers in ultralight axion dark matter cosmologies," *Phys. Rev. D*, vol. 94, p. 043513, 2016.

[116] L. Hui, J. P. Ostriker, S. Tremaine, and E. Witten, "Ultralight scalars as cosmological dark matter," *Phys. Rev. D*, vol. 95, p. 043541, 2017.

[117] Bañares-Hernández, Andrés, Castillo, Andrés, Martin Camalich, Jorge, and Iorio, Giuliano, "Confronting fuzzy dark matter with the rotation curves of nearby dwarf irregular galaxies," *Astronomy & Astrophysics*, vol. 676, p. A63, 2023.

[118] B. Dave and G. Goswami, "Self-interactions of ULDM to the rescue?," *Journal of Cosmology and Astroparticle Physics*, vol. 2023, no. 07, p. 015, 2023.

[119] J. Chen and H.-Y. Zhang, "Novel structures and collapse of solitons in nonminimally gravitating dark matter halos," *Journal of Cosmology and Astroparticle Physics*, vol. 2024, no. 10, p. 005, 2024.

[120] R. Brito, V. Cardoso, and H. Okawa, "Accretion of dark matter by stars," *Phys. Rev. Lett.*, vol. 115, p. 111301, 2015.

[121] R. Brito, V. Cardoso, C. F. B. Macedo, H. Okawa, and C. Palenzuela, "Interaction between bosonic dark matter and stars," *Phys. Rev. D*, vol. 93, p. 044045, 2016.

[122] D. Garfinkle, R. Mann, and C. Vuille, "Critical collapse of a massive vector field," *Phys. Rev. D*, vol. 68, p. 064015, 2003.

[123] M. Gorghetto, E. Hardy, J. March-Russell, N. Song, and S. M. West, "Dark photon stars: formation and role as dark matter substructure," *Journal of Cosmology and Astroparticle Physics*, vol. 2022, no. 08, p. 018, 2022.

[124] K. Aoki and M. Minamitsuji, "Highly compact Proca stars with quartic self-interactions," *Phys. Rev. D*, vol. 107, p. 044045, 2023.

[125] J. Chen, X. Du, M. Zhou, A. Benson, and D. J. E. Marsh, "Gravitational Bose-Einstein condensation of vector or hidden photon dark matter," *Phys. Rev. D*, vol. 108, p. 083021, 2023.

[126] R. Brito, V. Cardoso, C. A. Herdeiro, and E. Radu, "Proca stars: Gravitating Bose–Einstein condensates of massive spin 1 particles," *Physics Letters B*, vol. 752, pp. 291–295, 2016.

[127] N. Sanchis-Gual, C. Herdeiro, E. Radu, J. C. Degollado, and J. A. Font, "Numerical evolutions of spherical Proca stars," *Phys. Rev. D*, vol. 95, p. 104028, 2017.

[128] S. L. Liebling and C. Palenzuela, "Dynamical boson stars," *Living Reviews in Relativity*, vol. 26, no. 1, 2023.

[129] C. J. Lustri, S. Crew, and S. J. Chapman, "Exponential asymptotics using numerical rational approximation in linear differential equations," *The ANZIAM Journal*, vol. 65, no. 4, p. 285–307, 2023.

[130] M. Oliver and M. A. T. Kenfack, "Deterministic and stochastic surrogate models for a slowly driven fast oscillator," *SIAM Journal on Applied Dynamical Systems*, vol. 23, no. 2, pp. 1090–1107, 2024.

[131] A. H. Nayfeh, *Perturbation Methods*. John Wiley & Sons, Ltd, 1973.

[132] C. M. Bender and S. A. Orszag, *Advanced Mathematical Methods for Scientists and Engineers I*. Boston, MA: Springer New York, NY, 1978.

[133] J. Kevorkian and J. D. Cole, *Multiple Scale and Singular Perturbation Methods*. Springer New York, NY, 1996.

[134] H. Segur, S. Tanveer, and H. Levine, eds., *Asymptotics beyond All Orders*, Springer New York, NY, 1991.

[135] S. J. Chapman, J. R. King, and K. L. Adams, "Exponential asymptotics and Stokes lines in nonlinear ordinary differential equations," *Proceedings of the Royal Society of London. Series A: Mathematical, Physical and Engineering Sciences*, vol. 454, no. 1978, pp. 2733–2755, 1998.

[136] S. Crew and P. H. Trinh, "Resurgent aspects of applied exponential asymptotics," *Studies in Applied Mathematics*, vol. 152, no. 3, pp. 974–1025, 2024.

[137] M. Berry and C. Howls, "Infinity interpreted," *Physics World*, vol. 6, no. 6, p. 35, 1993.

[138] M. V. Berry and C. J. Howls, "Hyperasymptotics," *Proceedings of the Royal Society of London. Series A: Mathematical and Physical Sciences*, vol. 430, no. 1880, pp. 653–668, 1990.

[139] J. P. Boyd, "The devil's invention: Asymptotic, superasymptotic and hyperasymptotic series," *Acta Applicandae Mathematica*, vol. 56, no. 1, p. 1–98, 1999. [Deep Blue Repositories].

[140] R. Grimshaw and N. Joshi, "Weakly nonlocal solitary waves in a singularly perturbed Korteweg–De Vries equation," *SIAM J. Appl. Math.*, vol. 55, no. 1, pp. 124–135, 1995.

[141] T. Kakutani and H. Ono, "Weak non-linear hydromagnetic waves in a cold collision-free plasma," *Journal of the Physical Society of Japan*, vol. 26, no. 5, pp. 1305–1318, 1969.

[142] T. Kawahara, "Oscillatory solitary waves in dispersive media," *Journal of the Physical Society of Japan*, vol. 33, no. 1, pp. 260–264, 1972.

[143] C. J. Amick and J. B. McLeod, "A singular perturbation problem in water-waves," *Stability and Applied Analysis of Continuous Media*, vol. 1, pp. 127–148, 1991.

[144] B. T. N. Gunney, Y. A. Li, and P. J. Olver, "Solitary waves in the critical surface-tension model," *Journal of Engineering Mathematics*, vol. 36, no. 1, pp. 99–112, 1999.

[145] C. J. Amick and J. F. Toland, "Solitary waves with surface tension I: Trajectories homoclinic to periodic orbits in four dimensions," *Arch. Ration. Mech. Anal.*, vol. 118, pp. 37–69, 1992.

[146] S. M. Sun, "On the oscillatory tails with arbitrary phase shift for solutions of the perturbed Korteweg–de Vries equation," *SIAM J. Appl. Math.*, vol. 58, no. 4, pp. 1163–1177, 1998.

[147] C. Canuto, M. Y. Hussaini, A. Quarteroni, and T. A. Zang, *Spectral Methods, Fundamentals in Single Domains*. Springer Berlin, Heidelberg, 2006.

[148] J. Boyd, *Chebyshev and Fourier Spectral Methods: Second Revised Edition*. Dover Books on Mathematics, Dover Publications, 2001.

[149] "CLN - Class Library for Numbers." `https://www.ginac.de/CLN/`.

[150] "Arb - a C library for arbitrary-precision ball arithmetic." `https://arblib.org/`.

[151] F. Johansson, "Arb: efficient arbitrary-precision midpoint-radius interval arithmetic," *IEEE Trans. Comput.*, vol. 66, pp. 1281–1292, 2017.

[152] J. M. Hammersley and G. Mazzarino, "Computational aspects of some autonomous differential equations," *Proc. R. Soc. Lond. A*, vol. 424, pp. 19–37, 1989.

[153] J. P. Boyd, "Multiple precision pseudospectral computations of the radiation coefficient for weakly nonlocal solitary waves: Fifth-order Korteweg–DeVries equation," *Comp. Phys.*, vol. 9, no. 3, pp. 324–334, 1995.

[154] V. G. Makhankov, "Dynamics of classical solitons (in non-integrable systems)," *Physics Reports*, vol. 35, no. 1, pp. 1 – 128, 1978.

[155] G. Fodor, "A review on radiation of oscillons and oscillatons." arXiv:1911.03340 [hep-th], Hungarian version: Skalármezők által létrehozott lokalizált állapotok [pdf file], 2019.

[156] J. P. Boyd, "Weakly non-local solitary waves," in *Mesoscale/Synoptic Coherent structures in Geophysical Turbulence* (J. Nihoul and B. Jamart, eds.), vol. 50 of *Elsevier Oceanography Series*, pp. 103 – 112, Elsevier, 1989.

[157] J. P. Boyd, "A numerical calculation of a weakly non-local solitary wave: the ϕ^4 breather," *Nonlinearity*, vol. 3, no. 1, p. 177, 1990.

[158] G. L. Alfimov, W. A. B. Evans, and L. Vázquez, "On radial sine-Gordon breathers," *Nonlinearity*, vol. 13, no. 5, p. 1657, 2000.

[159] "LORENE, Langage Objet pour la RElativité NumériquE." `http://www.lorene.obspm.fr/`.

[160] V. M. Eleonskii, N. E. Kulagin, N. S. Novozhilova, and V. P. Silin, "Asymptotic expansions and qualitative analysis of finite-dimensional models in nonlinear field theory," *Theoretical and Mathematical Physics*, vol. 60, no. 3, pp. 896–902, 1984.

[161] R. Watkins, "Theory of oscillons." DART-HEP-96 preprint, unpublished, 1996.

[162] D. J. Kaup, "Klein-Gordon geon," *Phys. Rev.*, vol. 172, pp. 1331–1342, 1968.

[163] R. Ruffini and S. Bonazzola, "Systems of self-gravitating particles in general relativity and the concept of an equation of state," *Phys. Rev.*, vol. 187, pp. 1767–1783, 1969.

[164] P. Jetzer, "Boson stars," *Physics Reports*, vol. 220, no. 4, pp. 163 – 227, 1992.

[165] F. E. Schunck and E. W. Mielke, "General relativistic boson stars," *Classical and Quantum Gravity*, vol. 20, no. 20, p. R301, 2003.

[166] L. Visinelli, "Boson stars and oscillatons: A review," *International Journal of Modern Physics D*, vol. 30, no. 15, p. 2130006, 2021.

[167] S. Bird, C.-F. Chang, Y. Cui, and D. Yang, "Enhanced early galaxy formation in JWST from axion dark matter?," *Physics Letters B*, vol. 858, p. 139062, 2024.

[168] L. A. Ureña-López, T. Matos, and R. Becerril, "Inside oscillatons," *Classical and Quantum Gravity*, vol. 19, no. 23, p. 6259, 2002.

[169] M. Alcubierre, R. Becerril, F. S. Guzmán, T. Matos, D. Núñez, and L. A. Ureña-López, "Numerical studies of ϕ^2 -oscillatons," *Classical and Quantum Gravity*, vol. 20, no. 13, p. 2883, 2003.

[170] L. A. Ureña-López, S. Valdez-Alvarado, and R. Becerril, "Evolution and stability ϕ^4 oscillatons," *Classical and Quantum Gravity*, vol. 29, no. 6, p. 065021, 2012.

[171] T. Ikeda, C.-M. Yoo, and V. Cardoso, "Self-gravitating oscillons and new critical behavior," *Phys. Rev. D*, vol. 96, p. 064047, 2017.

[172] J. Balakrishna, R. Bondarescu, G. Daues, and M. Bondarescu, "Numerical simulations of oscillating soliton stars: Excited states in spherical symmetry and ground state evolutions in 3D," *Phys. Rev. D*, vol. 77, p. 024028, 2008.

[173] F. Muia, M. Cicoli, K. Clough, F. Pedro, F. Quevedo, and G. P. Vacca, "The fate of dense scalar stars," *Journal of Cosmology and Astroparticle Physics*, vol. 2019, no. 07, pp. 044–044, 2019.

[174] K. Clough, T. Dietrich, and J. C. Niemeyer, "Axion star collisions with black holes and neutron stars in full 3D numerical relativity," *Phys. Rev. D*, vol. 98, p. 083020, 2018.

[175] T. Helfer, E. A. Lim, M. A. G. Garcia, and M. A. Amin, "Gravitational wave emission from collisions of compact scalar solitons," *Phys. Rev. D*, vol. 99, p. 044046, 2019.

[176] S. H. Hawley and M. W. Choptuik, "Numerical evidence for "multiscalar stars"," *Phys. Rev. D*, vol. 67, p. 024010, 2003.

[177] M. Choptuik, R. Masachs, and B. Way, "Multioscillating boson stars," *Phys. Rev. Lett.*, vol. 123, p. 131101, 2019.

[178] "KADATH Spectral Solver." `https://kadath.obspm.fr/`. author: Philippe Grandclément.

[179] P. Grandclément, "Kadath: A spectral solver for theoretical physics," *Journal of Computational Physics*, vol. 229, no. 9, pp. 3334 – 3357, 2010.

[180] S. Kichenassamy, "Soliton stars in the breather limit," *Classical and Quantum Gravity*, vol. 25, no. 24, p. 245004, 2008.

[181] G. Fodor, P. Forgács, Z. Horváth, and M. Mezei, "Oscillons in dilaton-scalar theories," *Journal of High Energy Physics*, vol. 2009, no. 08, p. 106, 2009.

[182] I. M. Moroz, R. Penrose, and P. Tod, "Spherically-symmetric solutions of the Schrödinger-Newton equations," *Classical and Quantum Gravity*, vol. 15, no. 9, p. 2733, 1998.

[183] P. Tod and I. M. Moroz, "An analytical approach to the Schrödinger-Newton equations," *Nonlinearity*, vol. 12, no. 2, p. 201, 1999.

[184] L. Diósi, "Gravitation and quantum-mechanical localization of macro-objects," *Physics Letters A*, vol. 105, no. 4, pp. 199 – 202, 1984.

[185] R. Penrose, "Quantum computation, entanglement and state reduction," *Philosophical Transactions of the Royal Society of London. Series A: Mathematical, Physical and Engineering Sciences*, vol. 356, p. 1927, 1998.

[186] R. Friedberg, T. D. Lee, and Y. Pang, "Mini-soliton stars," *Phys. Rev. D*, vol. 35, pp. 3640–3657, 1987.

[187] N. Graham and N. Stamatopoulos, "Unnatural oscillon lifetimes in an expanding background," *Physics Letters B*, vol. 639, no. 5, pp. 541 – 545, 2006.

[188] E. Farhi, N. Graham, A. H. Guth, N. Iqbal, R. R. Rosales, and N. Stamatopoulos, "Emergence of oscillons in an expanding background," *Phys. Rev. D*, vol. 77, p. 085019, 2008.

[189] M. Gleiser, N. Graham, and N. Stamatopoulos, "Long-lived time-dependent remnants during cosmological symmetry breaking: From inflation to the electroweak scale," *Phys. Rev. D*, vol. 82, p. 043517, 2010.

[190] P. Bizoń and A. Rostworowski, "Weakly turbulent instability of anti–de Sitter spacetime," *Phys. Rev. Lett.*, vol. 107, p. 031102, 2011.

[191] M. Maliborski and A. Rostworowski, "Time-periodic solutions in an Einstein AdS–massless-scalar-field system," *Phys. Rev. Lett.*, vol. 111, p. 051102, 2013.

[192] Ó. J. C. Dias, G. T. Horowitz, D. Marolf, and J. E. Santos, "On the nonlinear stability of asymptotically anti-de Sitter solutions," *Classical and Quantum Gravity*, vol. 29, no. 23, p. 235019, 2012.

[193] M. W. Choptuik, J. E. Santos, and B. Way, "Charting islands of stability with multioscillators in anti–de Sitter space," *Phys. Rev. Lett.*, vol. 121, p. 021103, 2018.

[194] G. Fodor, P. Forgács, and P. Grandclément, "Scalar field breathers on anti–de Sitter background," *Phys. Rev. D*, vol. 89, p. 065027, 2014.

[195] G. Fodor, P. Forgács, and P. Grandclément, "Self-gravitating scalar breathers with a negative cosmological constant," *Phys. Rev. D*, vol. 92, p. 025036, 2015.

[196] Ó. J. C. Dias, G. T. Horowitz, and J. E. Santos, "Gravitational turbulent instability of anti-de Sitter space," *Classical and Quantum Gravity*, vol. 29, no. 19, p. 194002, 2012.

[197] Ó. J. C. Dias and J. E. Santos, "AdS nonlinear instability: moving beyond spherical symmetry," *Classical and Quantum Gravity*, vol. 33, no. 23, p. 23LT01, 2016.

[198] G. T. Horowitz and J. E. Santos, "Geons and the instability of anti-de Sitter spacetime," in *One hundred years of general relativity* (Y. Bieri, ed.), vol. 20 of *Surveys in Differential Geometry*, pp. 321 – 335, International Press of Boston, 2015.

[199] A. Rostworowski, "Comment on 'AdS nonlinear instability: moving beyond spherical symmetry' (2016 class. quantum grav. 33 23lt01)," *Classical and Quantum Gravity*, vol. 34, no. 12, p. 128001, 2017.

[200] J. A. Wheeler, "Geons," *Phys. Rev.*, vol. 97, pp. 511–536, 1955.

[201] D. R. Brill and J. B. Hartle, "Method of the self-consistent field in general relativity and its application to the gravitational geon," *Phys. Rev.*, vol. 135, pp. B271–B278, 1964.

[202] P. R. Anderson and D. R. Brill, "Gravitational geons revisited," *Phys. Rev. D*, vol. 56, pp. 4824–4833, 1997.

[203] G. Martinon, G. Fodor, P. Grandclément, and P. Forgács, "Gravitational geons in asymptotically anti-de Sitter spacetimes," *Classical and Quantum Gravity*, vol. 34, no. 12, p. 125012, 2017.

[204] G. Fodor and P. Forgács, "Anti–de Sitter geon families," *Phys. Rev. D*, vol. 96, p. 084027, 2017.